

Zeitschrift: IABSE reports of the working commissions = Rapports des commissions de travail AIPC = IVBH Berichte der Arbeitskommissionen

Band: 29 (1979)

Rubrik: Session IV: Numerical methods

Nutzungsbedingungen

Die ETH-Bibliothek ist die Anbieterin der digitalisierten Zeitschriften auf E-Periodica. Sie besitzt keine Urheberrechte an den Zeitschriften und ist nicht verantwortlich für deren Inhalte. Die Rechte liegen in der Regel bei den Herausgebern beziehungsweise den externen Rechteinhabern. Das Veröffentlichen von Bildern in Print- und Online-Publikationen sowie auf Social Media-Kanälen oder Webseiten ist nur mit vorheriger Genehmigung der Rechteinhaber erlaubt. [Mehr erfahren](#)

Conditions d'utilisation

L'ETH Library est le fournisseur des revues numérisées. Elle ne détient aucun droit d'auteur sur les revues et n'est pas responsable de leur contenu. En règle générale, les droits sont détenus par les éditeurs ou les détenteurs de droits externes. La reproduction d'images dans des publications imprimées ou en ligne ainsi que sur des canaux de médias sociaux ou des sites web n'est autorisée qu'avec l'accord préalable des détenteurs des droits. [En savoir plus](#)

Terms of use

The ETH Library is the provider of the digitised journals. It does not own any copyrights to the journals and is not responsible for their content. The rights usually lie with the publishers or the external rights holders. Publishing images in print and online publications, as well as on social media channels or websites, is only permitted with the prior consent of the rights holders. [Find out more](#)

Download PDF: 20.08.2025

ETH-Bibliothek Zürich, E-Periodica, <https://www.e-periodica.ch>



SESSION IV

Numerical Methods

Méthodes numériques

Numerische Methoden

Chairman: Prof. H. Okamura, Japan

Introductory Lectures: „On the Finite Element Method in the Field of Plasticity“
Prof. E. Anderheggen, Switzerland
„Collapse Load Analysis of Engineering Structures by
Using New Discrete Element Models“
Prof. T. Kawai, Japan

(The Introductory Lectures are published in the Introductory Report, Volume AK 28)

Leere Seite
Blank page
Page vide

IV**Reinforced Concrete Modeling for Protective Structure Analysis**

Modèles pour l'analyse d'éléments de protection en béton armé

Modellbildung für Stahlbeton bei der Berechnung von Schutzbauwerken

F. S. WONG

Associate
Weidlinger Associates
Menlo Park, CA, USA

J. ISENBERG

Associate Partner
Weidlinger Associates
Menlo Park, CA, USA

SUMMARY

A major limitation in 3D dynamic finite element analysis of protective structures is reinforced concrete modeling. The requirements of such a model and the approaches currently used are outlined in this paper. The advantages and consequences of using a simple composite continuum model are studied through a representative example. Promising directions of further research in this area of reinforced concrete modeling are also indicated.

RESUME

Une limite importante à l'analyse tridimensionnelle dynamique d'éléments de protection en béton armé est posée par le choix d'un modèle convenable. On montre les exigences posées à un tel modèle et on présente quelques modèles souvent utilisés. Les avantages et les conséquences de l'adoption d'un modèle continu simple sont étudiés à l'aide d'un exemple typique. Des possibilités de recherches sont indiquées.

ZUSAMMENFASSUNG

Eine Hauptschwierigkeit, die bei der dreidimensionalen, dynamischen Finite Elemente Berechnung von Schutzbauwerken auftritt, besteht in der Modellbildung für Stahlbeton. Anforderungen an derartige Modelle und heute übliche Vorgehensweisen werden dargestellt. Die Vorteile und Konsequenzen der Anwendung eines einfachen Kontinuummodells werden an einem Beispiel erläutert. Mögliche Richtungen weiterer Forschungstätigkeit werden angedeutet.



1. INTRODUCTION

Major advances have been made in dynamic, three-dimensional, nonlinear finite element methods in recent years[1] which enable the design of protective structures to be based on more rational estimates of structural response than was previously possible[2]. Simulation of geometric details using up to 20,000 constant strain hexahedral finite elements is possible and the cost of time-marching analyses is of the order of one to three hours. Work in simulating the nonlinear multiaxial properties of soil surrounding the structure has resulted in complementary advances [3]. Nonlinear models of reinforced concrete structures have been proposed (e.g. [4-6]) but their application to analysis of protective structures has lagged with the result that concrete modeling is the weakest aspect of the analysis.

The requirements for a reinforced concrete model of protective structures include its validity for short-time, monotonically-increasing deformation. There is occasionally a need to represent one or two cycles of load or deformation, but seldom more. The model must be valid for deformations up to and beyond those associated with the maximum load. It must be compatible with integration algorithms commonly used in dynamic, nonlinear analyses which include, at a minimum, guarantees of uniqueness, continuity and stability of solution. In addition, the algorithms for computing the properties must be economical of computer execution time and storage so as not to penalize overall execution time. Finally, the model should be expressed in terms of a few empirical parameters (order of 10) which can be defined by a limited experimental effort.

The types of concrete models which meet these criteria may be termed the continuum and structural element approaches. The continuum approach includes all models expressing multiaxial stress-strain relationships. Examples include models based on plasticity and endochronic theories and a variety of variable moduli models. The structural element formulation of concrete properties in terms of stress resultants (moments, membrane forces and shears) is attractive from the standpoint of describing structural properties in natural structural terms. Problems such as describing combined flexural and membrane behavior in terms of composite stress-strain relations, whose solution in the continuum approach requires through-the-thickness integration [8], are avoided. The same types of theoretical frameworks, including plasticity theory, can be used for the stress-resultant formulation [9].

The purpose of this paper is to illustrate by an example the advantages and disadvantages of the plasticity theory, continuum approach to reinforced concrete modeling. The example is a horizontal shelter which is subjected to airblast and local airblast-induced ground motion.

The response of this hypothetical structure, which has complicated reinforcing patterns, is simulated with a three-dimensional, nonlinear finite element analysis using the TRANAL computer program developed by Weidlinger Associates [10].

2. EXAMPLE OF STRUCTURE TO BE ANALYZED

Methods of analyzing protective structures will be illustrated by means of the example shown in Fig. 1. This structure is made up of a rectangular headworks section, including stiff frame,

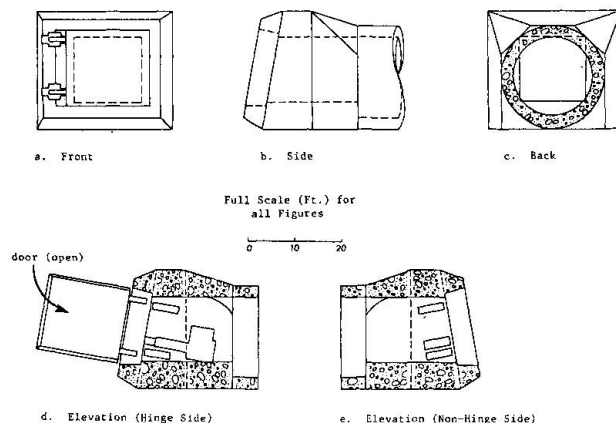


FIGURE 1. S4 HEADWORKS.

bearing surface and closure of door; and a transition section, which connects the headworks to a long horizontal tube. The main detail to be represented in the headworks frame is the circumferential reinforcing, including liner plate around the jamb of the door opening. The door is composed essentially of plain concrete poured into a steel tub; dowels connected to the interior of the tub act as connectors. At the transition region the cross-section changes from rectangular (headworks) to circular (tube). Both circumferential and longitudinal reinforcement are especially heavy in the transition section, whose cross-sectional area is significantly less than that of the front face of the closure which receives the direct load.

The loads on the structure derive from airblast applied to the front face and to the berm which covers the tube. The direct airblast on the front is amplified by dynamic reflection effects such that a high frequency pressure peak of about seven times the overpressure is applied to the door. The result is that direct airblast on the front of the closure is the dominant load in this example.

3. MODELING AND TEST OF STRUCTURE

3.1 Finite Element Discretization

Both the structure and soil media are represented by 3D continuum finite elements. The finite element model, consisting of about 20,000 hexahedrons, is shown in Fig. 2. Symmetry is assumed about the center vertical plane of the tube so that only half (the hinge side) of the shelter and berm is included. Special attention is given to details in the closure and in the headworks and transition region (Fig. 3). The dynamic analysis is performed using TRANAL, an explicit 3D nonlinear dynamic program for soil-structure interaction analysis developed especially for large-scale 3D problems [10]. On a CDC 7600, approximately 20,000 elements can be used with a solution time of 2500 element-time step per CP second. The sub-cycling feature permits different integration time steps in structural and soil elements; the penalty usually imposed on explicit integration methods by stringent requirements on time step is thereby imposed only where it is actually required, rather than on all equations of the system. The total computation time for the

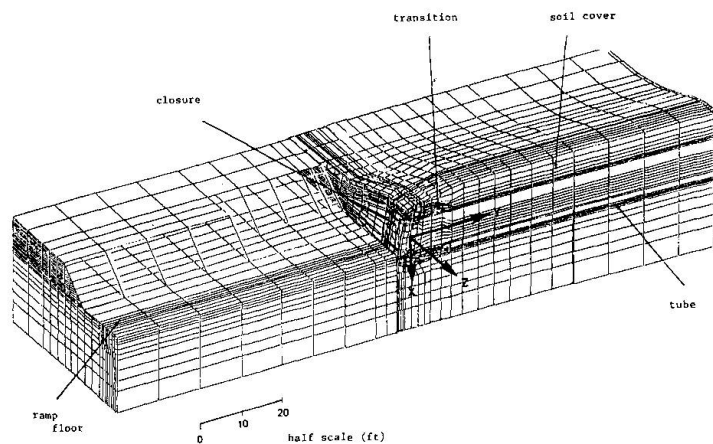


FIGURE 2. FE MODEL OF S4 TEST, COORDINATES SYSTEM.

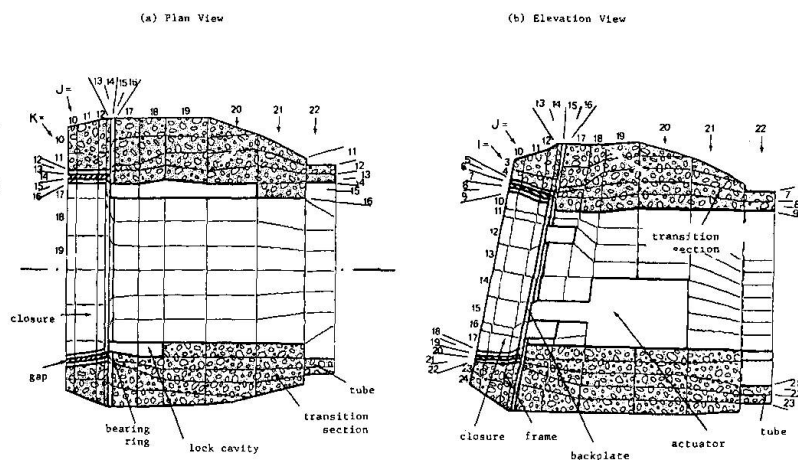


FIGURE 3. S4 HEADWORKS MODEL (IJK ARE FOR ELEMENT/NODE ACCOUNTING).



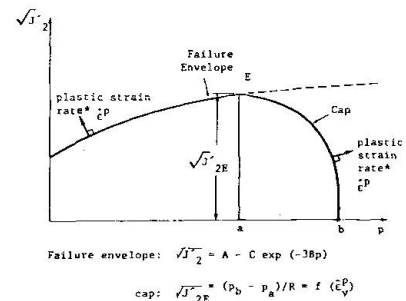
example is 50 CPU seconds for 0.1 msec of simulation time.

3.2 Soil Model

The in-situ soil and backfill are modeled as elastic-plastic materials defined by a modified Drucker-Prager yield function and a work-hardening cap (see Fig. 4 and also [7]) together with an associated, plastic potential flow rule. This formulation has been found to represent properties of a variety of soil and rock types [11, 12].

3.3 Structural Model

Both the plain concrete and structural steel are modeled as elastic, perfectly plastic materials, with associated flow rule (see failure envelope in Fig. 4). The concrete has a yield surface based on the dynamically enhanced compressive strength and the steel a von Mises' yield surface corresponding to A36 steel. The concrete strength is 10,000 psi for concrete in the closure and 6000 psi for concrete in other parts of the structure. The continuum elements which model the steel plates in the closure and bearing frame impose a stringent penalty on the local integration time step because of the dimension of the steel plate (5 in.) and because of the need to use a minimum of two elements across its thickness. The effect of the reinforcing steel in different parts of the structure, i.e. headworks, frame, tube, etc., is modeled by adjusting the amount of tension that the plain concrete model can accommodate. The basic yield surface is otherwise unchanged.



*The plastic strain rate $\dot{\epsilon}^p$ is governed by the associated flow rule whereby the plastic strain rate vector is normal to the yield surface when plotted to the appropriate scale parallel to the p-axis (plastic volumetric strain rate) and the $\frac{\sqrt{s}}{2}$ axis (plastic deviatoric strain rate)

FIGURE 4. TYPICAL YIELD SURFACE IN THE CAP MODEL FOR COMPRESSIVE STRESSES.

3.4 Test Description

The test program involved subjecting a half-size structure to blast loading using a high explosive simulation technique (HEST). Pressure generated within two HEST cavities and applied to the entire width of the front-face, wingwalls and soil berm covering the headworks is designed to match the prescribed loading.

The structure and its neighboring areas are heavily instrumented. There are approximately 400 channels of measurements, including concrete/rebar strain measurements, interface stress measurements, airblast pressures, accelerometers and velocity gages as well as pretest and post-test surveys. Some of the test data will be presented in Section 4 where they are compared with results obtained from the finite element analysis. The analysis was performed prior to the test event, based on predictions of airblast loading and estimates of soil properties.

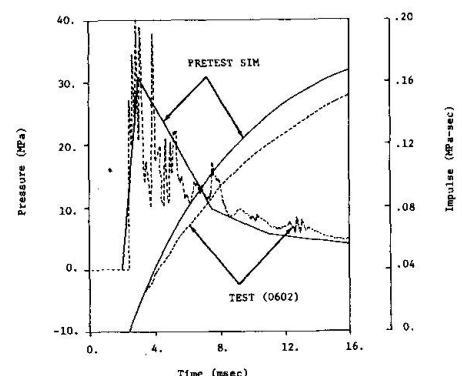


FIGURE 5. COMPARISON OF FRONT-FACE LOADING USED IN ANALYSIS AND ACHIEVED IN TEST.

4. STRUCTURAL RESPONSE AND PERFORMANCE OF MODEL

Due to inherent vibrations in the HEST cavity, the front load developed in the test differs from that assumed in the finite element analysis. An indication of this difference is given in Fig. 5,

which compares the measurement of a pressure gage on the upper right corner of the closure front face with its design value. While the peak HEST load is higher than the design value due to cavity vibrations, the impulse in the physical test is 10% low at 6 msec after detonation.

A comparison of the motion of the center of the closure backplate is given in Fig. 6. The initial peak is due to the front load and is higher for the test structure due to the higher peak load realized in the test. Consequently, the rebound is more severe in the test. There is also strong indication that the closure frequency for the test structure is less than that simulated, probably due to the support condition assumed in the analysis. Subsequent motion is dominated by the relatively rigid motion of the support or headworks given in Fig. 7. The spike at 11 msec coincides with the sudden failure of the transition section described later, and is absent in the analysis results. Despite these differences, however, both the test data (measurement and posttest observations) and analysis support the fact that the closure/headworks remains elastic, that the transient response of the closure is short-lived, and that the closure/headworks then moves as a rigid body.

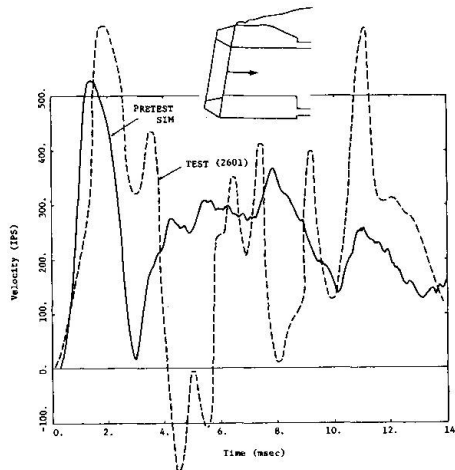


FIGURE 6. COMPARISON OF VELOCITY/TIME HISTORIES AT CENTER OF CLOSURE BACKPLATE.

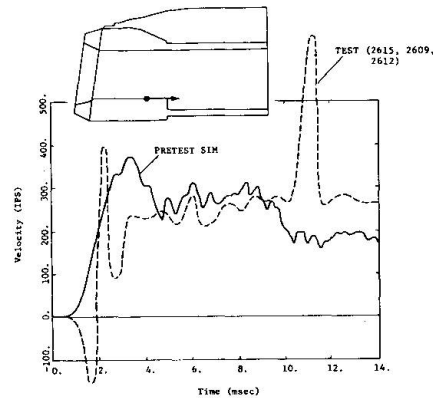


FIGURE 7. COMPARISON OF MOTION AT HEADWORKS FLOOR (LONGITUDINAL COMPONENT).

A comparison of the longitudinal tube concrete strain/time history immediately behind the headworks is given in Fig. 8. The correlation between analysis and test is in general quite good. Comparison of the circumferential strain at the same location as given in Fig. 9 is less favorable. Whereas dilatancy is dictated by the reinforced concrete model, test data seem to indicate the opposite.

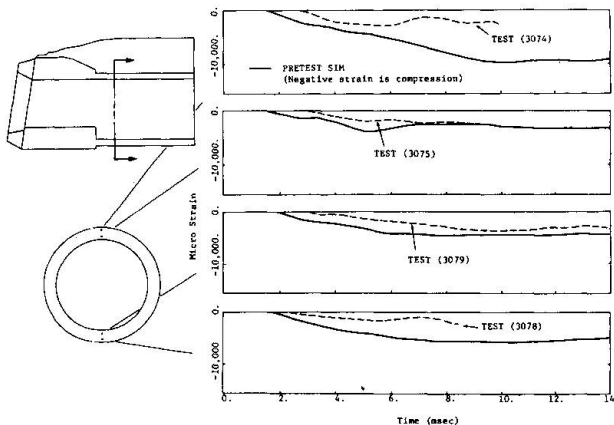
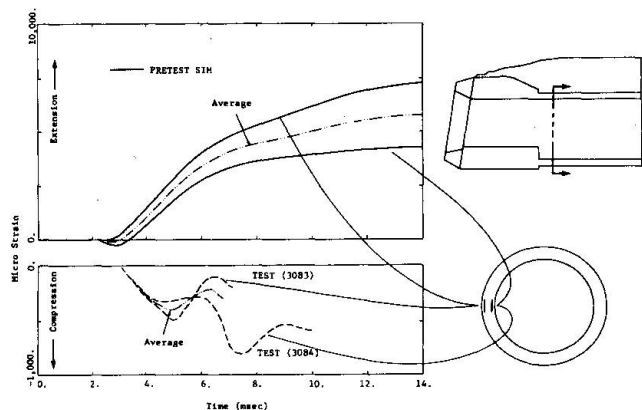


FIGURE 8. COMPARISON OF LONGITUDINAL STRAIN/TIME HISTORIES AT TUBE CROSS-SECTION BEHIND HEADWORKS.


FIGURE 9. COMPARISON OF CIRCUMFERENTIAL STRAIN/TIME HISTORIES AT TUBE CROSS-SECTION BEHIND HEADWORKS ($x = 2.995$ m).



Both test and analysis indicate crushing failure of concrete at that location, and posttest survey such as that reproduced graphically in Fig. 10 certainly confirms this finding. The present plasticity model does not simulate strain softening with resulting redistribution of load. Consequently, the longitudinal stress in the concrete is maintained at 9000 psi as shown in Fig. 11. This results in higher computed strains. Furthermore, this load is transmitted to the remainder of the tube section so that overall, a length of the tube from the transition to about one tube diameter behind is shown by the analysis to undergo significant plastic deformation. Physically, crushing failure of the concrete at the transition practically isolates the tube portion from the headworks, protecting the tube from further damage except for several major cracks along construction flaws (Fig. 10), and allowing the headworks to move impulsively as the spike in the velocity-time histories of Figs. 6 and 7 show.

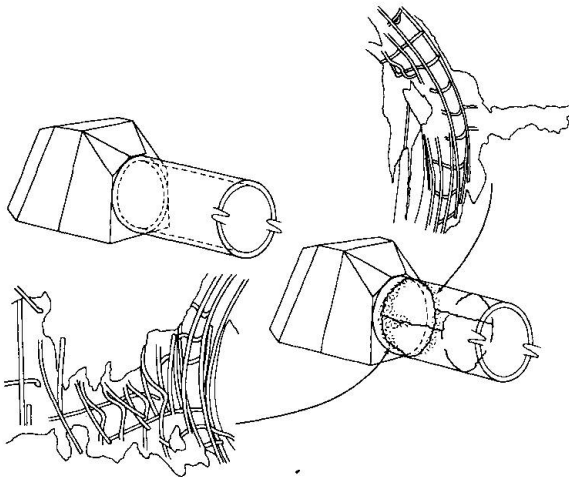


FIGURE 10. DAMAGE PATTERN OF TUBE, POSTTEST OBSERVATION.

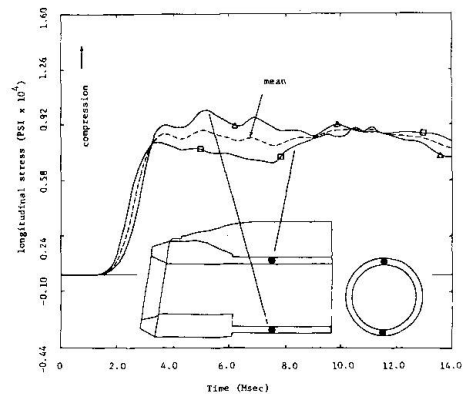


FIGURE 11. LONGITUDINAL STRESS/TIME HISTORIES FOR POINTS AT TUBE SECTION HALF-TUBE DIAMETER BEHIND HEADWORKS.

5. SUMMARY AND RECOMMENDATIONS

A major limitation in 3D dynamic finite element analysis of protective structures is reinforced concrete modeling. In this paper, we have outlined the requirements of such a model and approaches currently used. The performance of a simple composite continuum model is then studied, using a modified Prager-Drucker yield surface with the associated flow rule, and a tension region determined by the proportion of steel reinforcement. The advantages and consequences of using such a model are examined through a representative case study.

The simple plasticity model performs quite well when the inelastic deformation is minor. In the case study presented, good qualitative and quantitative agreements between test and analysis are obtained in portions of the structure which remain basically elastic. The performance of the analysis model is not as good in portions of the structure where extensive concrete failure occurs. Although the analysis results succeed in identifying areas of extreme distress in the structure, the concrete model is unable to reproduce some important features of failure and post-failure. Specifically, the absence of strain softening and load redistribution features in the model result in spreading out the zone of inelasticity. Since the major objective of protective structure design (and hence analysis) is not only its survivability and vulnerability in hostile environments, but also to strike a delicate balance between hardness and cost, it is essential that the reinforced concrete model used be able to discriminate conditions of near-failure from failure, and to reproduce the effect of different amounts of reinforcements and changes in reinforcement orientation.



Two directions of research in the area of reinforced concrete modeling for protective structure applications appear most promising. One approach is to refine the continuum representation of plain concrete in the tensile cracking, compressive failure and post-failure regions, which is then used in conjunction with an explicit representation of the reinforcement. In this approach, the dual-element strain-compatible finite element concept appears promising 4. The disadvantages of this approach are the additional input data required, numerical stability, and possible difficulty in the interpretation of results so obtained.

Alternately, structural elements can be used to model the structure. This is a natural representation of inelastic flexural properties of the structure and has an added advantage in that the model properties are easy to define experimentally. This approach requires careful implementation in order to maintain the efficiency required for large dynamic analyses 1.

ACKNOWLEDGMENT

The analysis described in this paper was performed by Weidlinger Associates under Contract No. DNA 001-77-C-0104 with the Defense Nuclear Agency of the United States Government. Computer programming support provided by John Baylor and Joseph Wright of Weidlinger Associates, New York, is gratefully acknowledged. We are thankful to Myrtle Carey for typing and revising the final manuscript and Penny Severson for preparing the illustrations.

REFERENCES

1. BAYLOR, J.L., and J.P. Wright: "Three Dimensional Transient Nonlinear Analysis," ASME Winter Meeting, Houston, Texas, December 1975.
2. LEVINE, H.S. et al: "Three Dimensional Soil Island Calculation of an Embedded Reinforced Concrete Structure Subjected to a Simulated Nuclear Explosion," 48th Shock and Vibration Symposium, Alabama, October 1977.
3. SANDLER, I.S., F.L. DiMaggio and G.Y. Baladi: "Generalized Cap Model for Geological Materials," Journal Geotechnical Engineering Division, ASCE, 102, No. GT7, July 1976.
4. CERVENKA, V., and K.H. Gerstle: "Inelastic Analysis of Reinforced Concrete Panels: Theory," 31-II, the Publications of the International Association for Bridge and Structural Engineering, 1971.
5. CHEN, A.C.T., and W.F. Chen: "Constitutive Relations for Concrete," Journal of the Engineering Mechanics Division, ASCE, August 1975.
6. ISENBERG, J., and S. Adham: "Analysis of Orthotropic Reinforced Concrete Structures," Journal of the Structural Division, Proceedings ASCE, 96, No. ST12, December 1970.
7. NELSON, I., M.L. Baron and I.S. Sandler: "Mathematical Models for Geological Materials for Wave Propagation Studies," Shock Waves and the Mechanical Properties of Solids, Syracuse University Press, Syracuse, New York, 1971, pp. 290-351.
8. BUYUKOZTURK, O.: "Nonlinear Analysis of Reinforced Concrete Structures," Computers and Structures, 7, 1977.
9. MCR paper on plasticity in plates.
10. BAYLOR, J.L., M.P. Bieniek, J.P. Wright: "TRANAL: A 3-D Finite Element Code for Transient Nonlinear Analysis," DNA 3501F, Weidlinger Associates, New York, NY, 1974.
11. DI MAGGIO, F.L., and I.S. Sandler: "Material Models for Soils," Journal of Engineering Mechanics, Proceedings, ASCE, June 1971, pp. 935-950.
12. SANDLER, I.S., and M.L. Baron: "Models of Geological Materials in Ground Shock," Num. Methods in Geomechanics, Proc. ASCE, New York, 1976, pp. 219-231.

Leere Seite
Blank page
Page vide



IV

Limit Analysis of Reinforced Concrete Shells of Revolution

Charge ultime de surfaces de révolution en béton armé

Traglast von rotationssymmetrischen Stahlbetonschalen

E. RAUE

Dozent Dr. sc. techn.

Hochschule für Architektur und Bauwesen

Weimar, German Democratic Republic

SUMMARY

The paper deals with a static and kinematic formulation of the collapse load problem of reinforced concrete shells of revolution. A numerical method of finding the collapse load intensity, the collapse mode and the stress resultants within the plastified zones is represented.

RESUME

L'article traite de la formulation statique et cinématique de la charge ultime de surfaces de révolution en béton armé. L'article présente une méthode numérique permettant de déterminer la charge ultime, le mode de rupture et les contraintes résultantes dans les zones plastiques.

ZUSAMMENFASSUNG

Eine statische und kinematische Formulierung des Traglastproblems von rotations-symmetrischen Stahlbetonschalen wird gegeben. Eine numerische Methode zur Bestimmung der Kollapslast, des Bruchmechanismus und der Spannungsergebnisse innerhalb der plastifizierten Bereiche wird angegeben.



1. INTRODUCTION

Tensile failure of concrete is the primary ingredient of the non-linear behaviour of concrete structures. Crack-initiation and slow crack-propagation up to failure form a very complex mechanism which is still not fully understood. Thus predictive statements must be treated with considerable caution in view of the limitations of the underlying fracture model, the high sensitivity of the constitutive parameters and the numerical distortion of the cracking process.

In two previous publications by the authors [1, 2], the smeared finite element approach to cracking was explored in detail. In particular the high sensitivity of the ultimate load of a thick-wall tube was noted with regard to small variations of the tensile strength as well as the finite element mesh. In view of the limited experimental evidence a careful study was proposed for crack-initiation and crack-propagation in plain concrete in the presence of large stress gradients. The primary objective was to assess the redistribution capacity of such a tensile specimen during the cracking process. In particular, the question of slow crack growth versus instable fracturing was of main concern. From the standpoint of numerical prediction, the study revolved around the fundamental postulates of smeared and discrete crack analysis methods.

As an example for the analysis of cracking we consider a thick-walled concrete ring subjected to internal pressure. This problem was selected to study the strength and deformation behaviour of a structural component with a non-uniform tensile stress field. The experimental study was carried out at the IBIW III of the Technical University Munich, the results of which were reported recently in reference [3] . Parallel, numerical investigations were carried out at the ISD of University of Stuttgart, of which some results are reported below [2] .

2. SMEARED CRACK APPROACH

It is this approach which is normally adopted for the ultimate load analysis of structures. In compression, this method is fully acceptable for modelling degrading material behaviour e.g. because of progressing micro-cracking in the form of nonlinear elastic, elastoplastic and endochronic constitutive models. In tension, the limited strength is of primary importance, rather than the nonlinear deformation behaviour. In particular the discontinuous reduction of strength to "no tension" behaviour is of interest in the case of brittle fracture. The ensuing stress redistribution is normally accomplished by initial load iteration which imposes this constitutive restraint by iterative correction of the linear elastic response. The smeared approach distributes the effect of localized cracking over a contributory area, for example a finite element, in which the strength degrades continuously according to the concepts of a continuum. Thus, the finite element method with its weak equilibrium statements is particularly suited for the smearing or better the averaging of constitutive statements in finite neighbourhoods.

At this stage there is no need for a detailed account of the finite element initial load strategy, the basic concepts are well established and are summarized for the analysis of concrete fracture for example in ref. [1] . In our example the pressurized ring is subjected to biaxial tension-compression, whereby the circumferential tension is responsible for radial cracking leading ultimately to fracture. Thus, the material behaviour is virtually linear elastic up to the tension cut-off, from which on ideally brittle and ideally plastic models bound the actual softening behaviour of the heterogeneous concrete material.

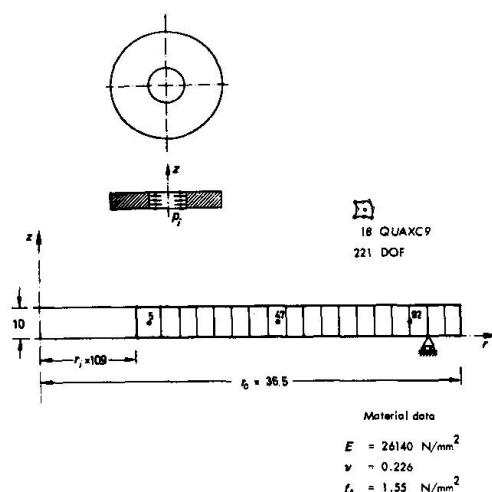


FIG. 1 Configuration and axisymmetric idealisation

Fig. 1 shows the axisymmetric idealisation of the concrete ring with 18 QUAXC9 elements and the underlying material data. Assuming that there is no axial effect due to friction at the supports or due to non-uniform shrinkage, we can restrict our analysis to a single element layer, in which cracking takes place in the radial direction only. Clearly, the axisymmetric idealization implies that the radial cracks are distributed uniformly over the circumference and that the non tension zones reduce the thickness of the ring accordingly. The material parameters are those of the original test data before they were adjusted for the age of the actual experiment, whereby the splitting tensile strength is used directly as strength parameter $f_t = \beta_{sz} = 1.55 \text{ N/mm}^2$ without further manipulation.

In the smeared crack analysis of brittle and ductile failure behaviour the excess tensile tangential stress is redistributed whence the tensile strength f_t is reached. In this way the actual softening behaviour is bounded by the two limiting cases of discontinuous strength reduction for no-tension behaviour and non strength reduction for ideally plastic behaviour. Clearly, plain concrete exhibits primarily brittle behaviour in tension, however, the localization of discrete cracks is always accompanied by extensive microcracking over a finite neighbourhood (analogous to the tributary area of the smeared approach), such that a continuous softening model would be most realistic. However, we should be aware that this softening branch is actually not a material property, it rather depends on the boundary conditions, the stress gradients or rather the redistribution capacity of the structure and last not least on the inhomogeneous composition of concrete. In this spirit, the softening model is a computational tool rather than a constitutive property for describing the reserve strength of the structure beyond that of an isolated material point.

The results of the smeared crack analysis are compared in Fig. 2 with the experimental results at sector 8, when the primary crack leads ultimately to rupture. For the proper assessment of the axisymmetric prediction the tangential strain data of the eight sectors is also averaged along the inner and outer surface of the ring and along the midsurface. For completion, Fig. 3 shows the overall load-deformation behaviour at the three surfaces, in which the circumferential variations of Fig. 2 are averaged. All figures illustrate clearly the low strength prediction of the brittle postulate and the high strength value of the ductile model. Similar, the rupture strain more than doubles when we go from the brittle model to the ductile one. The local behaviour in Fig. 2 illustrates the apparent ductility at the



sector 8 with the primary crack, where the deformation increases continuously up to

$\epsilon_r = 0.54\%$ at rupture (this includes the crack opening). On the other hand the average values of the eight sectors show strain levels which are of the order of those normally put forward by concrete technologists for the maximum level of tensile strain

$$\epsilon_{ave} = 0.15\%$$

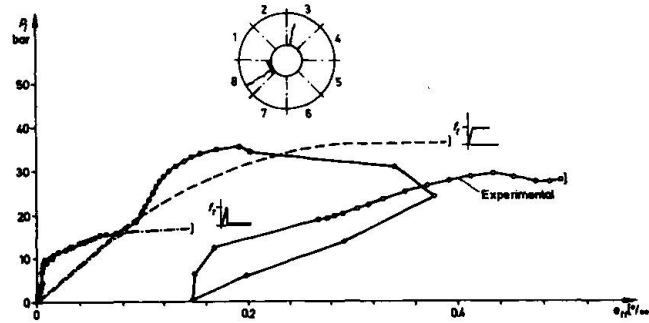


FIG. 2 Comparison of numerical and experimental results at the inside of sector 8

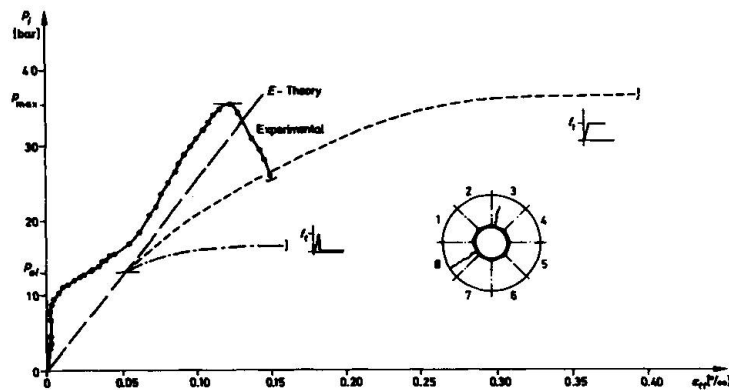


FIG. 3 Average response behaviour at inside

The tensile strength value of $f_t = 1.55 \text{ N/mm}^2$ restricts the elastic regime to pressure levels below $p_{max}^{el} = 13.0 \text{ bar}$. Table 1 summarizes these numerical and experimental results together with the average strain levels at the inner surface. We observe that the brittle failure model increases the maximum pressure only slightly from the elastic limit $p_{max}^{el} = 13.0 \text{ bar}$ to $p_{max}^{br} = 16.62 \text{ bar}$, while the ductile failure model mobilizes considerable strength reserves in the structure, $p_{max}^{du} = 36.50 \text{ bar}$. Note that these numerical strength values were obtained by an incremental iteration algorithm (initial load method with constant stiffness), where the ultimate load capacity was determined by successive refinement of the load steps. The actual failure load was localized by reducing the load step down to $\Delta p_{min} = 0.2 \text{ bar}$ near collapse and iterative corrections in order to assure that the cracking process reached the outside ring surface at ultimate pressure.


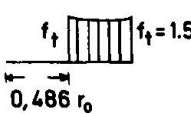

APPROACH	p_{\max} [bar]	ϵ_{tt} $r = r_i$ [‰]	$\sigma_{tt} = \sigma_{tt}(r)$ [N/mm ²]
Experiment	35,48	0,15	-
Elastic	13,00	0,06	
Brittle	16,62	0,16	
Ductile	36,50	0,40	

TABLE 1 Results of axisymmetric crack approach

The average response behaviour in Fig. 3 indicates clearly that there is some mechanism which delays the actual response as compared to the elastic prediction. If we neglect this initial stiffening regime, which is most likely caused by friction effects at the supports, then the subsequent response regime is nearly linear elastic. The gradual softening due to internal microcracking is most pronounced at the inner surface loading to a gradual deviation from the initial linear elastic behaviour before failure. Note that a tensile bending strength of $f_t = 4.05 \text{ N/mm}^2$ the most simple elastic failure postulate would lead to a very accurate strength prediction of the ring $p_{\max}^{el} = 33.86 \text{ bar}$. However, it is doubtful if the high tensile bending strength can be mobilised and applied to the ring where the circumferential stresses are entirely in tension (without crack arresters due to a compression zone).

Since the brittle and ductile failure models account for gradient effects by the stress redistribution capacity of the structure, they should resort to the centric strength values. Therefore, some gradual softening must be taking place in order to increase the ultimate load capacity of the brittle failure model (the ultimate strength of the brittle model is increased by approximately 20%). On the deformation side the ductility or rather the tangential rupture strain reaches twice the value at the elastic limit, see Table 1.

Altogether, the experimental data would compare quite well with a continuous softening model whose prediction of strength and ductility falls somewhere between the results the ideally brittle and ductile failure approach. The brittle postulate is certainly too low even if we would increase the strength of the value of the tensile bending test $f_t = 1.97 \text{ N/mm}^2$ since radial cracking does not lead to a uniform reduction of the load carrying area. In contrast, the ideally plastic model infers unlimited ductility, a material property which cannot be mobilized in plain concrete, not even in compression.



3. DISCRETE CRACK APPROACH

The experimental evidence clearly indicates that the initial micro-cracking leads ultimately to the localization of a single discrete crack at failure. Therefore, the question arises if a discrete crack analysis provides additional insight into the actual fracture mechanism. To this end, we examine first the concepts of linear fracture mechanics where we essentially start from an existing crack configuration and study its stability. Thereafter, we explore the possibility of predicting slow (stable) crack growth in the tensile ring specimen.

For the discrete crack analysis we consider a quarter of the ring configuration which implies symmetry along the x - and y -direction. With other words, we assume that the primary crack along the positive direction of the x -axis is accompanied by a secondary crack in the negative direction. Recall that the formation of two opposite cracks was actually observed in the experiment near the ultimate pressure.

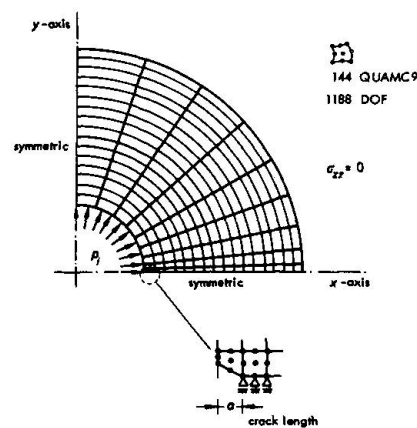


FIG. 4 Plane stress idealisation of discrete crack

Fig. 4 illustrates the finite element mesh with 144 QUAMC9 membrane elements. A discrete crack is introduced simply by releasing the kinematic nodal constraints at the x -axis of symmetry (for example in slow crack propagation the suppressed degrees of freedom are released node by node according to the crack criterion).

Traditionally, the principal question of fracture mechanics circles around the stability of a given crack configuration. In essence we start already from a predetermined discrete crack and study stability (stationary crack versus unbounded crack growth) by comparing for example the stress intensity K_I at the crack tip with the critical value K_{IC} from material testing. The basic postulate rests on the assumption that crack propagation is controlled exclusively by the local stress intensity at the crack tip. Thus, the linear theory of fracture mechanics is a priori not concerned with the initiation of cracks in intact specimens without flaws and even less with the slow extension of a given crack. The crucial stability problem is solved by testing of so-called fracture mechanics specimen which yield the critical value of stress intensity or equivalent quantities such as the crack opening displacement or the crack extension force.

In what follows, we apply these concepts which were originally established for the brittle fracture of metals. To this end a discrete crack is introduced along the x-axis of symmetry by releasing the nodal degrees of freedom in this zone. The stress intensity factor is computed for different crack lengths via the compliance method where K is a measure of the energy release rate as the crack length a is increased by Δa . Clearly, there are several other methods for the finite element analysis of K_I , such as the direct calculation from the resulting stress or displacement field, via contour integrals or singularity elements and nonlinear mappings. However, in conjunction with the finite element displacement method the energy approach is the most appropriate global technique.

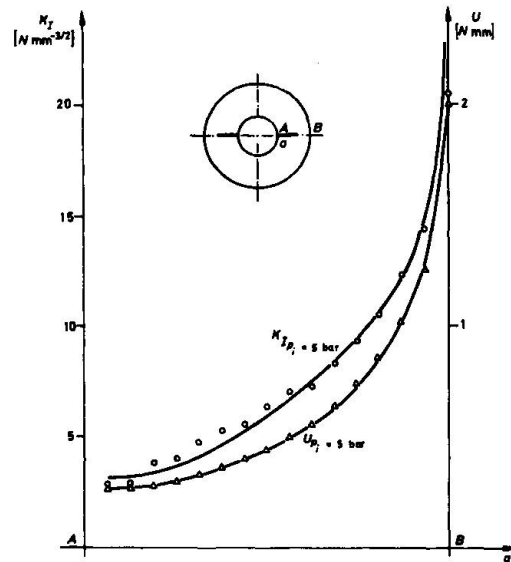


FIG. 5 Stress intensity K_I and strain energy versus crack length a

Fig. 5 illustrates the variation of the stress intensity value K_I in dependence of the crack length a together with the elastic strain energy U for an internal pressure $p = 5$ bar. Note that both results yield a continuous increase of stress intensity and strain energy with increasing crack length.

Traditionally the discrete crack analysis was the first approach which was adopted for tracing slow crack growth. Originally, this method was implemented by releasing the nodal compatibility whence the principal tensile stress was reached. At this stage the stress concentration or rather the stress singularity at the crack root was removed by a coarse finite element mesh (numerical damping) such that a simple strength criterion could be applied to propagate cracking. In subsequent proposals less sensitive variables such as the crack-opening displacement or the strain energy itself were utilized as criterion for crack extension. In this context we recall that the critical value of stress intensity or energy release rate predicts only catastrophic fracture and not slow crack extension. Thus, the appropriate criterion for crack initiation and slow crack propagation would have to be determined from a set of additional test data (calibration experiments) with a rather restrictive regime of application.

Independently of the choice of crack criterion it is intriguing that the discrete crack analysis is never able to predict slow crack growth in the tensile ring specimen. Fig. 5 clearly



shows that the energy (and correspondingly all local crack criteria) increases with the crack length; thus the crack extension cannot be arrested without introducing additional dissipation mechanisms, such as damping of the numerical solution, due to the spatial discretisation or continuous softening and gradual damage accumulation, respectively. It is surprising that in the case of a tensile stress field the discrete crack approach differs fundamentally from the smeared approach. While the former model predicts catastrophic failure immediately upon local crack initiation without further redistribution, the latter method accommodates slow crack extension with an associated stress redistribution. Thus spatial smearing of cracks implies in reality numerical damping because of the spatial distribution of cracks over a tributary area. In this way it corresponds to an intuitive concept of damage accumulation over a finite region, especially in conjunction with a gradual softening postulate, which is equivalent to a continuous degradation of strength until the tributary area is fully damaged.

3. CONCLUDING REMARKS

Clearly, the physical performance of the pressurized ring exhibits three response regimes, (i) the linear elastic region without damage, (ii) the hardening region with continuous damage accumulation due to progressive micro-cracking, and (iii) the localization of discrete cracks near the ultimate load accompanied by excessive damage accumulation up to rupture (continuous increase of strains at the expense of degrading strength).

None of the two numerical models is able to describe the entire process of cracking. Obviously, the smeared crack approach is most appropriate for the second response regime, which is however small in the present example, while the discrete crack method is better suited after localisation of a discrete crack takes place, although no stable crack growth can be predicted at this stage.

In our view point "smearing" and "continuous softening" are two computer-oriented strategies which introduce dissipation for stabilizing unbounded crack growth in tensile specimens. Clearly, other phenomena play a very important role for tensile fracture, here we only mention the stochastic nature of the cracking process which starts with a random distribution of strength and initial imperfections (flaws) and which continues with the probability of damage and damage accumulation with redistribution. In ref. [4] these stochastic concepts have been used successfully for interpreting size and gradient effects in tensile test specimens. However, at this stage the probabilistic fracture analysis of real concrete components is still unrealistic because of the large number of nonlinear analyses necessary for calculating the statistical distribution of strength.

REFERENCES

- [1.] J.H. ARGYRIS, G. FAUST, K.J. WILLAM, Limit Load Analysis of Thick-Walled Concrete Structures, A Finite Element Approach to Fracture, Comp. Meth. Appl. Mech. Eng. 8 (1976) 215-243.
- [2.] J.H. ARGYRIS, G. FAUST, K.J. WILLAM, Finite Element Analysis of Concrete Cracking, ISD-Report No. 254, University of Stuttgart (1979).
- [3.] J. NEUNER, S. STÖCKL, E. GRASSER, Versuche an dickwandigen unbewehrten Betonringen mit Innendruckbeanspruchung, Proceed. DAFStb, Vol. 299, Wilhelm Ernst und Sohn Berlin, 1978.
- [4.] G. IVANYI, Zugfestigkeit von Beton in örtlich veränderlichen Beanspruchungszuständen - Gradientenwirkung - Bericht IBStb, Technische Universität Braunschweig (1976).

IV

Nonlinear Behaviour of Reinforced Concrete Beams

Comportement non linéaire de poutres en béton armé

Nichtlineares Verhalten von Stahlbetonbalken

A.J. LAESSKER

dipl. Ing. ETH, PhD

Techdata AG

Basel, Switzerland

SUMMARY

The computer-oriented method for the analysis of reinforced concrete beams in the nonlinear range is based upon the finite-element approach. The method is suitable for the investigation of the structural behaviour taking nonlinear material properties into consideration, and allows the simulation of crack formation and crack propagation. The structures are analyzed as two-dimensional problems.

RESUME

La méthode, basée sur les éléments finis et sur le traitement électronique des données, est utilisée pour l'analyse des poutres en béton armé dans le domaine non linéaire. Elle permet l'étude du comportement des poutres, tenant compte des caractéristiques non-linéaires des matériaux, ainsi que la simulation de la formation et de la propagation de fissures dans le béton. La méthode de résolution se limite à l'étude des problèmes plans.

ZUSAMMENFASSUNG

Die hier beschriebene EDV-orientierte Methode zur Analyse von Stahlbetonbalken im nicht linearen Bereich beruht auf dem Finite-Element-Ansatz. Sie gestattet die Untersuchung des Trägerverhaltens unter Berücksichtigung nichtlinearer Materialeigenschaften sowie die Simulation der Bildung und Fortpflanzung von Rissen im Beton. Die Lösungsmethode beschränkt sich auf ebene Probleme.



1. INTRODUCTION

In this paper a method based on the finite element approach to simulate the behaviour of reinforced concrete beams is presented. The solution method is a combined iterative and step-by-step procedure based upon the matrix displacement method. The beam-structures are analyzed as plane stress problems. For each load increment, repeated elastic solutions are performed until the displacements meet a specific tolerance.

The mathematical model consists of an assemblage of triangular concrete plate elements, steel bar elements and bond links. The displacement fields are assumed to be linear for all three parts. The elastic constants which are needed in the derivation of the element stiffness matrices are extrapolated from the pertinent uniaxial stress-strain curves. For all elements, these functions are approximated by piecewise linear polygons. The appropriate values of the material constants are found by entering the stress-strain diagram at the correspondent values of principal strains. The random change in structural configuration due to cracking in the concrete is treated by cutting the concrete triangular element in the direction perpendicular to the principal tensile stress. Bond between concrete and steel reinforcements is simulated by discrete spring-like bond links. The influence of time-dependent effects such as creep or relaxation is neglected.

The method has proven to be an effective tool for the study of crack propagation.

2. FINITE ELEMENT PROPERTIES

The finite element idealization relevant to this investigation is displayed in Figure 1.

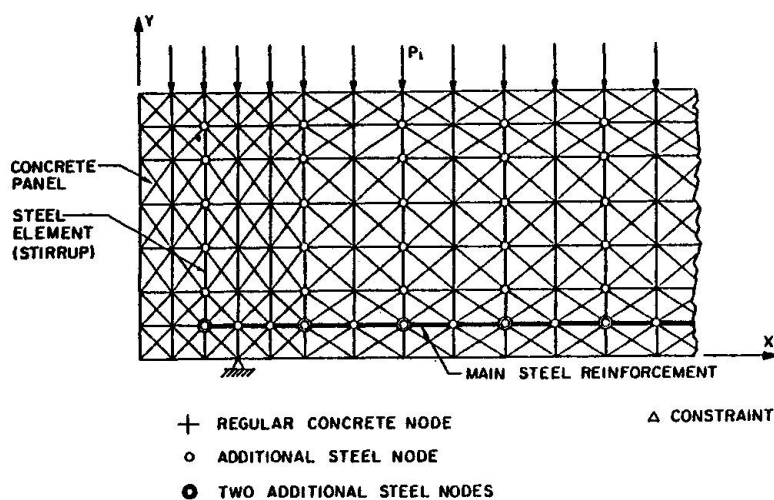


Figure 1. Finite element assemblage of a singly reinforced beam

Three kinematically and geometrically dissimilar elements as shown in Figure 2 have been chosen as basic components of the model.

For the concrete elements the constant-strain triangular panel has been adopted. This mainly because yielding takes place throughout the whole element. Thus, no problems arise in determining the state of stress. The displacement functions are:

$$u_x = c_1 x + c_2 y + c_3 \quad 1)$$

$$u_y = c_4 x + c_5 y + c_6 \quad 2)$$

The reinforcement occupies a relatively small volume compared to that of the concrete. It is therefore justifiable to idealize the steel tendons by simple two-force members.

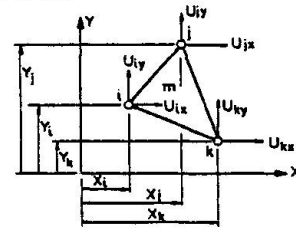
To account for bond slip, the steel must be attached to the concrete by a special connection mechanism. The bond link used here is designed to allow for relative displacements between the steel bars and the concrete panels. The links are dimensionless. Nevertheless, additional nodes must be provided to permit relative displacements between adjacent concrete and steel nodes.

For steel and bond elements the displacement function used is:

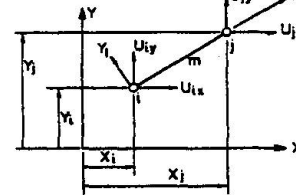
$$u_1 = c_7 x + c_8 \quad 3)$$

In the assemblage of Figure 3 the nodes of the steel bars and the connecting springs originally occupy the same geometrical position as their corresponding concrete joints.

a) CONCRETE PANEL



b) STEEL BAR



c) BOND LINK

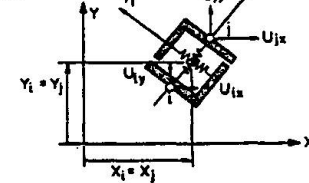


Figure 2.

Components of finite element model

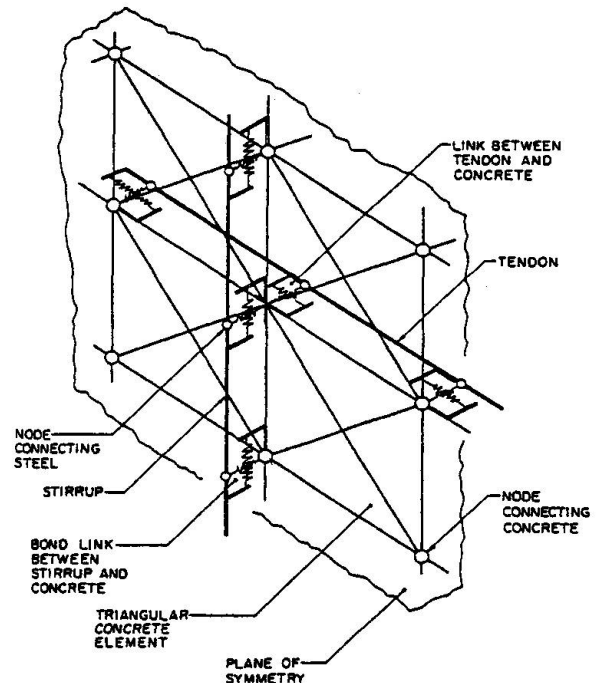


Figure 3.

Configuration of bond links



3. CONSTITUTIVE EQUATIONS

As constitutive equations for the concrete panels the following expressions in terms of principal values were used:

$$\begin{bmatrix} \sigma_1 \\ \sigma_2 \\ \sigma_3 \end{bmatrix} = \frac{E_1}{1 - \nu_{12}\nu_{21}} \begin{bmatrix} 1 & \nu_{21} & 0 \\ \nu_{12} & n & 0 \\ 0 & 0 & 0 \end{bmatrix} \begin{bmatrix} \epsilon_1 \\ \epsilon_2 \\ \epsilon_3 \end{bmatrix}$$

For steel and bond elements the constitutive equations are of the following form:

$$\begin{bmatrix} \sigma_{x1} \\ \sigma_{x2} \end{bmatrix} = \begin{bmatrix} k_1 & 0 \\ 0 & k_2 \end{bmatrix} \begin{bmatrix} \epsilon_{x1} \\ \epsilon_{x2} \end{bmatrix}$$

Where ϵ_{x1} and ϵ_{x2} are the relative displacements between the steel and the corresponding concrete node.

The influence of a crack on a continuous triangular concrete element is treated by introducing a cut in the direction perpendicular to the calculated principal tensile stress σ_1 .

In this new state the element no longer has any stiffness normal to the crack surface (Figure 4). Consequently, the concrete may be considered as a uniaxial stress condition parallel to the second principal axis. This assumption results in the following stress-strain relationship:

$$\begin{bmatrix} \sigma_1 \\ \sigma_2 \\ 0 \end{bmatrix} = \begin{bmatrix} 0 & 0 & 0 \\ 0 & E_2 & 0 \\ 0 & 0 & 0 \end{bmatrix} \begin{bmatrix} \epsilon_1 \\ \epsilon_2 \\ \epsilon_3 \end{bmatrix}$$

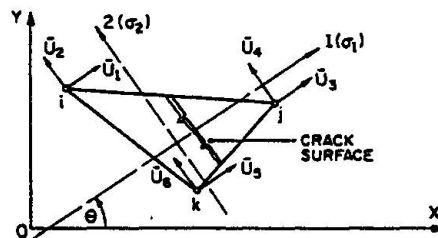


Figure 4. Cracked Element

4. STIFFNESS MATRICES

The stiffness matrices of the three types of elements may be derived by the standard equations

$$[K] = \iiint [b]^t [D] [b] dv$$

where $[b]$ is the strain-displacement transformation matrix and $[D]$ the matrix of elastic constants.

For the bond link the stiffness matrix is similar to the well-known matrix for a two-force member. The matrix for the cracked concrete element reduces to

$$[k_n] = \begin{bmatrix} 0 & & & & & \\ 0 & 0 & & & & \\ 0 & x_{32}^2 & 0 & & & \\ 0 & -x_{32}x_{31} & 0 & 0 & & \\ 0 & 0 & 0 & 0 & 0 & \\ 0 & x_{21}x_{32} & 0 & -x_{21}x_{31} & 0 & x_{21}^2 \end{bmatrix}$$

sym

5. ITERATIVE PROCEDURE

The method presented here is based upon an iterative, incremental load approach. For each load increment, the whole structure is repeatedly solved as an elastic problem until closure. Consider an arbitrary concrete element during load increment i . Assume that at the end of the previous step the principal strains $\{\epsilon_{p,i-1}\}$ and stresses $\{\sigma_{p,i-1}\}$ have been established. Based upon these values the element may be in any one of the following conditions:

- a. Type 1: Elastic, isotropic
- b. Type 2: Elastic, anisotropic
- c. Type 3: Inelastic, anisotropic
- d. Type 4: Cracked

The four cases may be visualized diagrammatically in Figures 6 and 7.

In the present computer program, principal strains $\{\epsilon_{i-1}\}$ are used to determine the relevant material constants. After the proper modulus of elasticity E_i , and Poisson's ratio, ν_i , have been found for each element, the $[D]$ matrices are generated.

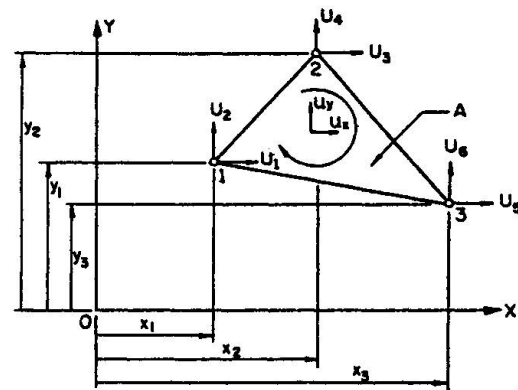
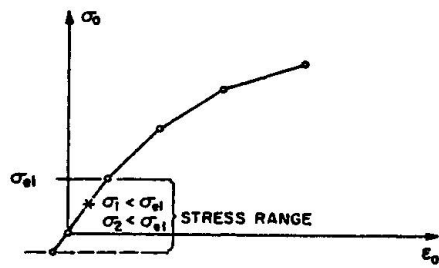
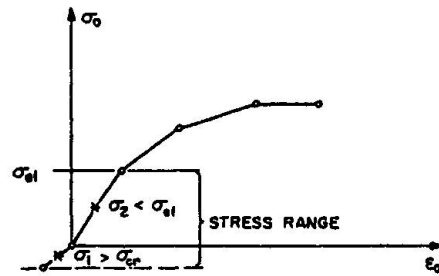


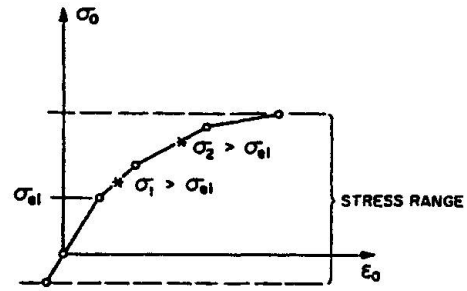
Figure 5.
Arbitrary triangular concrete element



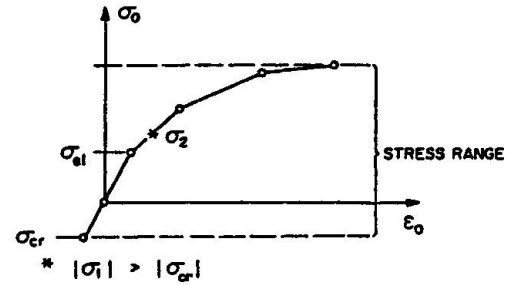
(a) TYPE 1



(b) TYPE 2



(a) TYPE 3



(b) TYPE 4

Figure 6.
Classification of concrete elements
in the elastic range

Figure 7.
Classification of concrete elements
in the inelastic range

The elemental stiffness matrices $[k_i]$ follow immediately

$$[k_i] = [b]^t [D] [b]$$

or, for cases 2, 3 and 4

$$[k_i] = [R]^t [b]^t [D_i] [b] [R]$$

Next, the total stiffness matrix is assembled and solved for the incremental displacements. The incremental strains are now evaluated as

$$\{\Delta e_i\} = [b_i] \{\Delta U_i\}$$

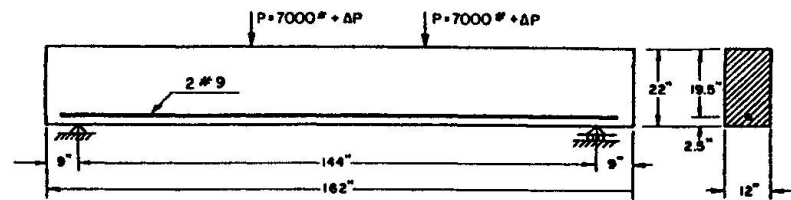
and added to the total strains e_{i-1} of the preceding step to give the new total strains

$$\{e_i^1\} = \{e_{i-1}\} + \{\Delta e_i\}$$

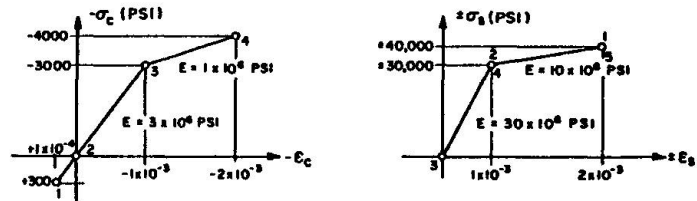
These values constitute a new strain situation with a corresponding new set of principal strains $\{\epsilon_{p,i}\}$. The material properties of the following iteration cycle are again extrapolated from the stress-strain curve. The iteration is stopped after a specified tolerance is reached. Before proceeding to the next increment, all total stress and strain values are updated and stored. Similar treatment is imposed upon the reinforcements and bond links. However, the procedure here is much less involved since the matrix $[D]$ reduces to a single term E_1 .



Example Problem 1:

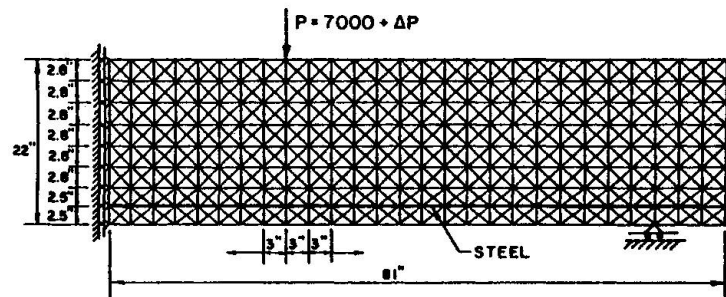


(a) SCORDELIS' BEAM A-1



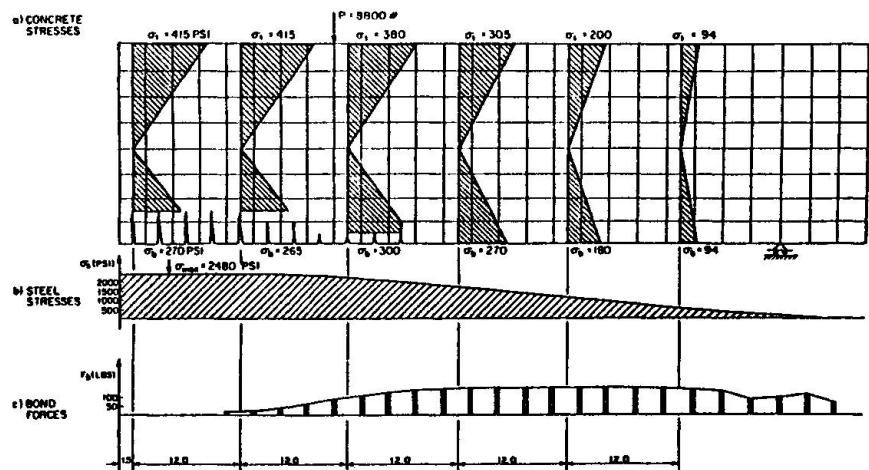
(b) MATERIAL PROPERTIES

Example Problem 1: Scordelis' Beam A-1



NUMBER OF TRIANG. ELEMENTS	NTEL = 864
NUMBER OF NODES (INCL. STEEL)	NUMNOD = 495
NUMBER OF LOADS	NLOAD = 1
NUMBER OF BOUND. COND.	NBOUND = 10

Mathematical Model of Beam A-1

Example Problem 1: Stresses at $P = 8800 \text{ Lbs.}$



Example Problem 2:

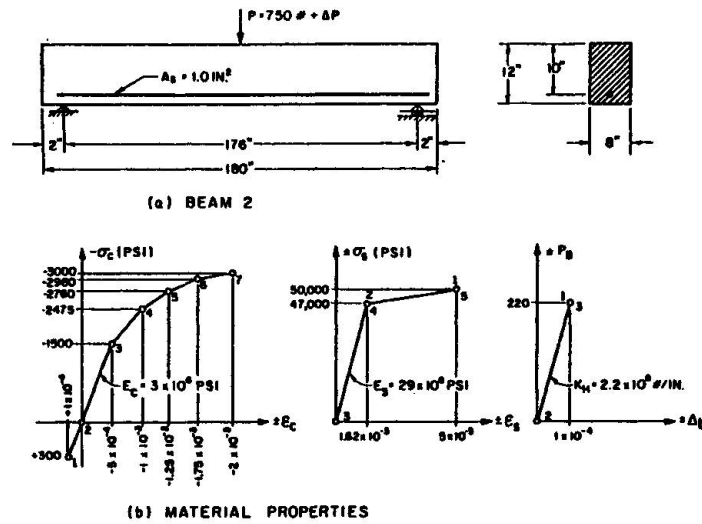
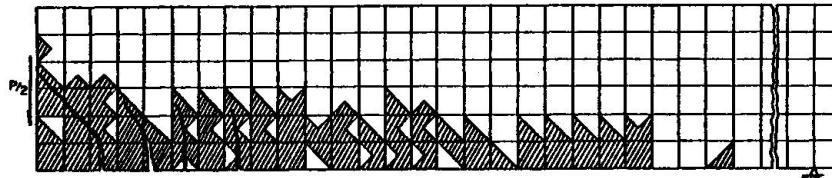
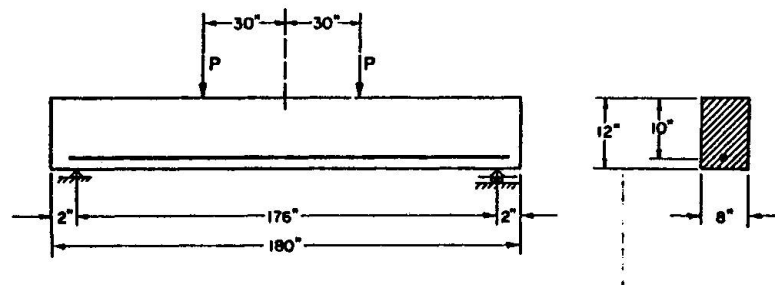


Figure 27. Example Problem 2: Simple Beam Loaded at Midspan

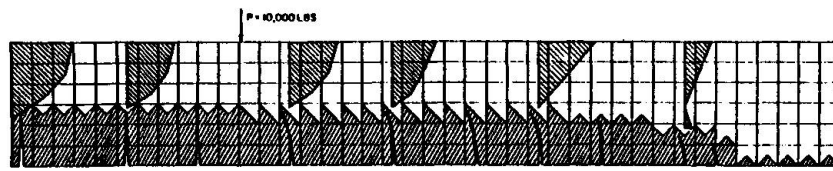
Figure 29. Example Problem 2: Crack Pattern at $P = 4000$ Lbs.

Example Problem 3:



FOR MATERIAL PROPERTIES, SEE FIGURE 27.

Figure 30. Example Problem 3: Simple Beam Loaded Symmetrically by Two Concentrated Loads

Figure 31. Example Problem 3: Crack Pattern and Stress Distribution at $P = 10,000$ Lbs.

IV

Nonlinear Dynamic Analysis of Reinforced Concrete Slabs

Analyse dynamique non linéaire des plaques en béton armé

Nichtlineare dynamische Analyse von Stahlbetonplatten

H.S. SINISALO

Research Assistant
Helsinki University of Technology
Espoo, Finland

M.T.E. TUOMALA

Research Assistant
Helsinki University of Technology
Espoo, Finland

M.J. MIKKOLA

Research Professor
Helsinki University of Technology
Espoo, Finland

SUMMARY

The paper is concerned with the analysis of reinforced concrete slabs subjected to transient impulsive loading. Tensile cracking, the plastic behaviour of concrete in multiaxial state of stress and the plastic deformation of the reinforcement are taken into account. Geometrical nonlinearity is included. The plate theories of Kirchhoff and Mindlin are used. The problem is discretized spatially and temporally by use of the finite element and finite difference methods, respectively. Some static and dynamic problems of slabs are analyzed and the results compared with experimental and numerical data obtained elsewhere.

RESUME

Cet article traite de l'analyse des plaques en béton armé soumises à des charges transitoires et impulsives. La fissuration, le comportement plastique du béton dans un état multiaxial de contrainte et la déformation plastique des armatures sont prises en considération. Les nonlinéarités géométriques sont considérées. Les théories de Kirchhoff et de Mindlin sont utilisées. Le problème est rendu discret spatialement et temporellement par les méthodes des éléments finis et des différences finies. Quelques problèmes statiques et dynamiques sont étudiés et les résultats comparés avec des résultats numériques et expérimentaux obtenus ailleurs.

ZUSAMMENFASSUNG

Die vorliegende Arbeit befasst sich mit der Analyse von impulsartig belasteten Stahlbetonplatten. Die Rissbildung im Zugbereich, die plastischen Deformationen des Betons unter dem mehrachsigen Spannungszustand und die plastischen Dehnungen der Stahlstäbe werden berücksichtigt. Geometrische Nichtlinearitäten werden ebenfalls berücksichtigt. Die Plattentheorien von Kirchhoff und Mindlin werden verwendet. Die Diskretisierung des Problems erfolgt räumlich nach der Finite Elemente Methode und zeitlich nach der Differenzenmethode. Einige statische und dynamische Plattenprobleme werden berechnet, und die Ergebnisse werden mit experimentellen und numerischen Resultaten anderer Untersuchungen verglichen.



1. INTRODUCTION

In problems of reactor safety and protective structures extreme dynamic loads can be encountered, and for safe and economic design the nonlinear behaviour of the material and the structure has to be considered. Major sources of nonlinearity in reinforced concrete structures are the progressive cracking in tension, the nonlinear response of reinforcing steel in tension and of concrete under compression, and other nonlinearities related to reinforcement and its interaction with concrete. In sudden loading the effect of high strain rate on the behaviour of concrete and steel should also be accounted for.

The finite element method has enabled the solution of the complicated problems represented by the nonlinear behaviour of reinforced concrete structures. Several studies on the nonlinear behaviour of reinforced concrete structures subjected to static loads have been published in recent years, see [1-6] and others. On the other hand, only few reports on dynamic analysis of reinforced concrete are available [7-12].

The purpose of this paper is to report on the study of reinforced concrete slabs subjected to transient impulsive loading. In initial state, elastic behaviour is assumed for the composite material formed by concrete and reinforcement. Tensile cracking of the concrete and the plastic behaviour of the concrete in biaxial compression and of the reinforcing steel are taken into account. The reinforcement is described as smeared and orientated steel layers. The equation of motion is derived using the principle of virtual displacements in total Lagrangian approach. The kinematic equations of plates are taken in accordance with the theories of Kirchhoff and Mindlin. The problem is discretized spatially and temporally by use of the finite element and finite difference methods, respectively. Some static and dynamic problems of slabs are analyzed and the results compared with available experimental or numerical values.

2. KINETIC AND KINEMATIC EQUATIONS

In total Lagrangian approach the principle of virtual displacements can be written in the form [13]

$$\int_{V_0} S \delta E dV - \int_{V_0} f \delta u dV - \int_{A_t} t \delta u dA + \int_{V_0} \rho \ddot{u} \delta u dV = 0 \quad (1)$$

where S is the 2nd Piola-Kirchhoff stress, E the Green-Lagrange strain, f and t the prescribed body force and surface traction, respectively, ρ the density, u the displacement, and \ddot{u} the acceleration. V_0 denotes the initial volume of the body and A_t the part of the initial boundary on which the traction is given. The use of finite element approximation $u = Nq$ results in matrix equation

$$R(q) + M\ddot{q} = Q \quad (2)$$

where q is the vector of nodal displacements, and

$$R = \int_{V_0} B^T S dV, \quad Q = \int_{V_0} N^T f dV + \int_A N^T t dA, \quad M = \int_{V_0} N^T \rho N dV \quad (3)$$

are the force of internal stresses, the load vector, and the mass matrix, re-

spectively. The matrix B , dependent on the current state, is defined by the strain variation $\delta E = B\delta q$. The incremental form of the equation of motion (2) is

$${}^1K_t \Delta q + M \ddot{q} = {}^2Q - {}^1R \quad (4)$$

where

$${}^1K_t = \int_{V_0} {}^1B^T {}^1D {}^1B dV \quad (5)$$

is the tangent stiffness matrix. Left superscripts 1 and 2 refer to the configurations of the body at times t and $t + \Delta t$, respectively. The constitutive matrix D relates the stress and strain rates, $\dot{S} = D\dot{E}$.

In Mindlin's thick plate theory, the assumption is made that normals to the midplane remain straight but not necessarily normal to the midsurface after deformation. The nonlinear strain-displacement relation can be written in the form [14]

$$\begin{pmatrix} \epsilon_x \\ \epsilon_y \\ \gamma_{xy} \\ \gamma_{xz} \\ \gamma_{yz} \end{pmatrix} = \begin{pmatrix} u_{,x} + w_{,x}^2/2 \\ v_{,y} + w_{,y}^2/2 \\ u_{,y} + v_{,x} + w_{,x}w_{,y} \\ w_{,x} + \varphi \\ w_{,y} + \psi \end{pmatrix} + z \begin{pmatrix} \varphi_{,x} \\ \psi_{,y} \\ \varphi_{,y} + \psi_{,x} \\ 0 \\ 0 \end{pmatrix} \quad (6)$$

where u and v are the in-plane displacements and w the deflection of the midplane and φ and ψ represent the rotations of the normal with respect to x - and y -axes. The corresponding relationships of the thin plate theory of Kármán-Kirchhoff are obtained by setting $\varphi = -w_{,x}$, $\psi = -w_{,y}$ in equation (6).

3. SOLUTION TECHNIQUE

The central difference method (CD) is used to solve the system of ordinary differential equations (2). The solution q_{n+1} at time t_{n+1} is computed from formula

$$q_{n+1} = h^2 M^{-1} (Q_n - R_n) + 2q_n - q_{n-1} \quad (7)$$

where $h = t_{n+1} - t_n$ is the step length. The strain and stress increments are calculated using equations

$$\Delta E = B_n (q_{n+1} - q_n), \quad \Delta S = D_n \Delta E$$

The internal force vector at time t_{n+1} is evaluated in accordance with equation (3) using B_{n+1} and $S_{n+1} = S_n + \Delta S$. The initial condition for \dot{q}_0 is used to



eliminate q_{-1} in the first step $\dot{q}_0 = (q_1 - q_{-1})/2\Delta t$. The CD-scheme with diagonal mass matrix is accurate and simple. As an explicit linear difference method its step length is limited by the largest natural frequency of the finite element mesh.

In the solution of equation (4) the trapezoidal rule or the Newmark scheme with parameters $\gamma = 0.5$ and $\beta = 0.25$ was applied

$$\begin{aligned}\dot{q}_{n+1} &= \dot{q}_n + h\ddot{q}_n/2 + h\ddot{q}_{n+1}/2 \\ q_{n+1} &= q_n + h\dot{q}_n + h^2\ddot{q}_n/4 + h^2\ddot{q}_{n+1}/4.\end{aligned}\quad (8)$$

Use of these formulae results in an implicit scheme and therefore iteration has to be used at each time step. The displacement vectors q_{n+1}^i and q_{n+1}^{i+1} in the i^{th} and $(i+1)^{\text{th}}$ iteration cycles correspond to configurations 1 and 2 in equation (4). Use of equations (4) and (8)₂ yields

$$(K_{t,n+1}^i + 4M/h^2)\Delta q^{i+1} = Q_{n+1} - R_{n+1}^i + M - 4(q_{n+1}^i - q_n)/h^2 + 4\dot{q}_n/h + \ddot{q}_n. \quad (9)$$

where $\Delta q^{i+1} = q_{n+1}^{i+1} - q_{n+1}^i$. For the first iteration cycle $q_{n+1}^1 = q_n$ is taken. The iteration is continued until $\|\Delta q^{i+1}\| < \epsilon \|q_{n+1}^{i+1} - q_n\|$ where ϵ is a tolerance parameter. To account for the drastic changes due to cracking the tangent stiffness K_t was updated in the first iteration cycle but held constant thereafter in order to reduce computing time when using consistent mass matrix.

In Kirchhoff's plate theory a 24 degree of freedom rectangular element was used with 4 nodes and the displacement parameters u, v, w, w_x, w_y , and w_{xy} at each node. Integration was performed by 2x2 Gauss quadrature formula. In Mindlin's plate theory 20 and 40 degrees of freedom rectangular elements were employed with 4 and 8 nodes, respectively. The displacement parameters at each node are u, v, w, ϕ , and ψ . 2x2 Gaussian integration rule was used, except in case of 20 DOF element only one Gaussian point for the shear deformation. In depthwise direction the integration was carried out by Simpson's rule with 7 integration points. Steel layers were considered separately at their proper places and their effects added to the internal force vector and the tangent stiffness.

4. MATERIAL PROPERTIES

The behaviour of concrete is illustrated by the uniaxial stress-strain diagram in Figure 1. At initial stage, concrete is linearly elastic, isotropic up to the level 30 % of the compressive strength and of the tensile strength. Then plastic strain hardening yield takes place according to a parabolic function. Cracking occurs when a cracking criterion is satisfied. Cracking is brittle and the stress at a discrete crack drops abruptly to zero. The descending part after cracking in Figure 1, however, describes average cracking behaviour over a finite distance and gradual release of tensile stress. In compression, strain softening occurs after the compressive strength in two linear parts, of which the latter corresponds the crushing region.

In multiaxial state of stress the yield criterion is defined as follows

$$F(\sigma, \epsilon^p) = 3\alpha g^2 J_2 + \beta \bar{\sigma} J_1 + \gamma J_1^2 - \bar{\sigma}^2 = 0 \quad (10)$$

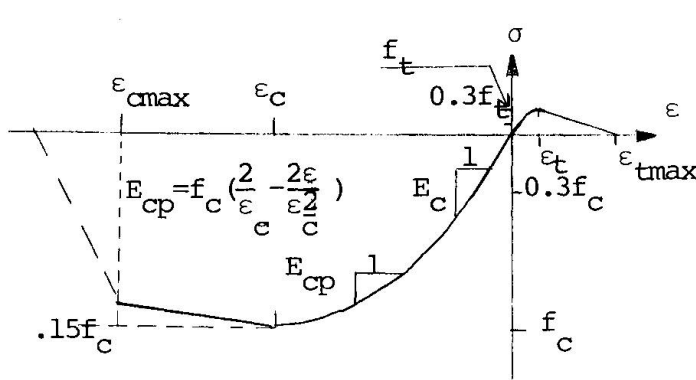


Fig. 1. Uniaxial stress-strain curve of concrete

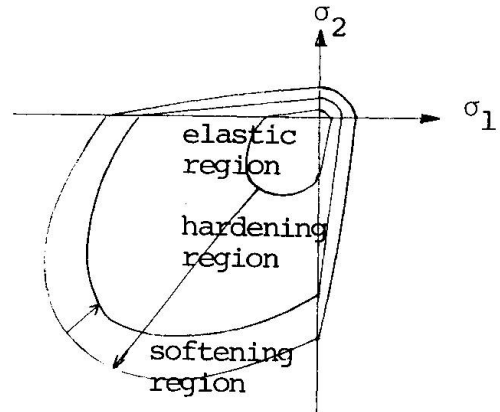


Fig. 2. Biaxial yield and failure criteria of concrete

where J_1 is the first invariant of stress tensor $J_1 = \sigma_{kk}$ and J_2 the second invariant of stress deviator $J_2 = \sigma'_{ij} \sigma'_{ij} / 2$. The function

$$g = \delta - (1 - \delta) \cos 3\theta = \delta - (1 - \delta) 3\sqrt{3} J_3 / 2J_2^{3/2} \quad (11)$$

determines the shape of the yield locus in the deviatoric stress plane. J_3 is the third invariant of stress deviator $J_3 = \sigma'_{ij} \sigma'_{jk} \sigma'_{ki} / 3$. α , β , γ , and δ are parameters to be determined on the basis of experimental data. The equivalent yield stress $\bar{\sigma}$ is a function of the equivalent plastic strain

$$\bar{\sigma} = \bar{\sigma}(\epsilon^p), \quad d\bar{\sigma}/d\epsilon^p = E_p(\epsilon^p), \quad d\epsilon^p = (2d\epsilon'_{ij} d\epsilon'_{ij} / 3)^{1/2} \quad (12)$$

It can be obtained from the uniaxial relationship by subtracting the elastic strain. The initial yield stress in equation (10) is $\bar{\sigma} = 0.3 f_c$. The yield locus expands when $\bar{\sigma}$ increases. Ultimate size is reached when $\bar{\sigma} = f_c$. Parameters α , β , and γ are determined at this stage to fit the experimental results for biaxial stress given in [15]. Using values: $\sigma_1 = -f_c$, $\sigma_2 = 0$; $\sigma_2 = -0.65 f_c$, $\sigma_1 = -1.25 f_c$; $\sigma_2 = \sigma_1 = -1.16 f_c$ one finds for compression-compression region $\alpha = 0.551$, $\beta = -0.872$ and $\gamma = -0.423$, and with values $\sigma_1 = -f_c$, $\sigma_2 = 0$; $\sigma_2 = -0.365 f_c$, $\sigma_1 = 0.075 f_c$; $\sigma_2 = 0$, $\sigma_1 = f_t = 0.1 f_c$ for tension-compression and tension-tension regions $\alpha = 27.49$, $\beta = 7.28$ and $\gamma = -19.22$. In tension-compression and tension-tension regions the ultimate yield locus serves as cracking criterion. Beyond the ultimate yield locus, the softening begins and the yield locus shrinks, see Figure 2. The parameter δ is chosen to be 1.14 in order to keep the yield surface convex.

The associated flow rule is employed. The constitutive equation in plastic flow is accordingly

$$\dot{\sigma} = D_{ep} \dot{\epsilon} \quad (13)$$

where the elastoplastic constitutive matrix is

$$D_{ep} = C - \frac{C n n^T C}{E_p + n^T C n} \quad (14)$$



C is the elasticity matrix of concrete. The vector $n \equiv \partial f / \partial \sigma$ is determined on the basis of the yield function (10).

The direction of the crack is taken perpendicular to the maximum tensile stress. After complete cracking concrete behaves uniaxially in the crack direction. The crack is assumed to close when the strain perpendicular to crack direction becomes compressive. After cracking some shear resistance still exists due to aggregate interlocking and dowel action. This is taken into account in reduced shear modulus of concrete [4]

$$G_{\text{red}} = \begin{cases} (1 - \varepsilon / \varepsilon_{t\text{max}}) \cdot 0.6 + 0.4 G, & \varepsilon_t < \varepsilon < \varepsilon_{t\text{max}}, \\ 0.4 G, & \varepsilon_{t\text{max}} < \varepsilon. \end{cases} \quad (15)$$

For the steel bars the elastic plastic linearly strain hardening idealization is used. Reinforcement takes axial and shear stresses. Reinforcement is described as smeared uniaxial layers. Complete compatibility between concrete and reinforcement is maintained. The effect of bond slip is taken into account by reducing the modulus of elasticity of reinforcement by 10-20 %.

5. NUMERICAL EXAMPLES

5.1 Statically loaded slabs

Two statically loaded slabs tested by Jofriet & McNeice [3] and Nilsson & Johansson [11] were analyzed numerically and compared with experimental data. In both cases good agreement was obtained.

5.2 Dynamically loaded beam

A freely supported beam tested in [7] was analyzed dynamically. The span, width and thickness of the beam were 2540 mm, 152 mm and 305 mm, respectively. Reinforcement of the beam was 1.23 %. The beam was loaded with a freely falling mass of 1030 kg. The mass time curve was approximated bilinearly. Central deflection vs. time curve is shown in Figure 3.

5.3 Dynamically loaded slabs

A clamped rectangular slab subjected to a jet force at the center is a structure analyzed by Stangenberg [8] using a difference method. In present analysis 2x2 and 3x3 finite element meshes for plate quadrant were used. The calculated time history of the deflection of the central point agrees closely with the curve given in [8] (Figure 4).

The one way roller supported slab [11] with 2280 mm span, 1230 mm width and 80 mm thickness with reinforcing steel 0.17 % and 0.085 % was tested under a uniformly distributed pressure load varying with time. The central deflection-time history was determined using four isoparametric elements for a plate quadrant (Figure 5).

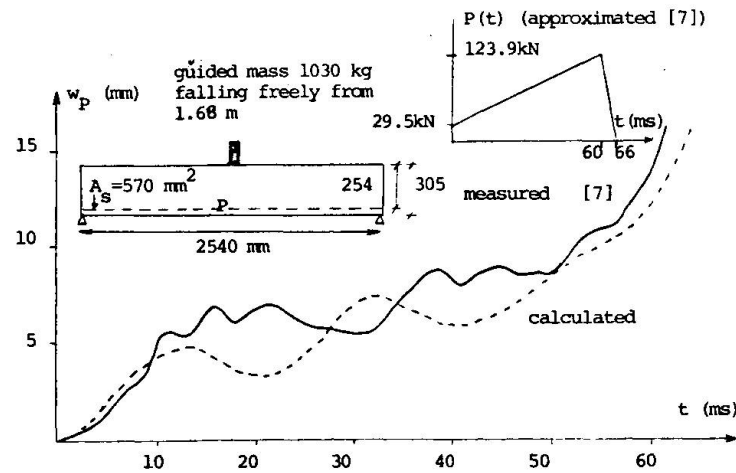


Fig. 3. Midspan deflection vs. time of RC beam, $E_c = 44$ GPa, $E_s = 100$ GPa, $f_c = 60$ MPa, $f_t = 6$ MPa, $\nu = 0.2$, $\rho = 0.24 \times 10^{-8} \text{ N s}^2/\text{mm}^4$, $E_s = 210$ GPa, $E_s = 1$ GPa, $f_c = 520$ MPa, $\nu = 0.3$, 5 elements for half span, time integration by trapezoidal rule.

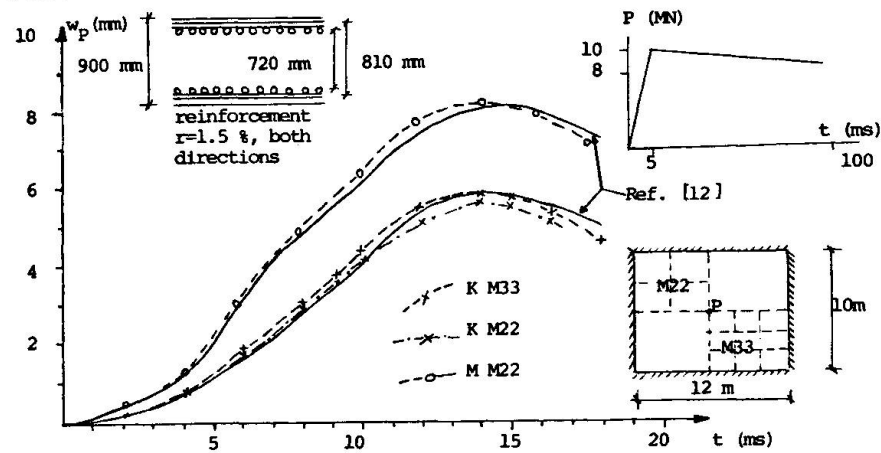


Fig. 4. Deflection vs. time of rectangular plate under central jet force. $E_s = 210$ GPa, $E_c = 33$ GPa, $\nu = 0.15$, $f_c = 22.7$ MPa, $f_t = 2.27$ MPa, $f_c = 400$ MPa, $\rho = 0.24 \times 10^{-8} \text{ N s}^2/\text{mm}^4$, $\epsilon_c = 0.002$, $\epsilon_c^{\max} = 0.004$, $\epsilon_t = 0.0002$, $K =$ Kirchhoff plate theory, $M =$ Mindlin plate theory.

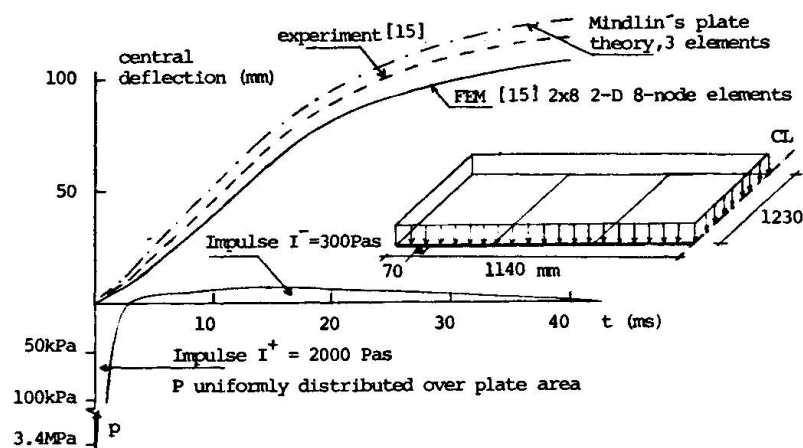


Fig. 5. One way roller supported slab under uniform pressure varying with time. Central deflection vs. time.



6. DISCUSSION

The numerical results obtained for the cases considered indicate that the method describes satisfactorily the behaviour of reinforced concrete slabs at least under static loading. More experimental evidence is needed for dynamic loading. The development of the proposed model is in progress. Systematic study of the factors, viz. cracking, elastic-plastic yield and strain rate effect of concrete, aggregate interlocking, dowel action, etc., affecting the behaviour of reinforced concrete structures and attempts to find realistic simplified models are continued.

REFERENCES

1. MIKKOLA, M.J., and SCHNOBRICH, W.C.: Material Behavior Characteristics for Reinforced Concrete Shells Stresses beyond the Elastic Range. Struct. Res. Series No. 367. University of Illinois. August, 1970.
2. CERVENKA, V.: Inelastic Finite Element Analysis of Reinforced Concrete Panels Under In-Plane Loads. Ph. D. Thesis. University of Colorado, Boulder, 1970.
3. JOFRIET, J.C., and MCNEICE, G.M.: Finite Element Analysis of Reinforced Concrete Slabs. J. Struct. Div., ASCE, Vol. 97, No. ST3, 1971, pp. 785-806.
4. LIN, C.S., and SCORDELIS, A.C.: Nonlinear Analysis of RC Shells of General Form. J. Struct. Div., ASCE, Vol. 101, No. ST3, 1975.
5. SCHNOBRICH, W.C.: Behavior of Reinforced Concrete Structures Predicted by the Finite Element Method. Computers & Structures, Vol. 7, 1977, pp. 365-376.
6. BUYUKOZTURK, O.: Nonlinear Analysis of Reinforced Concrete Structures. Computers & Structures, Vol. 7, 1977, pp. 149-156.
7. NOSSEIR, MOHAMED, S.E.B.: Static and Dynamic Behavior of Concrete Beams Failing in Shear. Ph. D. Thesis. University of Texas, Texas, 1966.
8. STANGENBERG, F.: Nonlinear Dynamic Analysis of Reinforced Concrete Structures. Nucl. Eng. and Design., Vol. 29, No. 1, 1974, pp. 71-88.
9. REBORA, B., ZIMMERMAN, Th., and WOLF, J.P.: Dynamic Rupture Analysis of Reinforced Concrete Shells. Nucl. Eng. and Design. Vol. 37, 1976, pp. 269-.
10. BUYUKOZTURK, O., and CONNOR, J.J.: Nonlinear Dynamic Response of Reinforced Concrete under Impulsive Loading: Research Status and Needs. Nucl. Eng. and Design, Vol. 50, 1978, pp. 83-92.
11. NILSSON, L., and JOHANSSON, I.: Analys med Finit Elementmetod av Luftstöt-vågsbelastade Enkelspända Betongplattor. FOA Raport C20204-D4, Stockholm, November 1977.
12. NILSSON, L.: Impact Loading on Concrete Structures., Chalmers University of Technology. Publication 79:1. Göteborg 1979.
13. BATHE, K.-J., RAMM, E., and WILSON, E.L.: Finite Element Formulation for Large Deformation Dynamic Analysis. Int. J. Num. Meth. Eng. Vol. 19, 1975, pp. 353-386.
14. HINTON, E., OWEN, D.R.J., and SHANTARAM, D.: Dynamic Transient Linear and Nonlinear Behaviour of Thick and Thin Plates. Mathematics of Finite Elements and Applications (ed. by J.R. Whiteman). Academic Press, 1976, pp. 423-438.
15. KUPFER, H.B., HILSDORF, H.K., and RUSCH, H.: Behavior of Concrete under Biaxial Stresses. J. of ACI, Vol. 66, No. 8, 1969, pp. 656-666.
16. SCHICKERT, G., and WINKLER, H.: Results of Test Concerning Strength and Strain of Concrete Subjected to Multiaxial Compressive Stresses. Heft 277, Deutscher Ausschuss für Stahlbeton. Berlin 1977.

IV

Comparison of Plastic Prediction with STANIL/1 Analysis

Comparaison de l'analyse plastique avec le programme STANIL/1

Vergleich plastischer Berechnungen mit Berechnungen nach STANIL/1

J. BLAAUWENDRAAD

dr.ir. (techn.)
Rijkswaterstaat-DIV
Rijswijk, Holland

S.F.C.H. LEIJTEN

ir. (techn.)
Rijkswaterstaat-DIV
Rijswijk, Holland

J.G.M. van MIER

ir. (techn.)
Technical University
Eindhoven, Holland

SUMMARY

The Danish group led by M.P. Nielsen published in 1978 a plastic analysis for the prediction of the ultimate shear failure load in beams. This method holds where unlimited ductility of steel and concrete can be assumed. In The Netherlands a nonlinear program, STANIL/1 is available to determine in which cases the plastic approach is admissible. The program uses concrete beam elements with main bending reinforcement and vertical web reinforcement. Results of some performed comparisons will be shown.

RESUME

Le groupe danois de Nielsen a publié en 1978 une méthode plastique pour calculer les charges ultimes de poutres soumises au cisaillement. Cette méthode est valable avec l'hypothèse d'une ductilité illimitée du béton et de l'acier. On a développé, aux Pays-Bas le programme non linéaire STANIL/1 à l'aide duquel on peut examiner si l'analyse plastique est applicable. Le programme utilise des éléments de poutre de béton avec une armature principale de flexion et une armature de cisaillement. Quelques résultats sont comparés.

ZUSAMMENFASSUNG

Nielsens Dänische Gruppe publizierte 1978 eine plastische Methode zur Berechnung der Schubbruchlast von Balken. Diese Methode ist anwendbar, wenn ein unbeschränktes Verformungsvermögen von Stahl und Beton angenommen werden darf. In den Niederlanden wurde das nichtlineare Rechenprogramm STANIL/1 entwickelt, mit dessen Hilfe beurteilt werden kann, in welchen Fällen die plastische Berechnung zulässig ist. Das Programm verwendet Beton-Balkenelemente mit Biegelängsbewehrung und vertikaler Schubbewehrung. Die Ergebnisse einiger durchgerechneter Vergleiche werden dargestellt.



1. INTRODUCTION AND SCOPE

During the IASS-symposium on Nonlinear behaviour of reinforced spatial structures at Darmstadt, 1978, a presentation has been given of the researchproject 'Beton-mechanica' in The Netherlands. A number of subprojects is on its way for experimental studies of a crackzone and a bondzone and also a subproject for numerical models. One of these models is called in the framework of the total project the Macro-model for framed structures. This Macro-model is a computerprogram Stanil/1 which enables us to analyse the nonlinear load displacement characteristics of beams, columns and frames. The program can be used to confirm the results of an existing ultimate load prediction via a plastic analysis, but above that additional information is provided on deformation restrictions and on the needed strain capacity of the reinforcement steel and the concrete.

The program Stanil/1 is an extension of an existing program which has been published by BLAAUWENDRAAD in 1972 [1]. That program had been based on the concept of a so called 'layered' beam-element as has been used parallelly by other investigators [2], [3]. The element has proven to give very good results for load combinations of pure bending and axial forces. However, the influence of shear forces could not be simulated adequately. This problem has been solved in the now presented new program Stanil/1 which uses a beam-element taking shear deformations and the action of vertical stirrups into account as well. The element-model will be briefly described in chapter 2.

NIELSEN, BRAESTRUP and BACH [4] presented a plastic analysis for the prediction of the ultimate shear failure load in beams. This method, which is in line with previous studies of THUERLIMANN et al [5], is used for the comparison with the Stanil/1 results. The plastic analysis is based on a theory of plasticity using an equilibrium method, providing a lower bound solution and a mechanism analysis, providing an upper bound solution. The method holds if unlimited ductility of steel and concrete may be assumed. Tuning of the method with experimental results showed that it was necessary to introduce a web effectiveness factor. In [4] this effectiveness factor was explained as to account for the limited ductility of the concrete. In case of complete accordance of the theoretical plastic model and the experimental results the web effectiveness factor should have the value 1.0. In practice the factor varies between 0.7 and 0.9.

Comparing the program Stanil/1 and the plastic analysis, it can be said that Stanil/1 is more general. The ultimate load prediction of the plastic analysis is a special case in the framework of Stanil/1. This program also is capable to calculate the ultimate load, but does not need the introduction of a web effectiveness factor. But more important, Stanil/1 provides information on the stiffness under work load conditions and on the amount of cracking. Stanil/1 also shows in which cases the strain capacity is insufficient to reach the plastic prediction for the ultimate load.

In cases in which the plastic analysis is valid, at failure both the nonlinear analysis of Stanil/1 and the plastic analysis of NIELSEN et al. should give the same results. To check this, in this paper two comparisons are presented. The first comparison regards the ideal plastic model in which the web effectiveness factor has the unit value. This situation can be simulated with Stanil/1 by making the axial concrete strains in the beam zero. This is the case for extremely high percentage of main reinforcement in the tensile region and for a compression flange which has an infinite rigidity. This comparison is shown in chapter 3. The second comparison in chapter 4 regards a situation for which the web effectiveness factor is less than unity. We use for this purpose experimental results for real beams of LEONHARDT and WALTHER [6].

2. THE MACRO-MODEL (STANIL/1)

2.1 General remarks about the beam-element

The beam-element has been based on an assumed field of displacements. Main bending reinforcement is schematized to two thin layers of steel; vertical stirrups are 'smeared out' to distributed vertical strings; cracks are smeared out on the beam. Nonlinearities are accounted for as follows: Each beam is divided over its height into imaginary concrete layers and steel layers (longitudinal reinforcement). Each layer may have different material properties corresponding to its stress or strain state and these properties can be different along one layer in the several cross-sections. The steel properties are defined for uniaxial states only but the concrete properties are defined for two-dimensional plane stress states. The behaviour of a beam-element is derived from the behaviour of a number of cross-sections of the beam-element, and the behaviour of the cross-section can be derived by totalizing the material properties of all layers in the cross-section in an appropriate way. Cracking and crushing of concrete are accounted for by modifying the material properties.

2.2 Possible deformations in the beam-element.

The assumed field of displacements allows for axial strains, bending and shear deformations and is capable of simulating bond slip of the main bending reinforcement and failure of the anchoring zone of this reinforcement. Above that vertical strains are allowed to occur, so that each admissible two-dimensional strain state can be simulated in the concrete, but also the stirrups can be activated. In this way one may expect to simulate truss action in the beam, needing in that case inclined concrete diagonals and vertical hangers.

Axial strains and bending deformations.

The chosen field of displacements allows a linear variation along the axis of the beam of both the axial strain e_{xx} and the curvature κ_{xx} , needing a total of 7 degrees of freedom (u_1, u_2, u_3 and w_1, w_2, ϕ_1, ϕ_2), see fig. 1.

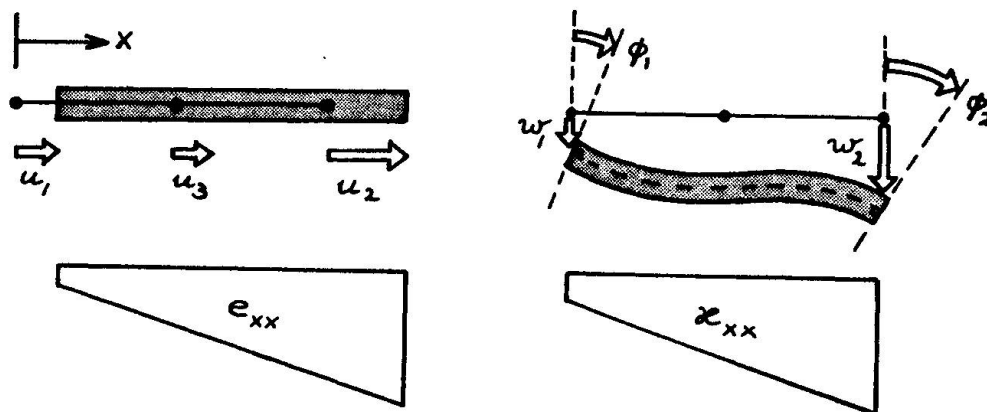


Fig. 1 Degrees of freedom and deformations for axial strain e_{xx} and curvature κ_{xx}



Shear deformation and tensile strain in stirrups.

More over the chosen field of displacements allows a linear variation along the axis of the beam of both the shear deformation γ_{xy} and the vertical strain e_s , needing another 4 degrees of freedom (γ_1 , γ_2 and Δh_1 , Δh_2), see fig. 2. This implies that the shear deformation and the strain in the stirrups is constant over the height of the beam. A perfect bond is assumed between the concrete and the stirrups.

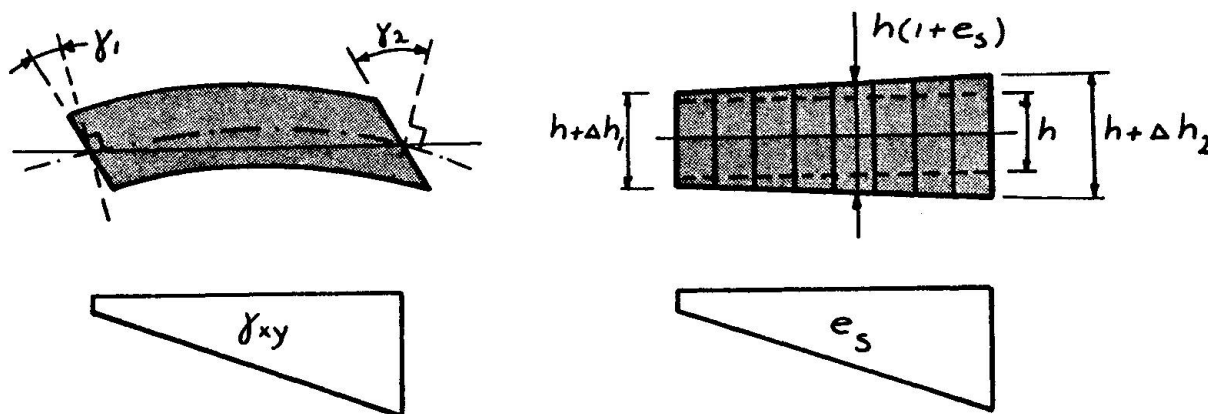


Fig. 2 Extra degrees of freedom and deformations for shear γ_{xy} and vertical strain e_s

Steel-concrete interaction.

In order to accomplish a stiffness-interaction between longitudinal reinforcement and concrete, a possibility is created for relative movement between steel and concrete, called bond slip. This is achieved by imagining a tubular bond-spring around the bars of reinforcement. The interaction takes place as follows. Besides the already chosen field of axial displacements (u_1 , u_2 , u_3) for concrete, a separate field of axial displacements is chosen for steel (interpolation of the same degree as for concrete). The relative movement (bond slip) is found as the difference between the displacements of steel and concrete, resulting in three additional degrees of freedom (Δu_1 , Δu_2 , Δu_3). Using these parabolic interpolations for bottom and top reinforcement 6 additional degrees of freedom are necessary.

The anchoring of the main reinforcement is in fact a complex three-dimensional state of strains and stresses. This is schematized with an extra point-spring between each end of the main reinforcement and the concrete in that position. Each spring results in an additional degree of freedom, being a relative axial displacement Δu .

2.3 Material properties.

The material properties of steel, concrete and bond can be inputted into STANIL/1 in multi-linear stress-strain relations c.q. multi-linear bond stress-slip relation. The failure surface for concrete is derived from the relevant relation, see fig. 3.

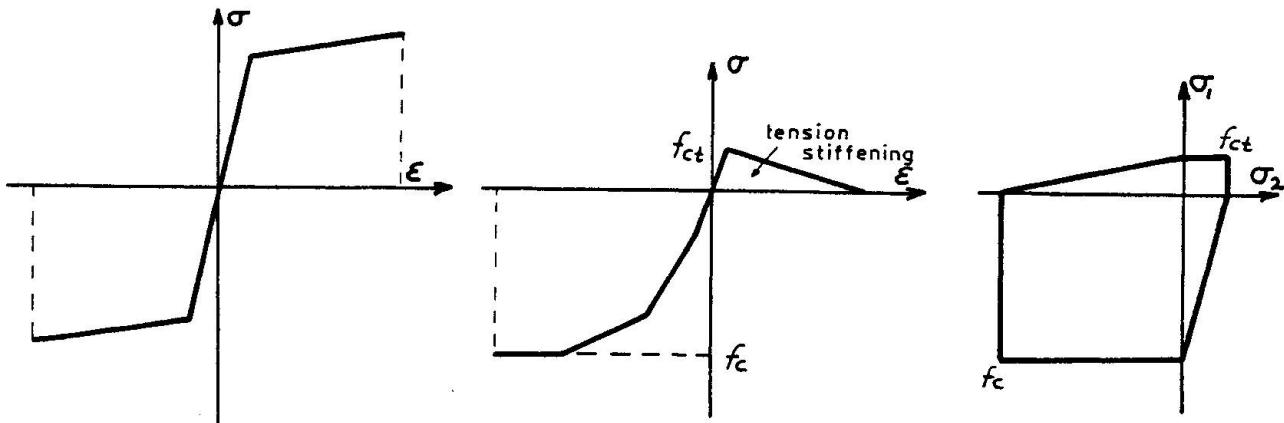


Fig. 3 Possible stress-strain relation for steel

Possible stress-strain relation for concrete together with assumed failure surface

The stress-strain relations that are used for concrete in biaxial stress-states, are also derived from the uni-axial stress-strain relations. At present the relations that are used can be expressed as:

uncracked region:
$$\begin{bmatrix} d\sigma_{xx} \\ d\sigma_{yy} \\ d\sigma_{xy} \end{bmatrix} = \begin{bmatrix} E & 0 & 0 \\ 0 & E & 0 \\ 0 & 0 & \frac{1}{2}E \end{bmatrix} \begin{bmatrix} d\epsilon_{xx} \\ d\epsilon_{yy} \\ d2\epsilon_{xy} \end{bmatrix}$$

If in one of the principal directions, say direction 1, the tensile strength is exceeded the relation used is:

cracked region:
$$\begin{bmatrix} d\sigma_{11} \\ d\sigma_{22} \\ d\sigma_{12} \end{bmatrix} = \begin{bmatrix} 0 & 0 & 0 \\ 0 & E & 0 \\ 0 & 0 & \alpha \frac{1}{2}E \end{bmatrix} \begin{bmatrix} d\epsilon_{11} \\ d\epsilon_{22} \\ d2\epsilon_{12} \end{bmatrix}$$

in which α is a constant to simulate the effect of aggregate interlock. If in future the other subprojects of 'Betonmechanica' on bond and cracking will be finished, it is expected to improve the three by three stiffnessmatrix and make it more dependent of the strains ϵ_{11} , ϵ_{22} and ϵ_{12}

Within the failure surface the stress-strain relation is regarded to be elastic. A similar assumption is made for steel and bond, the failure criteria (one-dimensional) being constituted by the extreme strains respectively extreme slip values given in the relevant relation.

3. COMPARISON FOR THE IDEAL MODEL (UNIT WEB EFFECTIVENESS FACTOR).

NIELSEN et al. [4] found for beams with vertical stirrups a relation between the nominal ultimate shearstress τ_u and a coefficient ω which is the mechanical degree for the amount of stirrups.

Fig. 4 displays this relation. The nominal shear stress τ_u is found by dividing the shear force V through the web cross-section area bh . The coefficient ω is defined by the quantities ρ , f_y and f_c , of which ρ is the degree of stirrup reinforcement, f_y the yield strength of steel and f_c the yield strength of concrete. The web effectiveness is indicated with the character ν .

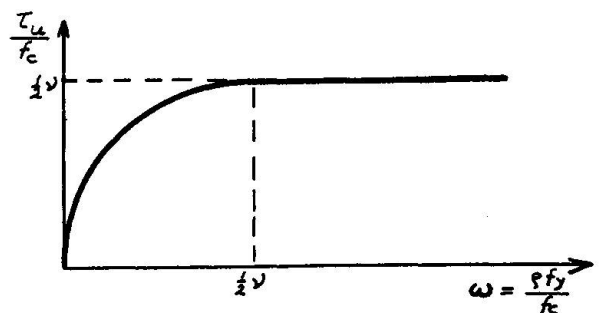


Fig. 4 Relation between τ_u , ω and ν according Nielsen et al.



As has been said in chapter 1, the unit web effectiveness factor corresponds with a Stanil/1 calculation for a beam with infinite rigid tensile and compression stringers. Fig. 5 shows which beam has been chosen and which material properties have been used.

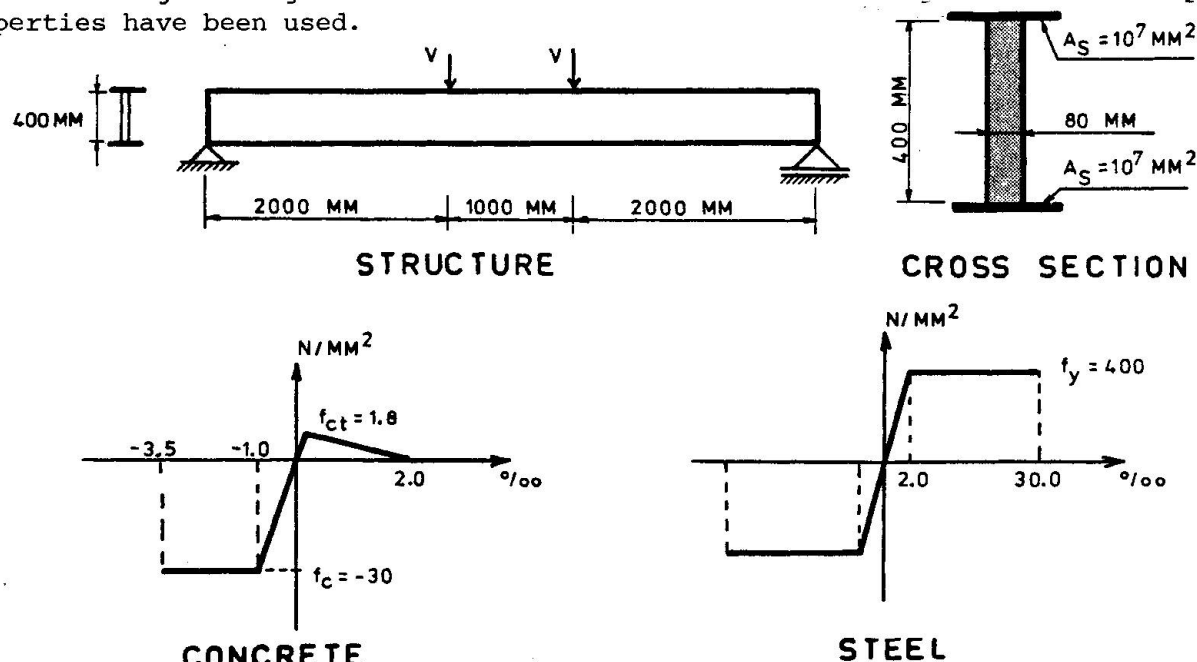


Fig. 5 Survey of the structure that was investigated and the stress-strain relations used for a unit web effectiveness factor.

The calculation with Stanil/1 has been executed for several amounts of web reinforcement, corresponding with ω -values 0.025, 0.05, 0.075, 0.1, 0.2, 0.35, 0.5, 0.6 and 0.8. In fig. 6 the results are plotted in the diagram for $\nu = 1$, showing perfect agreement. In all cases sufficient concrete ductility seems to be ensured to allow a plastic approach. It may therefore be concluded that in the plastic shear capacity prediction the web effectiveness factor is not needed because of the limited ductility of concrete but because of the fact that the axial strains caused by bending cannot be neglected in practical structures. The ductility of the structure as a whole is then limited due to the additional strains in the compressed concrete zone. This will be the subject of chapter 4.

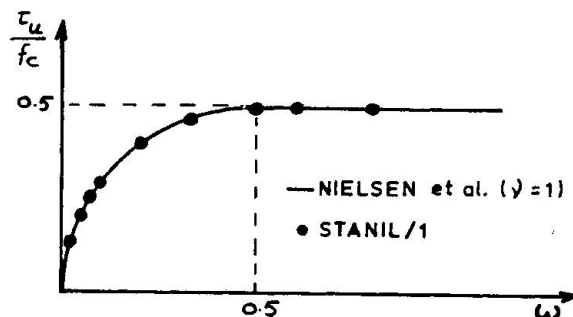
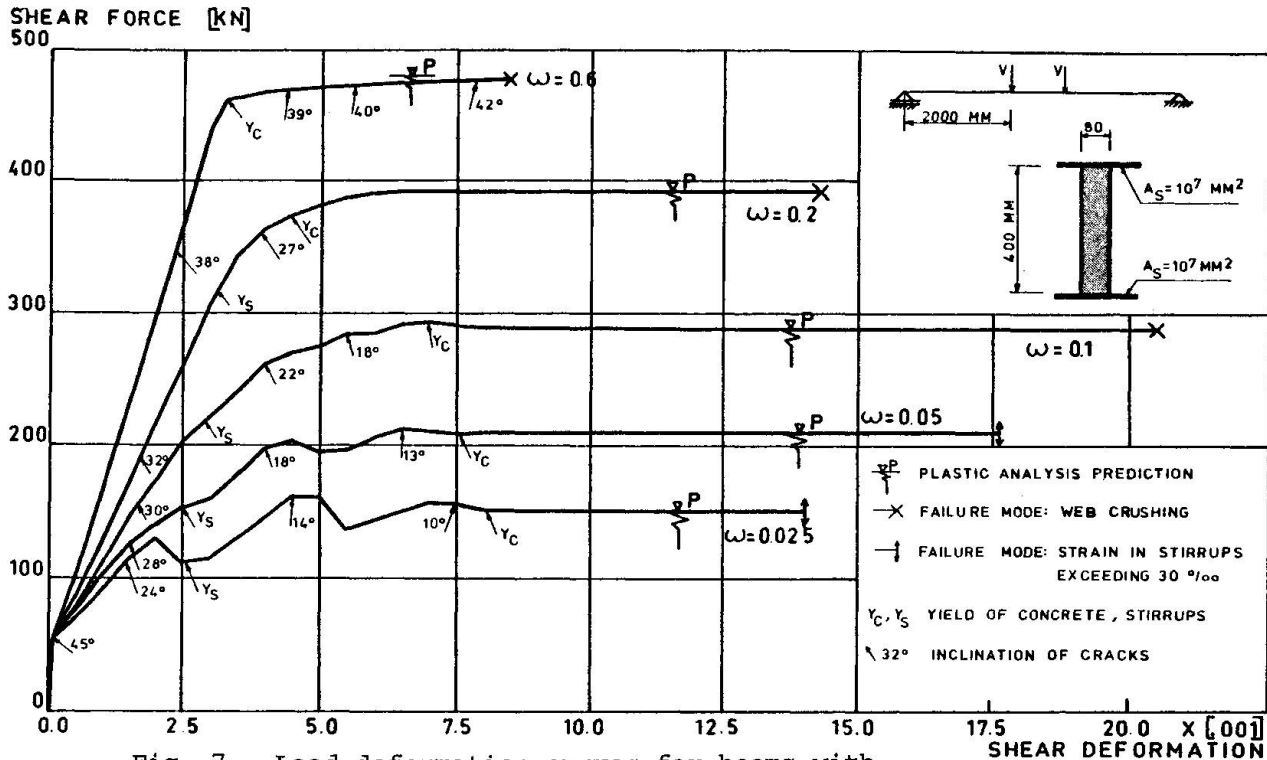


Fig. 6 Full agreement between Stanil/1 results and plastic analysis for $\nu = 1$

As has been said in chapter 1, the program Stanil/1 provides also additional information. In fig. 7 the load-deformation curves for the beams are shown for a number of ω -values. An extensive discussion cannot be given in this short paper, but the most important phenomena will be summarized.

- The stiffness after cracking decreases with decreasing amount of stirrups. The curves are less smooth in case of a low percentage web reinforcement. For these cases the stress-strain relation for concrete has to be refined, especially the tension stiffening.
- The initial crack inclination is 45° but it changes with increasing load



- At failure of the beam the web concrete yields for every value of ω , but the web reinforcement not always does. Depending on the value of ω one can notice three regimes with different failure phenomena:
 - For values of ω greater than 0.5 the failure mode is web crushing; the stirrups do not yield at failure.
 - For values of ω between 0.1 and 0.5 the failure mode is also web crushing, but now the stirrups do yield.
 - For values of ω smaller than 0.1 the yielding web concrete does not crush. Now the (average) strains in the yielding stirrups get very large and exceed 30‰. In practice this will probably mean that stirrups crossing dominant cracks will break. However, at this failure the shear deformation $2\varepsilon_{xy}$ has allready reached a big value, which means that sufficient ductility can be ensured.

4. COMPARISON FOR PRACTICAL CASE (WEB EFFECTIVENESS FACTOR SMALLER THAN UNITY)

It has been explained in chapter 1 that experimental results only correspond with the plastic model of NIELSEN et al. when a web effectiveness factor smaller than unity is introduced in the plastic model. In [4] it has been shown that test results of LEONHARDT and WALTHER agree with a plastic analysis for $v = 0.86$. Two of these tested beams (TA1 and TA4) have been analysed with STANIL/1. The load system is the same as applied in fig. 5. The distance between the support and the transverse load V was divided into three elements. The T-shaped beams have been modelled for this purpose into beams with by reinforcement steel in the compression zone with the same stiffness. This is allowable if the failure mode is not controlled by the flange. The geometrical data and material properties were taken from [6]. From experience gained so far we have learnt that the use of the prism strength in Stanil/1 shows a good agreement with tests. The results of the analysis are shown in fig.8. It can be seen to which extent they agree with the plastic analysis for $v = 0.86$ of NIELSEN et al. and with the test results of LEONHARDT and WALTHER. We may conclude that Stanil/1 is capable to predict the ultimate nominal shear load for such cases fairly well.

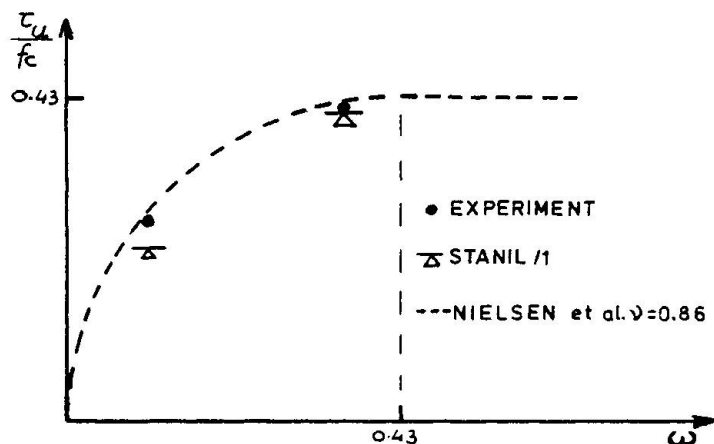


Fig. 8 Comparison of the ultimate strength from Stanil/1 and experiment.

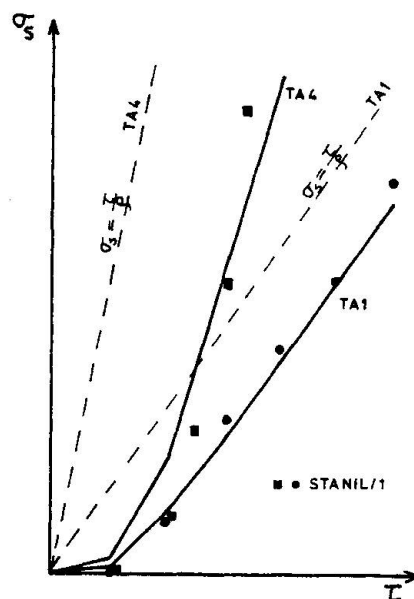


Fig. 9 Comparison of stirrup stresses σ_s from Stanil/1 and experiment

From the tests it is known in which way the steel stress σ_s in the vertical web reinforcement develops when the shear load (and thus the nominal shear stress τ) increases. This experimental result is reproduced in fig. 9, together with the dashed lines which would apply if the truss-analogy would hold (with inclined bars under 45 degrees). The shown curves were found by averaging the value of four stirrups in a certain position along the beam. The Stanil/1 results in fig. 9 are averaged values for the corresponding points. These results fit in a satisfactory manner with the experimental data, which means that the program Stanil/1 seems capable to simulate the beam phenomena under realistic conditions.

6. REFERENCES

1. BLAAUWENDRAAD, J: Realistic Analysis of Reinforced Concrete Framed Structures, Heron Vol. 18, 1972, no. 4.
2. MENEGOTTO, M; PINTO, P.E.: Method of Analysis for Cyclically Loaded R.C. Plane Frames ... under Combined Normal Force and Bending, IABSE-Symposium, Lisbon, 1973.
3. HAND, R.R; PECKNOLD, D.A.; SCHNOBRICH, W.C.: Nonlinear Layered Analysis of RC Plates and Shells, Journal of Struct. Div. ASCE, Vol. 99, 1973.
4. NIELSEN, M.P.; BRAESTRUP, M.W.; BACH, F: Rational Analysis of Shear in Reinforced Concrete Beams, IABSE Proceedings P-15/78
5. GROB, J; THUERLIMANN, B: Ultimate Strength and Design of Reinforced Concrete Beams under Bending and Shear, IABSE Mémoires, Vol. 36-II, 1976.
6. LEONHARDT, F; WALTHER, R: Schubversuche an Plattenbalken mit unterschiedlicher Schubbewehrung, Berlin, Deutscher Ausschuss für Stahlbeton, Heft 156, 1963.

IV

Finite Element Analysis of Beam Shear Problems

Analyse du cisaillement d'une poutre par la méthode des éléments finis

Finite Elemente Berechnung von Schubproblemen in Balken

T. NOMURA

Graduate Student
University of Tokyo
Tokyo, Japan

J. YAMAZAKI

Associate Professor
Tokyo Metropolitan University
Tokyo, Japan

H. OKAMURA

Associate Professor
University of Tokyo
Tokyo, Japan

SUMMARY

A non-linear finite element method of analysis was used to predict the behaviour of reinforced concrete beams. Special consideration was paid to the assumptions on change in stiffness of concrete due to cracking and bond. The results were compared with test results. The method of analysis used appeared to predict the behaviour of the beams subjected to shear and bending in terms of pattern and propagation of cracks, mode of failure and the shear at the failure.

RESUME

L'étude du comportement des poutres en béton armé est faite à l'aide d'une analyse non linéaire par la méthode des éléments finis. Les hypothèses concernant les changements de la rigidité du béton dues à la fissuration et à l'adhérence sont considérées avec soin. Les résultats analytiques et expérimentaux sont comparés. En appliquant la méthode décrite, on peut prédire le comportement d'une poutre soumise à la flexion et au cisaillement. On peut prédire la formation et la propagation des fissures ainsi que le mode de ruine.

ZUSAMMENFASSUNG

Eine nichtlineare Finite Elemente Berechnung wird durchgeführt, um das Verhalten von Stahlbetonbalken zu untersuchen. Den Annahmen über Steifigkeitsänderungen infolge Reißen des Betons sowie Verbund wird besondere Beachtung geschenkt. Den Ergebnissen werden Versuchsergebnisse gegenübergestellt. Die verwendete Methode gestattet die Voraussage des Verhaltens von Balken unter Biegung und Querkraft. Insbesondere können das Rissbild und die Rissentwicklung sowie die Art des Versagens verfolgt werden.



1. INTRODUCTION

1.1 Nature of the problem

The plastic behavior demonstrated by beams failing under the influence of bending and shear is complex and diverse, because it is affected by a broad variation in geometry of beams, distribution of reinforcing steel and boundary conditions. For confident application of plastic theory information is desirable for the behavior of beams at various stages of loading. The finite element analyses are one way of providing useful information. However, the idealization for the known inelastic behavior of concrete and a gradual destruction of bond between steel and concrete to be used in such methods of analysis is still in the process of development.

1.2 Scope

An attempt was made by a parallel study of analyses and tests for refinement for the method of analysis and better understanding of the behavior of the beams. A non-linear finite element method of analysis with several assumptions was used to predict the behavior of beams with rectangular cross section, containing flexural reinforcement only and subjected to bending and shear. The predicted results were compared with test results.

2. FINITE ELEMENT MODEL

2.1 Non-linear analysis

The finite element program used for this study was a two dimensional program which was a part of a general non-linear analysis program referred as COMPOSITE III and developed by Kokubu, Yamada and Sakurai (1). In this two dimensional analysis program conventional constant strain triangular elements and truss elements are used. Non-linear behavior is idealized by piece-wise linear analysis and modification of stiffness of elements according to stress or strain conditions as appropriate. The increments for applied loads can be prescribed to any required magnitude including zero. When the losses of stresses occur in an element due to cracking or crushing of concrete, the element stresses are transformed into nodal forces for the nodes connected to that element. In the next load increment, after modification of the stiffness of that element as required, the calculated set of the nodal forces is applied to the structure. Thus the relief of stresses in that element and redistribution of those stresses to the neighboring elements are approximated.

Four assumptions were made for this study. Those assumptions concerned : (1) stiffness of concrete, (2) failure criterion for concrete, (3) change in stiffness due to cracking, and (4) bond between steel and concrete.

2.2 Stiffness of concrete

The material stiffness matrix is defined by a shear modulus G and a bulk modulus K in this finite element program. The two moduli used for this study were identical to the tangent moduli given by Kupfer et al. for each load increment. If the moduli G and K are transformed into the modulus of elasticity E for a case of uniaxial compression, the resulting stress strain relationship is as indicated in Fig.1. If cracking occur in the concrete element, the procedure of this section is over-ridden by the provision given in Section 2.3.

2.3 Change in stiffness due to cracking

When the first cracking occurs, one of the axes of orthogonality is made coincident to the direction of the crack. Then, the coefficients in the material stiffness matrix related to the stress component which caused cracking are made equal to zero. If an element containing a crack is subjected to shear stress, displacements parallel to the crack may occur. The resistance against such displacements may be approximately expressed by the shear modulus, if the relation between the displacement and the stress is known. However, information is not sufficient for this behavior, and hence, it was assumed that the shear modulus was not changed due to cracking. This behavior implies that the interfaces of a crack are capable of transferring the same magnitude of shear as uncracked concrete. When the second crack occurs, the remaining coefficients in the material stiffness matrix are made practically equal to zero (one thousandth of the original values).

2.4 Failure criterion

The criteria for crushing and cracking of concrete are identical to those proposed by Kupfer et al., and are expressed in terms of principal stresses (2). A graphical representation is given in Fig.2.

2.5 Bond

The strength and behavior of beams failing under the influence of shear and bending was reported to vary with the bond characteristics of flexural reinforcement, and the reasons were explained by Kani (3), (4) in connection with the stress trajectories. Among the factors related to bond and influencing those trajectories, the variation in stress in flexural reinforcement with the distance from the section of maximum moment and distribution of flexural cracks were considered to be more significant. Therefore, for this analysis flexural cracks were forced to occur in the spacing approximately equal to those observed in actual beams, but the reinforcing steel was rigidly connected to the nodes of concrete elements without use of bond elements between the steel and the concrete. The flexural cracks were allowed to occur in only predetermined groups of elements by prescribing a very high value as fictitious tensile strength of concrete for the elements where cracking should be prevented. The elements for which cracking was prevented are indicated in Fig.3 with shades.

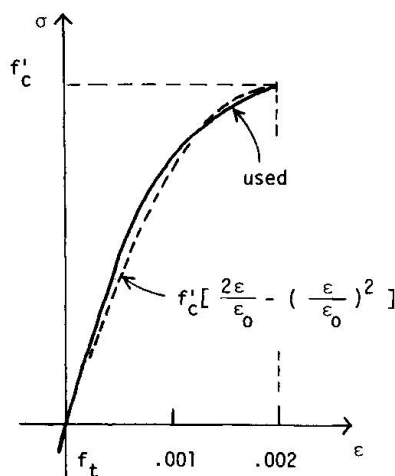


FIG.1 STIFFNESS OF CONCRETE

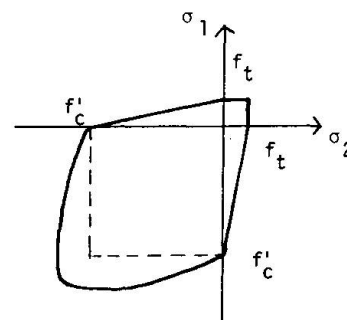


FIG.2 FAILURE CRITERION FOR CONCRETE



2.6 Structural model

The structural model used for this analysis is an idealization of a beam with rectangular cross section 15 cm in width, 25 cm in depth and 210 cm in length. The distance between the compression surface and the centroid of the flexural reinforcement, or effective depth, was 22 cm. The beam was simply supported and subjected to two symmetrical concentrated loads. The distance between the point of application of the load and the support, or shear span, was 66 cm. The finite element mesh layout and the boundary conditions are shown in Fig.3.

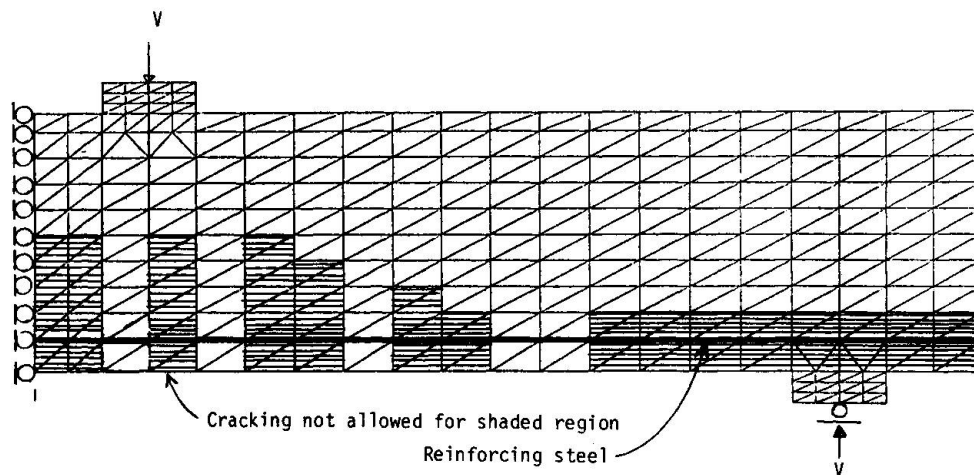


FIG.3 FINITE ELEMENT IDEALIZATION

3. COMPARISON OF PREDICTED AND OBSERVED BEHAVIOR

3.1 Loading

The load level, or applied shear was expressed as fractions of V_{flex} , where V_{flex} is a calculated shear which would cause flexural failure. When the concrete strength was 27 Mpa and the yield point of the flexural reinforcement was equal to 400 Mpa, and with the amount of flexural reinforcement equal to 11.6 cm² consisting of 3- Φ 22 mm bars (3 percent of steel ratio), the shear V_{flex} was 115 KN. The loads were applied in 16 steps, or with an increment of 0.044 V_{flex} .

The progressive propagation of cracks may not be predicted if the external loads are kept to increase at each increment of analysis, because of the provision used for this analysis in order to take into account of redistribution of stresses due to crushing and cracking of concrete as stated in Section 2.1. A particular analysis concerning this problem is to be reported in Section 3.7.

3.2 Cracking

Development of cracks with increasing load is shown in Fig.4 for the applied shear equal to 0.18, 0.44 and 0.53 V_{flex} . Cracks are denoted by outlining the triangular elements where cracking was predicted, and by lines representing the directions of the cracks in those diagrams. Flexural cracks in the tension surface of the beam were allowed to occur at only prescribed locations as explained in Section 2.5. At a shear equal to 0.44 V_{flex} inclined cracks appeared above the flexural cracks in a section about the beam effective depth away from the point of application of the load, at about the middle of the shear span, and in a section about the effective depth away from the support and at a level about

one third the beam depth from the tension side of the beam. Those cracks were to increase in number at higher loads, but those inclined cracks remained disconnected from each other. Long inclined cracks observed in beam tests were not predicted by this analysis. At a shear equal to $0.53 V_{flex}$, cracking were predicted in extensive portion of the top surface of the beam. At a section about the beam effective depth away from the point of application of the load the uncracked portion of concrete was significantly reduced due to development of inclined cracks developing from the flexural cracks as well as cracks developed on top surface of the beam.

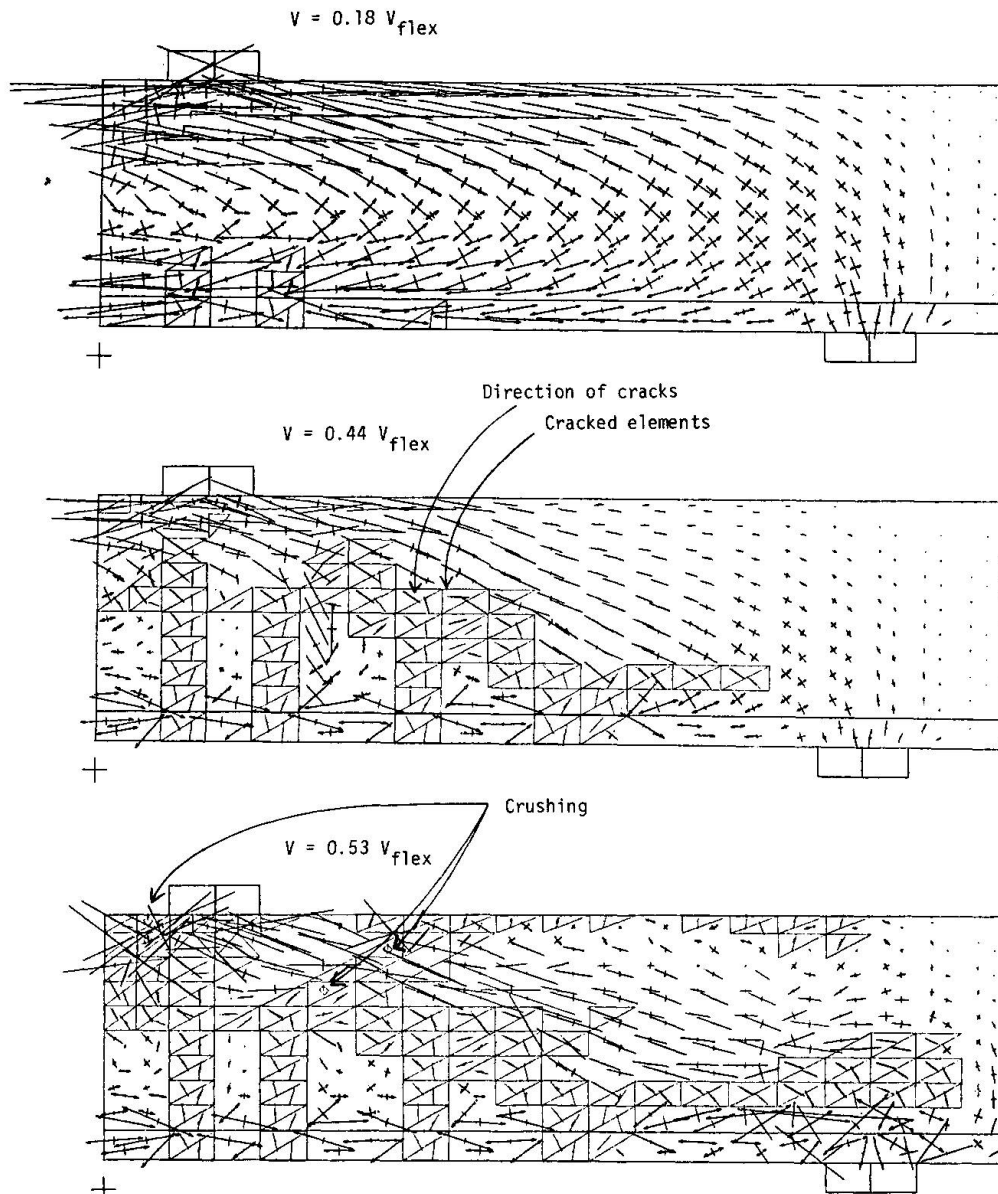


FIG. 4 PREDICTED PRINCIPAL STRESSES, CRACKING AND CRUSHING



3.3 Stress trajectory

At a shear equal to $0.18 V_{flex}$ cracking was locally contained in the region of maximum moment, and the most portion of the beam remained elastic. The compressive and tensile stress trajectories indicated in Fig.4 followed smooth curves which resembled arches and hanging arches. At a shear equal to $0.44 V_{flex}$ the compressive stress trajectories dominated in the middle of the shear span and in the compression zone in midspan sections. At a higher load directions of the trajectories flattened in both the upper and lower portions of the beam as apparent in the diagram for $0.53 V_{flex}$.

3.4 Crushing of concrete

The predicted crushing of concrete is denoted by a mark which has a shape of small rhombus in Fig.4 for a shear equal to $0.53 V$. Crushing was predicted in two sections in the beam. The first section was located adjacent to the loading plate and in the region of the maximum bending moment. The second section was situated about a beam effective depth away from the loading plate and in the direction of the reduced moment. In this section crushing was predicted in the narrowest path for the compressive stress trajectories.

3.5 Effect of bond

If the gradual breakage of bond between reinforcing steel and concrete was not taken into account in this method of analysis, the predicted cracking and trajectories are as indicated in Fig.5. Since the reinforcing bars were rigidly connected to the surrounding concrete elements, all of these concrete elements cracked.

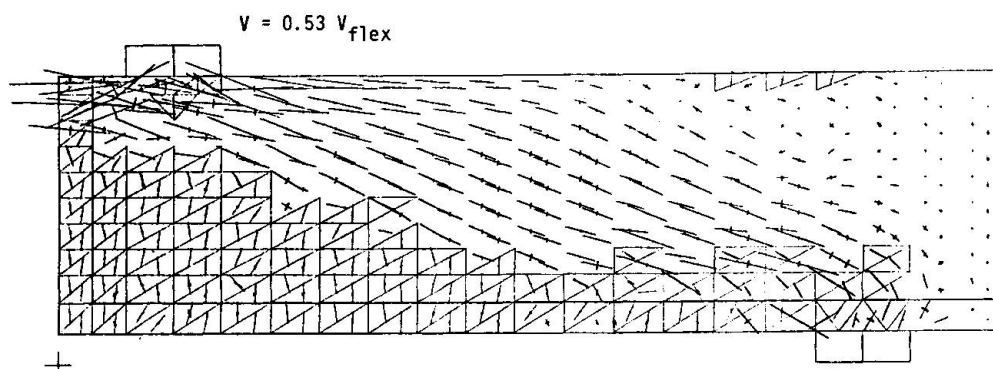


FIG.5 BEAM WITH CRACKING ALLOWED FOR ALL ELEMENTS

3.6 Compressive principal stress

For a more quantitative representation of the stress trajectories plot was made in Fig.6 for the distribution of the compressive principal stress along the vertical cross section of the beam located at 0.54, 1.18, 1.82 and 2.74 times the beam effective depth apart from the position of loading and for a section without shear. Three curves in each section represent stresses for applied shears equal to 0.18 , 0.44 and $0.53 V_{flex}$ respectively. At the lowest shear the distribution of this stress was as expected by elementary beam theory. However, at higher loads the distribution became markedly different. At the section closest to the position of the load a concentration of the stress occurred near the top surface of the beam. In contrast, at the next section moved toward the support the peak value for the stress occurred some distance apart from the top of the beam. At the sections closer to the support the distribution is more uniform and the peak gradually shifted downward. The manner in which those stresses are distributed is

understandable by referring the pattern of cracking.

3.7 Progressive propagation of cracks

So far report has been made for the analyses where the external loads were increased in increments at each increment of analysis. In order to predict the possible progressive propagation of cracks, one series of analysis was made where the external load was not increased after it reached $0.44 V_{flex}$. For the following increments of analysis the loads applied to the structure were only those resulting from stress redistribution. The results after three repetitions of such analyses are indicated in Fig.7. The results demonstrated that a crack propagated along the flexural reinforcement from the bottom end of an inclined crack to the end of the beam without an increase in the external load when the applied shear reached $0.44 V_{flex}$.

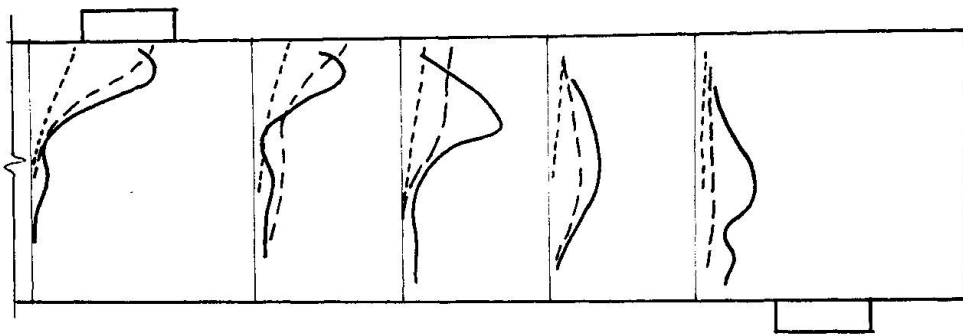


FIG.6 PREDICTED DISTRIBUTION OF COMPRESSIVE PRINCIPAL STRESSES FOR SHEAR 0.18, 0.44 AND 0.53 V_{flex}

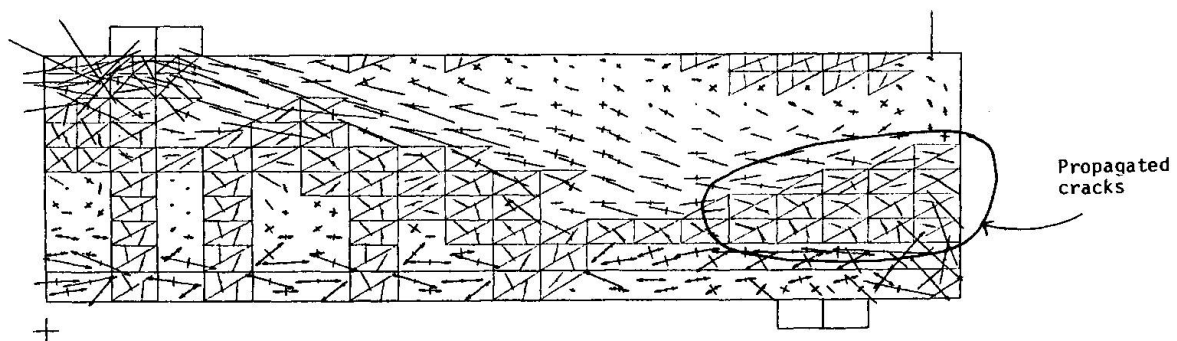


FIG.7 PREDICTED PROGRESSIVE PROPAGATION OF CRACKS ALONG REINFORCING BARS AT A SHEAR 0.44 V_{flex}



3.8 Failure of beam

In the beam failed in test the inclined crack propagated along the reinforcing bars and at the seemingly same instance crushing occurred in the upper portion of this inclined crack as well as cracks in the top surface of the beam. The shear at failure was $0.39 V_{flex}$. The mode of failure appeared to coincide with the prediction described in Section 3.7 and indicated by Fig.7. The prediction for the shear at failure was $0.44 V_{flex}$, or 12 percent higher than the measured.

The results predicted with monotonically increasing shear higher than $0.44 V_{flex}$ and reported in Section 3.2 through 3.6 are probably more indicative for the cases where the propagation of crack along flexural reinforcement was prevented by some measure. For the latter cases failure could occur due to crushing of concrete in the compression zone at cross sections some distance apart from the point of application of the load. This crushing may be attributed to the reduction in dimension of the path for compressive stress trajectories due to development of flexural and inclined cracks and cracks in the top surface of the beam.

4. CONCLUSIONS

The analytical and experimental study reported here was concerned with the shear failure of the beams with a rectangular cross section, without web reinforcement and where the ratio of shear span and beam effective depth was equal to three. Within the scope of this study the following conclusions appeared relevant.

1. The finite element method of analysis used here appeared to predict the behavior of the beams failing under the influence of shear and bending in terms of crack pattern, mode of failure and the shear at failure, if adequate considerations are made for bond between flexural reinforcement and concrete, criterion for crushing and cracking of concrete, and progressive propagation of cracks by the procedure given in this study.
2. The suppression of occurrence of flexural cracks at prescribed locations used in this study is a convenient practice to substitute a difficult but very important problem of idealizing the non-uniform bond between steel and concrete.
3. The finite element method of analysis used in this study enabled prediction of progressive development of cracks along the flexural reinforcement near the failure load by a few increments of analysis where the external load was set equal to zero and only the forces resulting from the stresses relieved from concrete elements which failed were considered.

ACKNOWLEDGMENT

This study was supported by the Grant-in-Aid for Scientific Research No.246118 from the Japanese Ministry of Education.

REFERENCES

1. Kokubu, M., Yamada, Y. and Sakurai, T., "Method of Analysis for Composite Materials", Report to Monbusho for the Special Project, March, 1977. (in Japanese)
2. Kupfer, H.B. and Gerstle, K.H., "Behavior of Concrete Under Bi-axial Stresses", ASCE, Vol.99, No.EM4, August, 1973, pp.853-866.
3. Kani, G.N.J., "The Riddle of Shear Failure and Its Solution", ACI Journal, Proceedings, Vol.61, No.4, April, 1964, pp.441-467.
4. Kani, G.N.J., "A Rational Theory for the Function of Web Reinforcement", ACI Journal, Proceedings, Vol.66, No.3, March, 1969, pp.185-197.

IV

Optimization of Reinforcement in Slabs by Means of Linear Programming

Optimisation de l'armature des plaques par la programmation linéaire

Optimierung der Bewehrung von Platten mit Hilfe der linearen Programmierung

H. PEDERSEN

Structural Engineer

Cowiconsult

Virum, Denmark

SUMMARY

This paper is concerned with the development of a numerical method for designing reinforced concrete slabs by linear programming. The total amount of reinforcement necessary in a slab with given concrete dimensions, subjected to given loads and with a given arrangement of the reinforcing bars, is minimized. The linear programming problem is formulated using the principles of the lower bound method. The continuum problem is discretized by means of equilibrium finite element types. The linearized yield conditions are established in a number of discrete points to ensure a safe stress field.

RESUME

Le développement d'une méthode numérique est présenté pour le dimensionnement de dalles en béton armé à l'aide de la programmation linéaire. Le volume total de l'armature nécessaire pour une dalle dont la géométrie, le chargement et le système d'armature sont donnés, est minimalisé. Le programme linéaire est formulé en appliquant les principes de la méthode statique de la théorie des charges ultimes. Le problème continu est discrétisé par des éléments finis du type modèle équilibre. Les conditions d'écoulement linéarisées sont établies pour un nombre de points afin d'assurer la stabilité du champ de contraintes.

ZUSAMMENFASSUNG

Die Entwicklung eines numerischen Verfahrens zur Bemessung von Stahlbetonplatten mit Hilfe der linearen Programmierung wird dargestellt. Der insgesamt erforderliche Aufwand an Bewehrung für eine Platte mit gegebenen Abmessungen, gegebenen Lasten und einer vorgewählten Bewehrungsanordnung wird minimiert. Gestützt auf die statische Methode wird das lineare Programm formuliert. Das kontinuierliche Problem wird mit Finiten Elementen vom Gleichgewichtstyp diskretisiert. Die Stabilität des Spannungszustandes wird gesichert, indem die linearisierten Fließbedingungen für die Anzahl diskreter Punkte aufgestellt werden.



1. INTRODUCTION

Bound methods of limit analysis have proved to be powerful tools for the determination of the ultimate limit load for many structures. Also in the calculations of reinforced concrete slabs plastic theory has been successfully used for years. Johansen [1] formulated the yield-line theory leading to upper bound solutions which theoretically are unsafe solutions.

Since then, many attempts have been made to create safe methods. The establishment of a general plastic theory for reinforced concrete slabs has made it possible to use lower bound methods giving results on the safe side. The major part of this work was done by Nielsen [2] in the early sixties. Based on the theory of perfectly plastic materials, Nielsen [2] formulated the general yield conditions for orthotropic slabs.

The great advantages of using lower bound methods are really achieved when computerizing the construction of the equilibrium solutions. The statically admissible stress fields can be created for instance by means of finite element methods. Overall equilibrium requirements result in a set of linear equations in the stress parameters. A safe stress field is ensured by establishing the yield conditions in a set of discrete points in each element.

Many authors have adopted this approach in the evaluation of the bearing capacity for a given slab subjected to proportional loading. As the yield conditions are not linear, the optimization problem is non-linear. If the yield conditions are linearized, one gets a case of linear programming, LP, which can be solved by general available standard routines. Calculations of this kind for concrete slabs have been performed by Anderheggen and Knöpfell [3] and Knöpfell [4]. For materials governed by the Tresca yield criteria, Faccioli and Vitiello [5] have carried out a similar calculation.

Most of the numerical methods leading to LP-problems include both upper- and lower bound techniques expressing the analogy between the duality of the limit analysis theorems and the duality theorem of LP.

It has been concluded by the author [6] that with the present knowledge of the existing optimization techniques - especially concerning reliability and efficiency - an automatic limit design method for practical use should be based on LP. Moreover, it is stated that using LP no results can be achieved by upper bound methods that cannot be produced by lower bound methods alone. The most economic design will often be obtained by varying the reinforcement over the slab area. This case can be treated directly by the lower bound method but can hardly be done by upper bound methods. Further, it has been demonstrated by the author [7] that based on lower bound techniques the limit analysis problem as well as the limit design problem can easily be handled by means of the same computer programme. Thus the LP-problem should be formulated using the principles of the lower bound method.

The general approach adopted here in the development of a rational and safe design method was at first presented by Wolfensberger [8], who used Hillerborgs [9] strip method to generate a parametric moment field.

In this paper, only thin slabs are dealt with. The Kirchhoff plate theory is adopted and the material is assumed to be rigid plastic. The optimization criteria is the minimum of the total amount of tensile reinforcement. The arrangement of the reinforcing bars can be chosen a priori to ensure a design for direct practical use. Arbitrarily reinforced slabs with given directions of the reinforcing bars can be handled. Slabs with various geometry and different types of boundary conditions, together with column supports are dealt with. The design is carried out for a set of given loading cases.

As examples to illustrate the method designs of an isotropic square built-in slab and a flat plate construction are shown.

2. MATHEMATICAL FORMULATION OF THE DESIGN PROBLEM

Equilibrium element types are used to discretize the continuum problem. The moment field for the slab is represented by the NM global parameters contained in the vector \underline{M} . The moment field for an element, e , is given by the nm parameters \underline{m}^e . The relation between these and the global parameters is for each element given by:

$$\underline{m}^e = \underline{G}^e \times \underline{M} \quad (2.1)$$

By means of interpolation functions the moments referring to a global x-y-system, $\underline{m} = (m_x, m_{xy}, m_y)$, can be expressed in the form:

$$\underline{m} = \underline{a}^e \times \underline{m}^e \quad (2.2)$$

For each element the boundary forces, \underline{r}^e , necessary to express the required statical continuity conditions are calculated from:

$$\underline{r}^e = \underline{k}^e \times \underline{m}^e \quad (2.3)$$

By means of (2.1-3) all equilibrium requirements such as internal requirements, continuity requirements along the element boundaries and the statical boundary conditions lead to a set of linear equations in the global parameters:

$$\underline{K} \times \underline{M} = \underline{P} \quad (2.4)$$

where the vector \underline{P} represents the effects of the given loads.

The design variables, which are the steel areas, for the slab are established in the ND-dimensional design vector \underline{D} . For each element the plastic moments, $\underline{m}_p^e = (m_{Fx}, m_{Fy}, m_{Fxy}, m'_{Fx}, m'_{Fy}, m'_{Fxy})$, see section 4, are expressed by the relevant steel areas by:

$$\underline{m}_p^e = \underline{E}^e \times \underline{D} + \underline{m}_{p,o}^e \quad (2.5)$$

where $\underline{m}_{p,o}^e$ are plastic moments due to given reinforcement.

By means of (2.1-2) and (2.5) the linearized yield conditions set up in some a priori selected points for each element, lead to a set of linear inequalities in the global moment parameters and the design variables:

$$\underline{R}^1 \times \underline{M} + \underline{R}^2 \times \underline{D} \leq \underline{R}_0 \quad (2.6)$$

where \underline{R}_0 expresses the contribution of given reinforcement in (2.5).

Several explicit linear constraints in the design variables such as given intervals for certain steel areas, desired linear relationships between different steel areas etc. can be handled. For clarity, such relationships will be assumed to be included in (2.6).

The total amount of reinforcement is expressed as a linear function in the design variables:

$$\underline{Z} = \underline{C} \times \underline{D} \quad (2.7)$$

In this way, the design problem is formulated as a case of LP:

$$\begin{aligned} &\text{minimize:} && \underline{Z} = \underline{C} \times \underline{D} \\ &\text{subject to} && \underline{K} \times \underline{M} = \underline{P} \quad \text{and:} \quad \underline{R}^1 \times \underline{M} + \underline{R}^2 \times \underline{D} \leq \underline{R}_0 \end{aligned} \quad (2.8)$$



3. ELEMENT TYPES, STATICAL EQUATIONS

For many equilibrium slab elements used in elastic calculations the corresponding stress field can be used here directly to generate parametric statically admissible fields. Two such element types are given below, i.e. the triangular element with a constant moment field, TRIC, and the triangular element with a linear moment field TRIL. A direct way can also be used to derive applicable element types considering only the statical properties. An example of this is given by the rectangular element RECT. For the element matrices the reader is referred to reference [6].

Triangular element, TRIC

The geometrical and statical properties of the element are shown in Fig. 3.1. The element parameters can be chosen as:

$$\tilde{m}^e = (m_{b1}, m_{b2}, m_{b3})^T \quad (3.1)$$

The only vertical forces acting at an element are the concentrated corner forces due to discontinuities in the torsional moments. These are established in the vector:

$$\tilde{r}^e = (P_1, P_2, P_3)^T \quad (3.2)$$

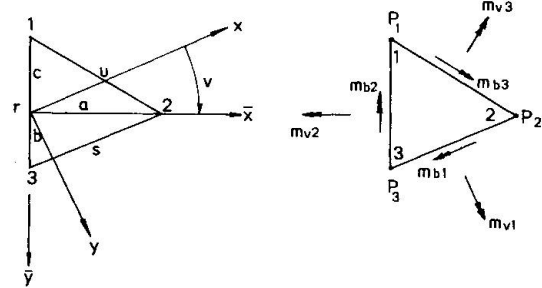


Fig. 3.1: Triangular element, TRIC

It is thus seen that only concentrated forces acting at the nodes of the element mesh can be handled.

Triangular element, TRIL

This element is due to Veubeke [10], who used it in elastic slab analysis.

The moment field is linear and can thus be represented by nine parameters for each element. The analysis is most easily carried out in a local ablique reference system as shown in Fig. 3.2 where sign conventions and the nine parameters are also shown. The parameters are:

$$\tilde{m}^e = (\bar{m}_1, \bar{m}_2, \bar{m}_3)^T$$

$$\text{where } \bar{m} = (m_{\bar{x}}, m_{\bar{x}\bar{y}}, m_{\bar{y}}) \quad (3.3)$$

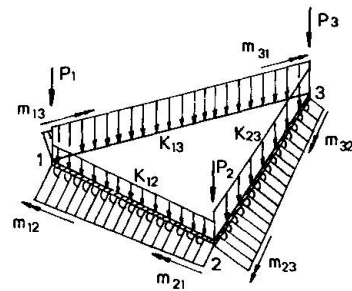
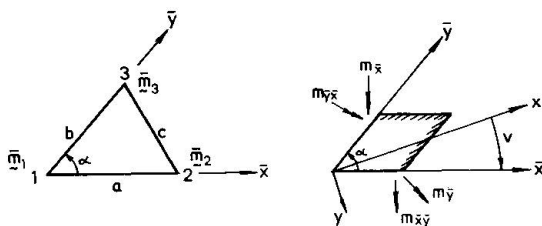


Fig. 3.2 Triangular element, TRIL.

Fig. 3.3 Boundary forces.

The corresponding boundary and nodal forces, shown in Fig. 3.3, are contained in the following vector:

$$\underline{r}^e = (m_{12}, m_{21}, m_{13}, m_{31}, m_{23}, m_{32}, K_{12}, K_{13}, K_{23}, P_1, P_2, P_3)^T \quad (3.4)$$

Line loads with constant intensity along element boundaries and concentrated loads acting at the nodes of the element mesh can be handled.

Rectangular element, RECT

The slab area is subdivided into rectangular elements by lines parallel to the axes of the global reference system.

The moment field for an element is given by the ten parameters:

$$\underline{m}^e = (m_x^1, m_x^2, m_{xy}^1, m_{xy}^2, m_{xy}^3, m_{xy}^4, m_y^1, m_y^2, p_x, p_y)^T \quad (3.5)$$

These parameters are shown in Fig. 3.4. The variation of the m_x -moment is parabolic in the x-direction and constant in the y-direction. Analogous for the m_y -moment. The torsional moment m_{xy} is represented by a hyperbolic paraboloid and is thus linear at the element boundaries.

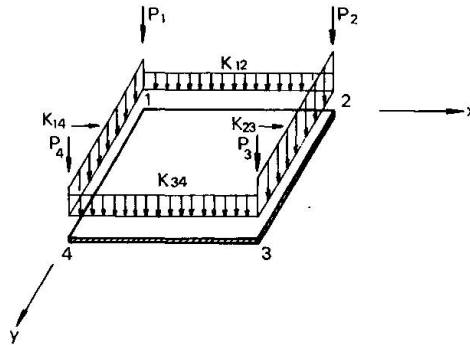
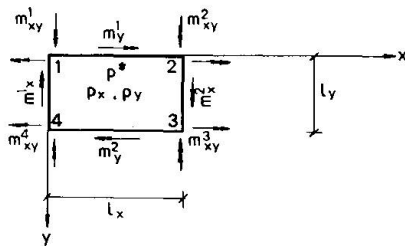


Fig. 3.4 Rectangular element, RECT

Fig. 3.5 Boundary forces.

The Kirchhoff' shear forces and the concentrated forces acting at the corners of the element, see Fig. 3.5, are expressed by the following vector:

$$\underline{r}^e = (K_{12}, K_{23}, K_{34}, K_{41}, P_1, P_2, P_3, P_4)^T \quad (3.6)$$

One equation needs to be satisfied to ensure internal equilibrium. From the \underline{a}^e -matrix one gets directly:

$$m_{xy}^1 + m_{xy}^3 - m_{xy}^2 - m_{xy}^4 = \frac{1}{2} l_x l_y (p^* - p_x - p_y) \quad (3.7)$$

Distributed loads with constant intensity for each element, line loads acting at element boundaries and concentrated loads acting at the nodes can be handled.

4. YIELD CONDITIONS

Yield conditions for arbitrarily reinforced concrete slabs have been derived by many authors on the basis of Johansen's suggestions for the moments in a yield-line. For instance, this has been done by Bræstrup [11], who used polar diagrammes to formulate the yield conditions.

$$\left. \begin{aligned} \varphi_1 &= - (m_{Fx} - m_x) (m_{Fy} - m_y) + (m_{xy} - m_{Fxy})^2 \leq 0 \\ \varphi_2 &= - (m'_{Fx} + m_x) (m'_{Fy} + m_y) + (m_{xy} - m'_{Fxy})^2 \leq 0 \end{aligned} \right\} \quad (4.1)$$



Here, m_{Fx} is the numerical value of the positive yield moment in pure bending in an x-section and m'_{Fx} is the numerical value of the negative yield moment in that section. Analogous for m_{Fy} and m'_{Fy} . m_{Fxy} and m'_{Fxy} are the plastic torsional moments due to reinforcement at the bottom and the top respectively. The yield conditions (4.1) include the conditions for orthotropic slabs ($m_{Fxy} = m'_{Fxy} = 0$) as a special case, see reference [2].

A safe linearization of the yield conditions has been suggested by Wolfensberger [8], leading to the following eight inequalities:

$$\left. \begin{aligned} -m_{Fx} + m_x + \frac{1}{2}(m_{xy} - m_{Fxy}) &\leq 0 \\ -m_{Fy} + m_y + \frac{1}{2}(m_{xy} - m_{Fxy}) &\leq 0 \\ -m'_{Fx} - m_x + \frac{1}{2}(m_{xy} - m'_{Fxy}) &< 0 \\ -m'_{Fy} - m_y + \frac{1}{2}(m_{xy} - m'_{Fxy}) &< 0 \end{aligned} \right\} \quad (4.2)$$

This linearization has also been used in reference [3] and [4].

As the relationships between the plastic moments and the corresponding steel areas are assumed to be linear, which is a good approximation for such small degrees of reinforcement for which the yield conditions (4.1) are valid, the linearized conditions (4.2) are also linear in the design variables. The plastic moments are assumed to be constant within each element and are given by the vector \underline{m}^e as shown in section 2. For example, the linear expression for m_{Fx} is:

$$m_{Fx} = F_1 \cos^2 u_1 + \dots + F_{ND} \cos^2 u_{ND} \quad (4.3)$$

where u_i is the angle relative to the x-axis for the reinforcement with steel area D_i . If the reinforcement with steel area D_i is not to be represented at the bottom of the element the F_i -factor for m_{Fx} , m_{Fy} and m_{Fxy} is set to zero.

From the given arrangement of reinforcing bars formulated in (4.3), the linear objective function is derived automatically. The c_i -value simply represents the slab area in which the reinforcement with corresponding steel area D_i is extended.

For the element type with constant moment field, TRIC, the linearized yield conditions only have to be established at one point per element. For the element with linear moment field, TRIL, establishment in the three corners of each element will ensure overall fulfillment. For the rectangular element, RECT, the yield conditions (4.2) are set up in the corners and in the centre of the element. For no loading cases this alone can ensure a true lower bound solution. For the solution obtained the yield conditions (4.1) are checked in a finer mesh and the solution is proportioned if needed to fulfil (4.1) in all check-points.

5. NUMERICAL TREATMENT OF THE LP-PROBLEM

The LP-problem stated in (2.8) can be solved directly by means of many LP-codes. However, it can be considerably reduced, and an easy way of treating different loading cases simultaneously can be obtained by solving the linear equations (2.4) first. By means of a rank-method, some moment parameters, \underline{M}_a , can be expressed in terms of the redundancies, \underline{M}_u , by:

$$\underline{M}_a = \underline{K}^r \times \underline{M}_u + \underline{M}_0 \quad (5.1)$$

where \underline{M}_0 represents a particular solution for the actual loading case.

The LP-problem is then reduced to:

$$\left. \begin{array}{l} \text{minimize:} \quad Z = \underline{c} \times \underline{D} \\ \text{subject to:} \quad \underline{R}_u \times \underline{M}_u + \underline{R}^2 \times \underline{D} \leq \underline{R}_o \end{array} \right\} \quad (5.2)$$

where the particular solution is now introduced into the \underline{R}_o -vector.

If the slab is to be designed according to different loading cases, one only has to establish (5.1) once. For each loading case, i , the particular solution, \underline{M}_u^i , is calculated and the right-hand sides, \underline{R}_o^i , in the linear constraints are obtained by substitution in (2.6). By this procedure the following LP-problem is formulated:

$$\left. \begin{array}{l} \text{minimize:} \quad Z = \underline{c} \times \underline{D} \\ \text{subject to:} \quad \left. \begin{array}{l} \underline{R}_u \times \underline{M}_u^1 + \underline{R}^2 \times \underline{D} \leq \underline{R}_o^1 \\ \vdots \\ \underline{R}_u \times \underline{M}_u^n + \underline{R}^2 \times \underline{D} \leq \underline{R}_o^n \end{array} \right\} \\ \text{and:} \end{array} \right\} \quad (5.3)$$

Solving this problem, the global optimum (according to the linear model) will be obtained.

An approximate optimum can be achieved by solving the LP-problem:

$$\left. \begin{array}{l} \text{minimize:} \quad Z = \underline{c} \times \underline{D} \\ \text{subject to:} \quad \underline{R}_u \times \underline{M}_u + \underline{R}^2 \times \underline{D} \leq \underline{R}_o^{\min} \\ \text{and:} \quad R_{o,j}^{\min} = \min (R_{o,j}^1, \dots, R_{o,j}^n) \end{array} \right\} \quad (5.4)$$

The design, considering more than one loading case, can also be carried out by successive calculations. For the loading case, i , all reinforcement quantities as obtained earlier are treated as given through \underline{m}_p^i , and only necessary additional reinforcement, if any, is determined.

The computer time needed to solve the LP-problem, either (5.3) or (5.4), can be reduced by solving the corresponding dual LP-problem. Concerning this, the reader is referred to reference [7].

Numerical calculations using the described method have been performed on the IBM/360-system at the Technical University of Denmark, Copenhagen, using the MPS/360 linear programming code.

6. RESULTS

The design of two different types of concrete slabs with orthogonal reinforcement (orthotropic slabs) is shown.

Square built-in slab

The isotropic square slab with clamped edges is designed using the RECT-element ($m_{Fx} = m_{Fy} = m'_{Fx} = m'_{Fy} = m_F$). The load is uniformly distributed and denoted by p . The result is represented by the quantity $\rho = p l^2 / m_F$. In Fig. 6.1 the result is shown as a function of the mesh size.

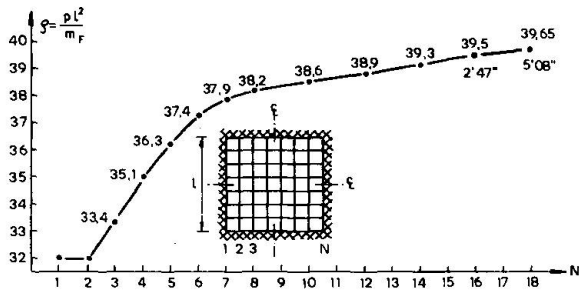


Fig. 6.1 Rectangular element.

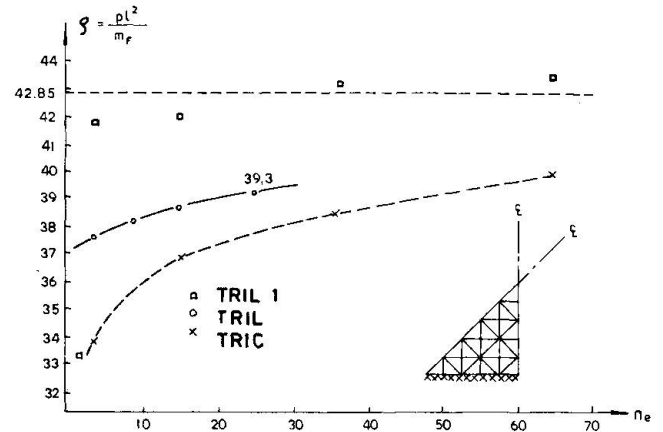


Fig. 6.2 Triangular elements.

This slab has also been calculated by means of triangular elements. The results are given in Fig. 6.2 where n_e is the number of elements in the considered eighth part of the slab.

The results obtained by the TRIC-element have been determined by Anderheggen and Knöpfell [3], who have also given the results according to the element here called TRIL 1. This element has a linear moment field with continuous torsional moments along element boundaries. Considering linear displacement fields for each element, statical equilibrium requirements are established using virtual work methods. In this way, overall equilibrium can never be ensured. Thus the results obtained do not represent true bound solutions.

In comparison, it should be mentioned that Chan [12], using non-linear optimization has determined the value 41.78 for a computer time considerably larger than those met here using linear programming. The exact solution of this problem is $\rho = 42.851$ and was found by Fox [13].

Flat Plate Structure

For the uniformly loaded flat plate structure shown in Fig. 6.3, the total amount of steel is minimized for different arrangement of the reinforcement. The RECT element is used. The three cases: a) $m_{Fx} = m_{Fy} = m_F' = m_F'' = m_F \sim D_1$, b) $m_{Fx} = m_{Fy} = m_F \sim D_1$, $m_F' = m_F'' = m_F' \sim D_2$ and c) $m_{Fx} = m_{Fy} = m_F \sim D_1$, $m_F' = m_F'' = 0$ all give the same total amount of reinforcement denoted by A. In case a) is found $m_F = 0.0685 p l^2$.

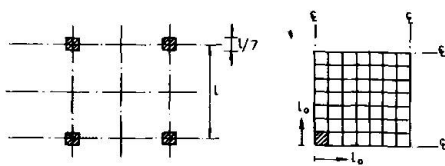


Fig. 6.3 Flat plate structure.

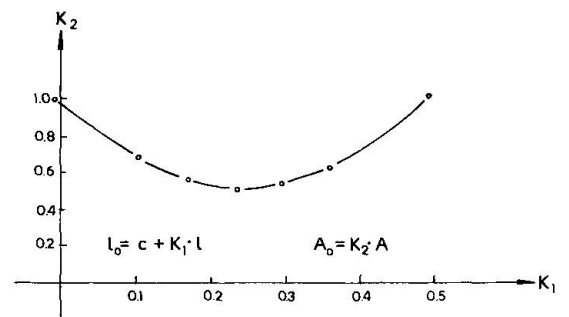


Fig. 6.4 Restricted top reinforcement.



Johansen [14] suggests from yield-line calculations that if the bottom reinforcement is homogenous throughout the slab, and the top reinforcement is homogenous only in a square at the column (zero elsewhere), the latter must have an extension from the centre of the column given by $l_o = c + 0.3 l$, where c is the radius of the circle with the same area as the cross section of the column. This problem has been calculated for different values of l_o (l_o is shown in Fig. 6.3). The corresponding amounts of reinforcement, A_o , are given in Fig. 6.4 as a function of l_o .

The results show that a minimum is obtained for $l_o \sim c + 0.23 l$, for which the amount of reinforcement is reduced to $A_o \sim 0.5 A$.

7. FINAL REMARKS

Results show that linear programming methods require longer computer times compared to those required for calculations on linear elasticity. However, continued developments in the field of electronic computers can be expected to result in reduced prices so that practical design will be able to profit by these methods in the near future.

Moreover, the advantages of these automatic methods in the area of practical design should be emphasized. In this case, the alternative methods are normally not the very sophisticated methods available in the field of structural analysis.

Concerning the finite element discretization, it should be mentioned that procedures like the one adopted by Anderheggen and Knöpfell [3], leading to approximate bound solutions, will probably be successful in practical design methods. This is due to the fact that concerning calculations in practice, one will often accept a design which is safe for a loading case a little different from the prescribed one.

ACKNOWLEDGMENT

The present paper is based on a part of a Ph.D.-thesis (lic. techn.) written under the general supervision of Prof., dr.techn. M.P. Nielsen, Structural Research Laboratory, Technical University of Denmark.

REFERENCES

- 1 Johansen, K.W.: Brudlinieteorier, København, 1943.
- 2 Nielsen, M.P.: Limit Analysis of Reinforced Concrete Slabs, Acta Polytechnica Scandinavia, Copenhagen, 1964.
- 3 Anderheggen, E. and Knöpfell, H.: Finite Element Limit Analysis using Linear Programming, Int. J. Solids Structures, Vol. 8, pp. 1413-1431, 1972.
- 4 Knöpfell, H.: Berechnung Starr-plastischen Platten Mittels Finiten Elementen, Diss. No. 5034, ETH, Zürich, 1973.
- 5 Faccioli, E. and Vitiello, E.: A Finite Element Linear Programming Method for the Limit Analysis of Thin Plates, Int. J. Numm. Eng., Vol. 5, pp. 311-325, 1973.
- 6 Pedersen, H.: Optimizing af Jernbetonplader, Ph.D.-thesis, Structural Research Laboratory, Technical University of Denmark, to be published.
- 7 Pedersen, H.: Optimum Design of Thin Concrete Plates, Proc. Int. Symp. Discr. Meth. Eng., CISE-SEGRATE, Milan, pp. 374-389, 1974.



- 8 Wolfensberger, R.: Traglast und optimale Bemessung von Platten, Diss., ETH, Zürich, 1964.
- 9 Hillerborg, A.: Strimlemetoden, Stockholm, 1959.
- 10 Veubeke, B.F. and Sander, G.: An Equilibrium Model for Plate Bending, Int. J. Solid Structures, Vol. 4, pp. 447-468, 1968
- 11 Bræstrup, M.W.: Yield-line Theory and Limit Analysis of Plates and Slabs, Magazine of Concrete Research, Vol. 27, No. 71, pp. 99-106, 1970.
- 12 Chan, H.S.Y.: The Collapse Load of Reinforced Concrete Plates, Int. J. Numm. Meth. Eng., Vol. 5, pp. 57-64, 1972.
- 13 Fox, E.N.: Limit Analysis for Plates: The Exact Solution for a Clamped Square Plate of Isotropic Homogenous Material Obeying the Square Yield Criterion and Loaded by Uniform Pressure. Phil. Trans. Roy. Soc., Vol. 277A, pp. 121-155, 1974.
- 14 Johansen, K.W.: Yield-line Formulae for Slabs, Cement and Concrete Association, London 1972.

IV

Mesh Formulation of the Yield Line Method by Mathematical Programming

La formulation en mailles de la méthode des lignes de rupture par la programmation mathématique

Die Netzformulierung der Bruchlinienmethode mit Hilfe der mathematischen Programmierung

A.M.A. DA FONSECA

Civil Engineering Department
University of Oporto
Portugal

J. MUNRO

Civil Engineering Department
Imperial College
London, England

SUMMARY

The yield line method has been formulated as a mathematical programming problem using a mesh description of a finite element network. The fundamental structural relations have been transformed to an equivalent primal-dual pair of mesh linear programs using the Kuhn-Tucker theory. These programs, along with the primal-dual pair of nodal linear programs derived previously, provide a choice of four programs available for computation. A comparison has been made of the relative computational effort required for these programs when using a simplex-based computer code.

RESUME

La formulation en mailles développée pour la méthode des éléments finis a été appliquée à la méthode des lignes de rupture. On a obtenu une paire „primal-dual“ de programmes linéaires équivalente aux relations structurales qui gouvernent la dite description, en utilisant la théorie de Kuhn-Tucker. Ces programmes offrent, avec la paire „primal-dual“ de programmes linéaires déjà dérivée pour la description nodale, un éventail de quatre programmes de calcul. On a finalement comparé les difficultés de calcul inhérentes à chacun de ces programmes en utilisant l'algorithme du Simplex.

ZUSAMMENFASSUNG

Die Bruchlinienmethode wurde mit Hilfe einer Netzbeschreibung eines finiten Element-Netzes dargestellt. Die grundlegenden strukturellen Beziehungen wurden unter Verwendung der Kuhn-Tucker Theorie zu einem entsprechenden „primal-dualen“ Paar von linearen Programmen transformiert. Diese, und das früher hergeleitete „primal-duale“ Paar von linearen Programmen für die Knotenbeschreibung, liefern eine Auswahl von vier für die Berechnung verfügbaren Programmen. Schliesslich wurde der für jedes dieser Programme erforderliche relative Rechenaufwand bei Verwendung des Simplex Algorithmus verglichen.



1. INTRODUCTION

The plastic limit analysis and synthesis of structural *frames* may be formulated conveniently as linear programs (LPs) using either a mesh [1] or nodal [2] description of the structure to formulate the fundamental static and kinematic relations. Each description leads to a primal-dual pair of LPs and thus, for the numerical computation, a choice must be made between four possible programs. Whilst the nodal description is most commonly used, it has been shown [3] [4] recently that the required computational effort with respect to simplex-based algorithms is greatly reduced when the mesh description is employed.

A particularly simple and convenient form of manually-computed plastic limit analysis is embodied in the yield line method (YLM) [5] [6]. This method may be automated to the plastic limit analysis [7] and synthesis [8] of r.c. slabs through FEs and linear programming. The LPs formulated in this way have the same algebraic structure as those obtained previously for frames using the *nodal* description. Since the programs obtained from the *mesh* description for frames had computational advantages, it would appear logical to seek a corresponding mesh formulation for the slab problem and to see if these advantages carry over to this different class of problem.

The nodal description commences with a statement of the (nodal) fundamental kinematic relations and then seeks the corresponding static relations such that an appropriate criterion of consistency is satisfied. The criterion adopted [7] is that of static-kinematic duality (SKD) [1]. The mesh description to be presented herein commences with a statement of the (mesh) fundamental static relations and then derives the corresponding kinematic relations such that SKD is maintained.

2. STATICS

The normal bending moments (\underline{m}) at the FE sides are considered as the superposition of a particular solution (\underline{m}_0) which equilibrates the loading and a complementary solution (\underline{m}_c) which consists of a linear combination of independent self-equilibrating moment fields.

$$\underline{m} = \underline{m}_0 + \underline{m}_c \quad (1)$$

The particular solution can be readily obtained if, as indicated on Fig. 1, the slab is split into cantilevers.

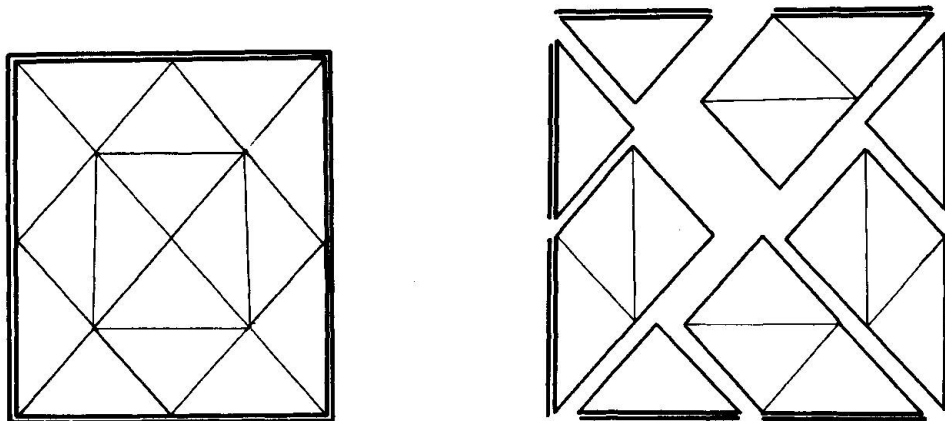
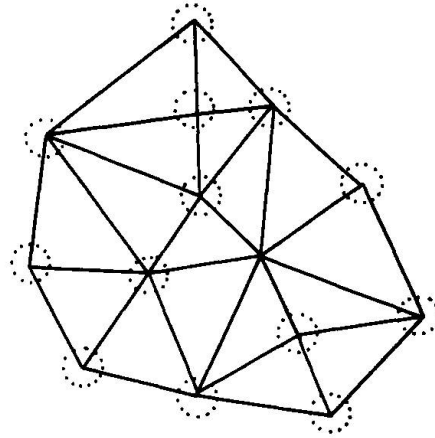


Fig.1: Cantilever Slabs

Clearly, such a procedure implies edge fixity. However, if other boundary conditions pertain, then they can be incorporated as outlined elsewhere [9].

The complementary solution (\tilde{m}_c) will be based on a set of linearly independent meshes. The simplest such set will be obtained from the FEs which are incident on each of the nodes except one. Such a set is shown in Fig. 2 and these meshes are analogous to the regional meshes of frame theory [4].

Fig. 2: Linearly independent set of finite element meshes



For example, the complementary solution total normal bending moments at the FE sides of the mesh represented in Fig. 3 may be expressed in terms of two static parameters (p_1 and p_2) in the following form

$$\begin{bmatrix} m_{s1} \\ m_{s2} \\ m_{s3} \\ m_{s4} \\ m_{s5} \end{bmatrix} = \begin{bmatrix} \sin \alpha_1 & \cos \alpha_1 \\ \sin \alpha_2 & \cos \alpha_2 \\ \sin \alpha_3 & \cos \alpha_3 \\ \sin \alpha_4 & \cos \alpha_4 \\ \sin \alpha_5 & \cos \alpha_5 \end{bmatrix} \begin{bmatrix} p_1 \\ p_2 \end{bmatrix} \quad (2)$$

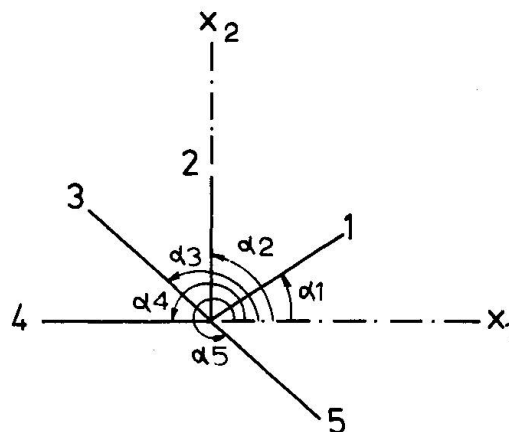
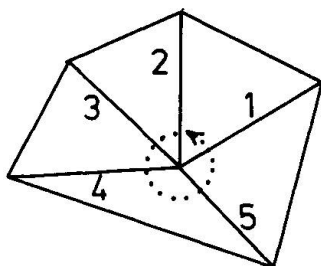


Fig. 3: Example of finite element mesh

Now, if relations (2) are established for all such regional meshes, then they can be assembled in the following compact form

$$\tilde{m}_c = \tilde{B} p \quad (3)$$



and the parameters \underline{p} will be termed the *mesh actions*. Thus, the mesh equilibrium equations (1) become

$$\boxed{\underline{m} = \underline{m}_0 + \underline{B} \underline{p}} \quad (4)$$

3. KINEMATICS

The conditions of compatibility for every mesh must ensure that the modal angular deformation rates ($\dot{\underline{\theta}}$) across yielding FE sides correspond to continuity of vertical displacements. For example, for the FE sides of the mesh represented in Fig. 3,

$$\begin{bmatrix} \sin \alpha_1 & \sin \alpha_2 & \sin \alpha_3 & \sin \alpha_4 & \sin \alpha_5 \\ \cos \alpha_1 & \cos \alpha_2 & \cos \alpha_3 & \cos \alpha_4 & \cos \alpha_5 \end{bmatrix} \begin{bmatrix} \dot{\theta}_1 \\ \dot{\theta}_2 \\ \dot{\theta}_3 \\ \dot{\theta}_4 \\ \dot{\theta}_5 \end{bmatrix} = \begin{bmatrix} 0 \\ 0 \end{bmatrix} \quad (5)$$

Now, if these compatibility conditions are imposed on every mesh of a FE system, then they can be stated in the following compact form

$$\boxed{\underline{B}^T \dot{\underline{\theta}} = \underline{0}} \quad (6)$$

The contragredient relation connecting equations (3) and (6) is a manifestation of their consistency with respect to SKD.

Once again, the special treatment of various boundary conditions is discussed more fully elsewhere [9].

4. CONSTITUTIVE RELATIONS

The YLM employs a simple yield criterion

$$\underline{N}^T \underline{m} - \underline{m}_* \leq \underline{0} \quad (7)$$

where \underline{m}_* is the vector of the magnitudes of plastic moments of resistance and the normality matrix \underline{N} is given by

$$\underline{N} = \begin{bmatrix} \underline{I} & \underline{I} & -\underline{I} \end{bmatrix}$$

where \underline{I} is the identity matrix.

It is convenient to express the plastic modal deformations ($\dot{\underline{\theta}}$) in terms of non-negative components

$$\dot{\theta}_i = x_i^+ - x_i^- \quad \text{where} \quad x_i^+ \geq 0, \quad x_i^- \geq 0$$

Thus

$$\dot{\tilde{\theta}} = \tilde{N} \tilde{x} \quad (8)$$

where

$$\tilde{x} \equiv \begin{bmatrix} \tilde{x}^+ \\ \tilde{x}^- \end{bmatrix} \geq 0$$

and \tilde{N} is the normality matrix as previously described. Relations (8) constitute the flow rule for the considered problem.

The parity rule linking the static and kinematic variables can be expressed in the following complementary way.

$$\tilde{x}^T [\tilde{N}^T \tilde{m} - \tilde{m}_*] = 0 \quad (9)$$

5. FUNDAMENTAL STRUCTURAL RELATIONS

The particular solution bending moments (\tilde{m}_o) may be expressed as the sum of those due to dead load (\tilde{m}_{do}) and those due to live load (\tilde{m}_{lo}).

$$\tilde{m}_o = \tilde{m}_{do} + \tilde{m}_{lo} \quad (10)$$

If the \tilde{m}_{lo} vector is expressed in terms of a single load parameter (λ),

$$\tilde{m}_o = \tilde{m}_{do} + \tilde{r}_o \lambda \quad (11)$$

where \tilde{r}_o is the vector of live load particular solution bending moments per unit value of the load parameter (λ).

Substituting from (11) into (4), the equilibrium equations become

$$\tilde{m} = \tilde{m}_{do} + \tilde{r}_o \lambda + \tilde{B} \tilde{p} \quad (12)$$

and the static admissibility conditions are obtained by substituting from (12) into the yield conditions (7),

$$\tilde{A}^T \tilde{y} - \tilde{c} + \tilde{t} = 0 \quad (13)$$

where

$$\tilde{A} \equiv \begin{bmatrix} \tilde{r}_o^T & \tilde{N} \\ \tilde{B}^T & \tilde{N} \end{bmatrix} \quad \tilde{y} \equiv \begin{bmatrix} \lambda \\ \tilde{p} \end{bmatrix} \quad \tilde{c} = \tilde{m}_* - \tilde{N}^T \tilde{m}_{do}$$

and \tilde{t} are non-negative slack variables.

The plastic collapse deformation rates ($\dot{\tilde{\theta}}$) for a single-degree-of-freedom mode are fixed only up to a single parameter whose magnitude remains arbitrary. It will therefore be necessary to introduce some form of scaling so that the problem will have a finite kinematic solution. A convenient scaling is

$$\tilde{r}_o^T \tilde{N} \tilde{x} = 1 \quad (14)$$



The compatibility relations (6) and the flow rule (8) lead to

$$\tilde{B}^T \tilde{N} \tilde{x} = \tilde{0} \quad (15)$$

The kinematic admissibility conditions are obtained from equations (14) and (15)

$$\begin{bmatrix} \tilde{r}_0^T & \tilde{N} \\ \tilde{B}^T & \tilde{N} \end{bmatrix} \tilde{x} = \begin{bmatrix} 1 \\ 0 \end{bmatrix}$$

or, more compactly,

$$\tilde{A} \tilde{x} = \tilde{b} \quad (16)$$

Thus, the full set of fundamental structural relations in mesh form becomes

Statical Admissibility	$\tilde{A}^T \tilde{y} - \tilde{c} + \tilde{t} = \tilde{0}$	(17)
Kinematical Admissibility	$\tilde{A} \tilde{x} = \tilde{b}$	
Parity	$\tilde{x}^T \tilde{t} = 0$	
Sense restrictions	$\tilde{x} \geq 0 \quad \tilde{t} \geq 0$	

6. LINEAR PROGRAMS

The relations (17) constitute a linear complementarity problem (LCP). If they are regarded as Kuhn-Tucker conditions [10] then, from Kuhn-Tucker equivalence, their solution is also the solution of the following mesh primal-dual LPs of the YLM

$\begin{aligned} \text{Min } z &= \tilde{c}^T \tilde{x} \\ \tilde{A} \tilde{x} &= \tilde{b} \\ \tilde{x} &\geq 0 \end{aligned}$	$\begin{aligned} \text{Max } w &= \tilde{b}^T \tilde{y} \\ \tilde{A}^T \tilde{y} &\leq \tilde{c} \end{aligned}$	(18) (19)
Mesh Primal LP	Mesh Dual LP	

7. SOLUTION BOUNDS

From the duality theory [11] of LP, it follows that the optimal values of the two objective functions coincide and are equal to the collapse load (λ_c) for the YLM-FE model,

$$z_* = w_* = \lambda_c \quad (20)$$

Since the necessary compatibility requirements are satisfied, the plastic collapse load parameter (λ_c) for the YLM-FE model is an *upper bound* to the collapse load parameter (λ_c^c) for the continuous model.

$$\lambda_c \geq \lambda_c^c \quad (21)$$



Clearly, if the FE boundaries contain the yield lines of the true collapse mode of the continuous model, then the strict equality applies in relation (21).

The upper bound nature of the YLM-FE model also applies when a nodal description [7] is adopted. However, it has been shown elsewhere [9][12][13] that an FE formulation using approximating field functions can be devised such that the collapse load parameter is a lower bound on that of the continuous model.

8. COMPUTATIONAL EFFORT

If n_c is the number of constraints and n_v is the number of variables in the standard form of an LP, then the computational effort involved in a simplex-based computer code varies as $(n_c^3 n_v)$. It can be shown that the primal (unsafe) LP always involves less computation than the dual (safe) LP, irrespective of the description (nodal or mesh) used. The choice therefore lies between the nodal primal LP and the mesh primal LP for a YLM-FE model. The comparison between these two programs with respect to computational effort depends, to some extent, on the boundary conditions. However, as the number of FEs increases and the FE network tends to an infinitely fine one, then the influence of boundary conditions becomes less important and the nodal primal LP tends to require 450% of the computational effort of the corresponding mesh LP.

Another important consideration is the complexity of data preparation and organisation prior to entering the simplex-based code. Here the position with regard to the mesh description is, as yet, less satisfactory. However, this was also considered to be a disadvantage with respect to the mesh LPs for frames, but recent developments have largely overcome the problems and further research should improve the position with regard to slabs.

9. CONCLUSIONS

The mesh description, which has proved to be particularly convenient with respect to frames, can readily be adapted to a YLM-FE model of a reinforced concrete slab. The mesh primal-dual LPs for the slab problem have the same algebraic form as those for frames. Whilst the data preparation may require more attention, the computational effort required for the solution of the mesh primal LP is generally considerably less than that for the corresponding nodal primal LP.

10. ACKNOWLEDGEMENTS

This work was carried out in the Systems and Mechanics Section of the Civil Engineering Department, Imperial College, London, with the partial sponsorship of A M A Da Fonseca by the Instituto Nacional de Investigação Científica of Portugal.

11. REFERENCES

- [1] MUNRO J and D L SMITH. Linear Programming in Analysis and Synthesis, Proc. Int. Symp. Computer-Aided Struct. Design, Univ. of Warwick, vol. 1, pp A1/22-A1/54, July 1972.
- [2] MAIER G, R SRINIVASAN and M A SAVE. On Limit Design of Frames using Linear Programming, Proc. Int. Symp. Computer-Aided Struct. Design, Univ. of Warwick, vol. 1, pp A2/32-A2/59, July 1972.



- [3] SMITH D L. Plastic Limit Analysis and Synthesis of Structures by Linear Programming, PhD Thesis, Univ. of London, 1974.
- [4] MUNRO J. Optimal Plastic Design, NATO Advanced Study Institute on Engineering Plasticity by Mathematical Programming, Univ. of Waterloo, Ontario, Canada, 1977. To be published by Pergamon Press, 1979.
- [5] JOHANSEN K W. "Brudlinieteorier" (in Danish), Thesis, Copenhagen, Jul. Gjellerups Forlag, 1943. Eng. Trans: Yield-Line Theory, Cement and Concr. Assn, London, 1962.
- [6] JOHANSEN K W. "Pladeformler" (in Danish), Polyteknisk Forlag, Copenhagen, 1946. Eng. Trans: Yield-Line Formulae for Slabs, Cement and Concr. Assn, London, 1972.
- [7] MUNRO J and A M A DA FONSECA. Yield Line Method by Finite Elements and Linear Programming, The Structural Engineer, vol. 56B, no. 2, pp 37-44, June 1978.
- [8] MUNRO J and A M A DA FONSECA. Plastic Limit Design of Reinforced Concrete Slabs, Proc. IASS Symp. on Nonlinear Behaviour of Reinf. Concr. Spatial Structs, vol. 1, pp 163-176, Darmstadt, West Germany, Werner-Verlag Dusseldorf, July 1978.
- [9] DA FONSECA A M A. Plastic Limit Analysis and Synthesis of Plates and Shells by Mathematical Programming, Thesis to be submitted for PhD degree, Univ. of London, 1979.
- [10] KUHN H W and A W TUCKER. Nonlinear Programming, Proc. 2nd Berkeley Symp. Math. Statistics and Probability, pp 481-492, 1950.
- [11] DANTZIG G B. Linear Programming and Extensions, Princeton Univ. Press, New Jersey, 1963.
- [12] ANDERHEGGEN E and H KNÖPFEL. Finite Element Limit Analysis using Linear Programming, Int. Journ. of Solids Struct., vol. 8, pp 1413-1431, 1972.
- [13] DA FONSECA A M A, J MUNRO and D L SMITH. Finite Element Limit Analysis of Plates by Linear Programming, Proc. IASS Int. Conf. on Lightweight Shell and Space Structures for Normal and Seismic Zones, vol. 1, pp 95-106, Alma-Ata, USSR, MIR Publishers, Sept. 1977.

IV

Finite Element Aspects of Concrete Cracking

Eléments finis et fissuration du béton

Gesichtspunkte zur Rissberechnung im Beton

J.H. ARGYRIS G. FAUST K.J. WILLAM

Institut für Statik und Dynamik der Luft- und Raumfahrtkonstruktionen
Universität Stuttgart
Stuttgart, Fed. Rep. of Germany

SUMMARY

Two techniques are examined for the finite element analysis of cracking: The smeared approach and the discrete crack formulation are compared and illustrated with the example of a thick-walled concrete ring for which extensive experimental results have been made available by the IBIW III at the Technical University Munich.

RESUME

Deux procédés de calcul de la fissuration par la méthode des éléments finis sont examinés: Le modèle „barbouillé” et la formation discrète de fissures sont comparés et illustrés par l'exemple d'un anneau de béton à paroi épaisse, pour lequel de nombreux résultats de mesures existent.

ZUSAMMENFASSUNG

Zwei Verfahren werden untersucht zur Rissberechnung mit finiten Elementen: Das verschmierte Modell und die diskrete Rissformulierung werden am Beispiel eines dickwandigen Betonringes illustriert, an dem umfangreiche Messdaten des IBIW III, Technische Universität München, vorliegen.



INTRODUCTION

The knowledge of the inelastic behaviour and collapse of reinforced shell structures has been improved and increased in the past by experimental research. Early theoretical estimations of the collapse load were mainly based on the investigation into collapse modes and the use of a kinematical method similar to that known as the theory of yield lines for plates. This method permits to find an upper bound solution of the collapse load problem, but it is hardly suitable for reinforced concrete shells of more complex geometry and loading conditions.

Requirements on more generally applicable techniques led to the further development of numerical methods. One of the main ways of describing mathematically the inelastic behaviour of structures and calculating the collapse loads is based on the two fundamental theorems on lower and upper bounds and on the use of optimization procedures for linear and non-linear programming. A detailed description of the limit analysis of shells of revolution under axi-symmetric loads as an optimization problem by means of the Ritz method, the Bubnov-Galerkin method, the collocation method, the difference method and the method of finite elements is given in /1/.

METHOD OF SOLUTION

For rotationally symmetric shells under axi-symmetric one-parameter loading the collapse load intensity is found by solving the problem

$$\max_{p, N_\psi, N_\phi, M_\psi, M_\phi} \min_{\dot{v}_\psi, \dot{v}_\zeta, \lambda, \lambda_p} \Lambda(p, N_\psi, N_\phi, M_\psi, M_\phi, \dot{v}_\psi, \dot{v}_\zeta, \lambda, \lambda_p) \quad (1)$$

$p \geq 0$ on R_p

or

$$\min_{\dot{v}_\psi, \dot{v}_\zeta, \lambda, \lambda_p} \max_{N_\psi, N_\phi, M_\psi, M_\phi, p} \Lambda(p, N_\psi, N_\phi, M_\psi, M_\phi, \dot{v}_\psi, \dot{v}_\zeta, \lambda, \lambda_p) \quad (2)$$

$\lambda \geq 0$ in V
 $\lambda_p \geq 0$ on R_p

with the Lagrange functional

$$\Lambda = p + 2\pi \left[\int_{s_0}^{s_n} r_0 \left\{ [\dot{v}_\psi - r_\psi^{-1} \dot{v}_\zeta] N_\psi + r_0^{-1} [\cos\psi \dot{v}_\psi - \sin\psi \dot{v}_\zeta] N_\phi \right. \right. \\ \left. \left. + [-(r_\psi^{-1} \dot{v}_\psi)' - \dot{v}_\zeta'] M_\psi + r_0^{-1} [-r_\psi^{-1} \cos\psi \dot{v}_\psi - \cos\psi \dot{v}_\zeta] M_\phi \right\} ds \right]$$

$$\begin{aligned}
 & \left\{ + \lambda [c - f(N_\Psi, N_\Phi, M_\Psi, M_\Phi)] - [\bar{p}_\Psi \dot{v}_\Psi + \bar{p}_\zeta \dot{v}_\zeta] p + \lambda_p p \right\} ds \\
 & - p \left\{ [r_o P_\Psi \dot{v}_\Psi]_{R_{p\Psi}} + [r_o P_\zeta \dot{v}_\zeta]_{R_{p\zeta}} + [r_o M_s \dot{\chi}_\Psi]_{R_{p\chi}} \right. \\
 & \left. - [r_o n_s N_\Psi \dot{v}_\Psi]_{R_{v\Psi}} - [r_o n_s Q_\Psi \dot{v}_\zeta]_{R_{v\zeta}} - [r_o (-n_s) M_\Psi \dot{\chi}_\Psi]_{R_{v\chi}} \right\}
 \end{aligned} \quad (3)$$

In these expressions N_Ψ , N_Φ are the normal forces, M_Ψ , M_Φ the bending moments in the meridional and circumferential direction, respectively, \dot{v}_Ψ , \dot{v}_ζ the velocities of displacements tangential and perpendicular to the middle surface of the shell, $\dot{\chi}_\Psi$ the slope velocity, λ , λ_p flow parameters, and n_s the cosinus of the normal direction at the edges of the shell.

Along the meridian $s_0 \leq s \leq s_n$ the shell is subdivided into n intervals of the length Δs . The internal forces, displacement velocities, and flow parameters are approximated by functions of discrete argument (fig.).

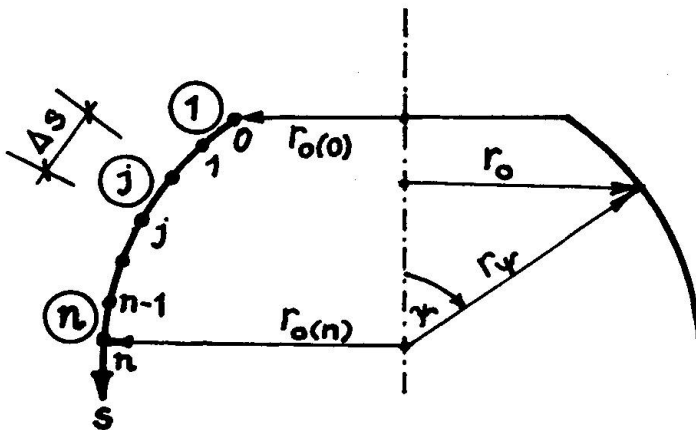


FIG. 1

Assuming that N_Ψ, N_Φ, M_Φ are constant within each interval j ($j=1, \dots, n$), they can be written as vectors in the form

$$\begin{aligned}
 N_\Psi(s) & \rightarrow \vec{\tilde{N}}_\Psi = [\tilde{N}_{\Psi(1)}, \dots, \tilde{N}_{\Psi(j)}, \dots, \tilde{N}_{\Psi(n)}]^T \\
 N_\Phi(s) & \rightarrow \vec{\tilde{N}}_\Phi = [\tilde{N}_{\Phi(1)}, \dots, \tilde{N}_{\Phi(j)}, \dots, \tilde{N}_{\Phi(n)}]^T \\
 M_\Phi(s) & \rightarrow \vec{\tilde{M}}_\Phi = [\tilde{M}_{\Phi(1)}, \dots, \tilde{M}_{\Phi(j)}, \dots, \tilde{M}_{\Phi(n)}]^T
 \end{aligned}$$

Both displacement velocities and meridional bending moment were approximated by their values at the discrete points j ($j=0, \dots, n$)



$$\begin{aligned}\dot{\mathbf{v}}_{\Psi}(s) &\longrightarrow \dot{\mathbf{v}}_{\Psi} = [\dot{v}_{\Psi}(0), \dots, \dot{v}_{\Psi}(j), \dots, \dot{v}_{\Psi}(n)]^T \\ \dot{\mathbf{v}}_{\zeta}(s) &\longrightarrow \dot{\mathbf{v}}_{\zeta} = [\dot{v}_{\zeta}(0), \dots, \dot{v}_{\zeta}(j), \dots, \dot{v}_{\zeta}(n)]^T \\ \mathbf{M}_{\Psi}(s) &\longrightarrow \mathbf{M}_{\Psi} = [M_{\Psi}(0), \dots, M_{\Psi}(j), \dots, M_{\Psi}(n)]^T\end{aligned}$$

The actual loading is replaced by concentrated forces $pP_{\Psi}(0), \dots, p\bar{P}_{\Psi}(n)$ and $p\bar{P}_{\zeta}(0), \dots, p\bar{P}_{\zeta}(n)$ at the points j .

As to the yield condition

$$f(N_{\Psi}, N_{\phi}, M_{\Psi}, M_{\phi}) \leq c$$

it will in general be more convenient to express it by a set of linear inequalities

$$a_{Fi}^{N_{\Psi}} N_{\Psi} + a_{Fi}^{N_{\phi}} N_{\phi} + a_{Fi}^{M_{\Psi}} M_{\Psi} + a_{Fi}^{M_{\phi}} M_{\phi} \leq b_{Fi} \quad (i=1, \dots, m) \quad (4)$$

For shells under consideration it is justified to neglect the interaction between circumferential and meridional response of the shell, and for practical calculations it will be sufficient to approximate the yield locus in each direction by 6 or 7 straight lines (fig.2)

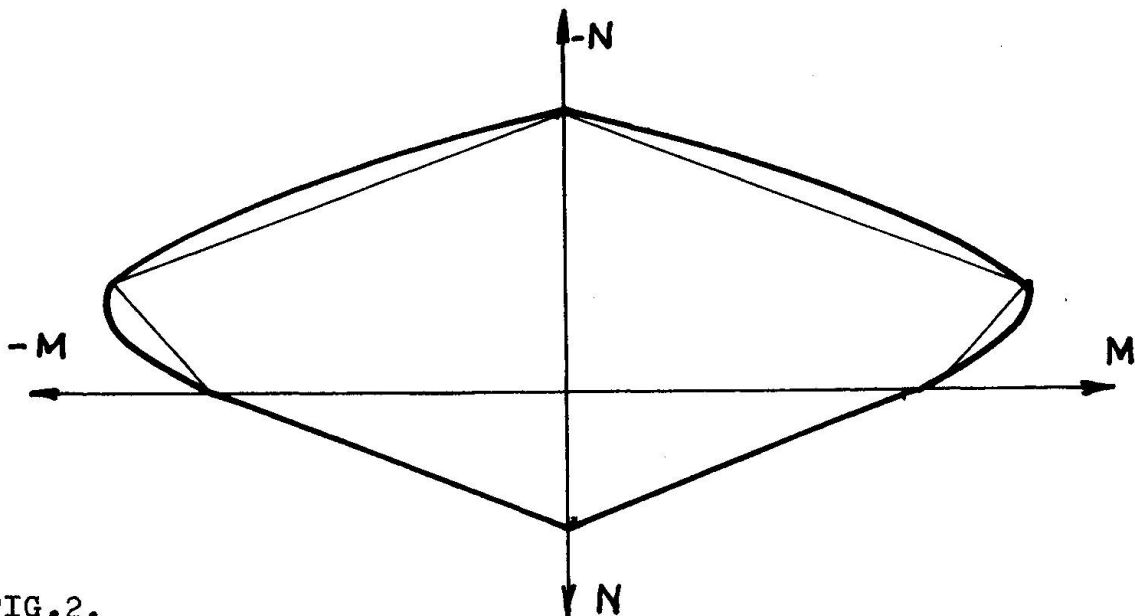


FIG.2.

Thus, instead of one flow parameter λ a set of parameters λ_i ($i=1, \dots, m$) is obtained. Assuming all λ_i to be constant within each interval j ($j=1, \dots, n$) they can be written in the form

$$\lambda(s) \rightarrow \vec{\lambda} = [\vec{\lambda}_1, \dots, \vec{\lambda}_i, \dots, \vec{\lambda}_m]^T$$

where

$$\lambda_i = [\tilde{\lambda}_{i(1)}, \dots, \tilde{\lambda}_{i(j)}, \dots, \tilde{\lambda}_{i(n)}]^T$$

By replacing the integration by a summation and the differential operators by finite differences the Lagrange functional (3) is transformed into

$$\Lambda(p, N_\Psi, N_\Phi, M_\Psi, M_\Phi, v_\Psi, v_\zeta, \lambda, \lambda_p) \rightarrow \Lambda(p, \vec{N}_\Psi, \vec{N}_\Phi, M_\Psi, \vec{M}_\Phi, \vec{v}_\Psi, \vec{v}_\zeta, \lambda, \lambda_p) \quad (5)$$

Thus the original problem (1), (2) is reduced to the minimization or maximization of a function.

With the conditions

$$\frac{\Lambda}{\dot{v}_\Psi(j)} = 0, \quad \frac{\Lambda}{\dot{v}_\zeta(j)} = 0, \quad \frac{\Lambda}{\lambda_{i(j)}} = 0 \quad (6)$$

the static formulation of the collapse load problem is finally obtained

$$p \rightarrow \text{maximum} \quad (7.1)$$

with

$$\begin{aligned} (\Delta s)^{-1} E_{1,\Psi} D_3^{(1)} \vec{R}_0 \vec{N}_\Psi - E_{7,\Psi} \vec{C}_\Psi \vec{N}_\Phi - (\Delta s)^{-1} E_{1,\Psi} R_\Psi^{-1} D_1^{(1)} R_0 M_\Psi \\ + E_{7,\Psi} \vec{R}_\Psi^{-1} \vec{C}_\Psi \vec{M}_\Phi + (\Delta s)^{-1} E_{1,\Psi} R_0 \vec{P}_\Psi p = 0 \end{aligned} \quad (7.2)$$

$$\begin{aligned} E_{7,\zeta} R_\Psi^{-1} R_0 \vec{N}_\Psi + E_{7,\zeta} \vec{S}_\Psi \vec{N}_\Phi + (\Delta s)^{-2} E_{1,\zeta} D_1^{(2)} R_0 \vec{M}_\Psi \\ - (\Delta s)^{-1} E_{1,\zeta} D_3^{(1)} \vec{C}_\Psi \vec{M}_\Phi + (\Delta s)^{-1} E_{1,\zeta} R_0 \vec{P}_\zeta p = 0 \end{aligned} \quad (7.3)$$

$$\vec{A}_{Fi}^{N_\Psi} \vec{N}_\Psi + \vec{A}_{Fi}^{N_\Phi} \vec{N}_\Phi + \vec{A}_{Fi}^{M_\Psi} E_7 \vec{M}_\Psi + \vec{A}_{Fi}^{M_\Phi} \vec{M}_\Phi \leq \vec{b}_{Fi} \quad (i=1, \dots, m) \quad (7.4)$$

$$-(\Delta s)^{-1} r_{o(0)} E_5 \vec{M}_\Psi + (\Delta s)^{-1} r_{o(0)} \vec{M}_s(0) p = 0 \quad \text{on } R_p \quad (7.5)$$

$$(\Delta s)^{-1} r_{o(n)} E_6 \vec{M}_\Psi + (\Delta s)^{-1} r_{o(n)} \vec{M}_s(n) p = 0 \quad \text{on } R_p \quad (7.6)$$

$$p \leq 0 \quad (7.7)$$



Considering the conditions

$$\frac{\Lambda}{N_{\Psi(j)}} = 0, \quad \frac{\Lambda}{N_{\Phi(j)}} = 0, \quad \frac{\Lambda}{M_{\Psi(j)}} = 0, \quad \frac{\Lambda}{M_{\Phi(j)}} = 0, \quad \frac{\Lambda}{p} = 0 \quad (8)$$

the kinematic formulation is found to be

$$\sum_{i=1}^m \vec{b}_{Fi} \vec{\lambda}_i^* \longrightarrow \text{minimum} \quad (9.1)$$

with

$$-(\Delta s)^{-1} \tilde{R}_0 D_4^{(1)} E_{1,\Psi}^T \vec{v}_{\Psi} + \tilde{R}_0 \tilde{R}_{\Psi}^{-1} E_{7,\zeta}^T \vec{v}_{\zeta} + \sum_{i=1}^m \tilde{A}_{Fi}^{N\Phi} \vec{\lambda}_i^* = 0 \quad (9.2)$$

$$-\tilde{C}_{\Psi} E_{7,\Psi}^T \vec{v}_{\Psi} + \tilde{S}_{\Psi} E_{7,\zeta}^T \vec{v}_{\zeta} + \sum_{i=1}^m \tilde{A}_{Fi}^{N\Phi} \vec{\lambda}_i^* = 0 \quad (9.3)$$

$$\begin{aligned} & (\Delta s)^{-1} \tilde{R}_0 D_2^{(1)} \tilde{R}_{\Psi}^{-1} E_{1,\Psi}^T \vec{v}_{\Psi} + (\Delta s)^{-2} \tilde{R}_0 D_1^{(2)} E_{1,\zeta}^T \vec{v}_{\zeta} \\ & - \left[(\Delta s)^{-1} r_{o(0)} E_5^T \dot{f}_{\Psi(0)} + (\Delta s)^{-1} r_{o(n)} E_6^T \dot{f}_{\Psi(n)} \right] R_{p\chi} + \sum_{i=1}^m E_7 \tilde{A}_{Fi}^{M\Psi} \vec{\lambda}_i^* = 0 \end{aligned} \quad (9.4)$$

$$\tilde{R}_{\Psi}^{-1} \tilde{C}_{\Psi} E_{7,\Psi}^T \vec{v}_{\Psi} + (\Delta s)^{-1} \tilde{C}_{\Psi} D_4^{(1)} E_{1,\zeta}^T \vec{v}_{\zeta} + \sum_{i=1}^m \tilde{A}_{Fi}^{M\Phi} \vec{\lambda}_i^* = 0 \quad (9.5)$$

$$\begin{aligned} & (\Delta s)^{-1} \vec{P}_{\Psi}^T R_0 E_{1,\Psi}^T \vec{v}_{\Psi} + (\Delta s)^{-1} \vec{P}_{\zeta}^T R_0 E_{1,\zeta}^T \vec{v}_{\zeta} \\ & + \left[(\Delta s)^{-1} r_{o(0)} \bar{M}_s(0) \dot{f}_{\Psi(0)} + (\Delta s)^{-1} r_{o(n)} \bar{M}_s(n) \dot{f}_{\Psi(n)} \right] R_{p\chi} \geq 1 \end{aligned} \quad (9.6)$$

$$\begin{aligned} \tilde{\lambda}_{1(0)}^* &= 0,5 \quad r_{o(0)} \tilde{\lambda}_{1(0)} = 0 \\ \tilde{\lambda}_{1(j)}^* &= r_{o(j)} \tilde{\lambda}_{1(j)} = 0 \quad (i=1, \dots, m), (j=1, \dots, n-1) \\ \tilde{\lambda}_{1(n)}^* &= 0,5 \quad r_{o(n)} \tilde{\lambda}_{1(n)} = 0. \end{aligned} \quad (9.7)$$

In this equations are

$$D_1^{(1)} = \begin{bmatrix} -0,5 & +0,5 & & & \\ -0,5 & 0 & +0,5 & & \\ & \dots & \dots & \dots & \\ & & -0,5 & 0 & +0,5 \\ & & & -0,5 & +0,5 \end{bmatrix}, \quad D_3^{(1)} = -D_4^{(1)T} = \begin{bmatrix} +1 & & & & \\ -1 & +1 & & & \\ & \dots & \dots & & \\ & & -1 & +1 & \\ & & & & -1 \end{bmatrix}$$

$$D_1^{(2)} = \begin{bmatrix} -1 & +1 & & & \\ +1 & -2 & +1 & & \\ & \dots & \dots & \dots & \\ & & +1 & -2 & +1 \\ & & & +1 & -1 \end{bmatrix} \quad \begin{aligned} E_5 &= [1 \ 0 \ \dots \ 0 \ 0] \\ E_6 &= [0 \ 0 \ \dots \ 0 \ 1] \end{aligned}$$

\tilde{R}_0 , \tilde{R}_ψ , \tilde{C}_ψ , \tilde{S}_ψ , $\tilde{A}_{Fi}^{N_\psi}$, $\tilde{A}_{Fi}^{N_\phi}$, $\tilde{A}_{Fi}^{M_\psi}$, $\tilde{A}_{Fi}^{M_\phi}$, R_ψ are diagonal matrices with the diagonal elements $\tilde{r}_0(j)$, $\tilde{r}_\psi(j)$, $\cos \tilde{\psi}(j)$, $\sin \tilde{\psi}(j)$, $\tilde{a}_{Fi}^{N_\psi}(j)$, $\tilde{a}_{Fi}^{N_\phi}(j)$, $\tilde{a}_{Fi}^{M_\psi}(j)$, $\tilde{a}_{Fi}^{M_\phi}(j)$ ($j=1, \dots, n$), and $r_\psi(j)$ ($j=0, \dots, n$).

According to the boundary conditions, the shell edges will either belong to R_p if they are loaded by external forces $p\bar{P}_\psi(k)$, $p\bar{P}_\zeta(k)$ and bending moments $p\bar{M}_s(k)$ ($k=0, n$), or to R_v if slopes and displacements are restricted. Depending upon the boundary conditions the matrices $E_{1,\psi}$, $E_{1,\zeta}$, $E_{7,\psi}$, $E_{7,\zeta}$ are obtained by modification of the matrices

$$E_1 = \begin{bmatrix} 1 & & & & \\ & 1 & & & \\ & & \cdot & & \\ & & & 1 & \\ & & & & 1 \end{bmatrix} \quad \text{and} \quad E_7 = \begin{bmatrix} 0,5 & & & & \\ 0,5 & 0,5 & & & \\ & \dots & \dots & \dots & \\ & & 0,5 & 0,5 & \\ & & & & 0,5 \end{bmatrix}$$

For the solution of the collapse load problem in the form (7) or (9) various optimization techniques for linear programming are available.

The coefficient matrix will be formed very easily, because only a few of the matrix elements differs from zero.



Besides the collapse load intensity, the field of displacements and internal forces in the plastified zones are found without any additional computations. This is a certain advantage in comparison to methods, where the unknown functions are represented in form of series.

As the static and kinematic formulations are dual to each other the same collapse load intensity will be obtained. Therefore, it is not possible to characterize the results as upper or lower bound solutions without additional considerations.

The method described in this paper was used for the investigation into reinforced concrete cylindrical shells under various loading conditions. The calculations were carried out by an electronic computer of the type ROBOTRON 300.

REFERENCES

- /1/ Raue, E.: Beitrag zur Berechnung rotationssymmetrischer Flächentragwerke nach der Theorie des Grenzgleichgewichts, Hochschule für Architektur und Bauwesen Weimar, Dissertation (Promotion B), 1975.



SUMMARY OF DISCUSSION - SESSION 4

Due to shortage of time there were only five discussions - from G. Mehlhorn, A.M.A. Da Fonesca, T. Kawai and E. Anderheggen. The main point of discussion was on whether the current FEM can be applied to the analysis of nonlinear behaviour of reinforced concrete. G. Mehlhorn pointed out that there were many examples which had shown the applicability of FEM to these problems.

T. Kawai explained his unique idea which is described below in detail.

1. Slip is the essential source of plastic deformation

The influence of slip may be neglected if it is uniformly distributed. However, it usually appears discontinuously. Even in this case current plastic theory requires the continuity of displacement. Therefore, it should be said that the current FEM, which is based on continuum mechanics, cannot follow the non-linear behaviour of solid materials until failure.

2. Constitutive equations should be essentially investigated

It is quite easy to point out the examples which indicate that the elasto-plastic deformation field obtained from the mathematical theory of plasticity does not coincide with that obtained from the experimental result.

It may be extremely difficult to draw failure criteria from the stress strain relationship obtained from the test of materials since this represents the average. The true stress strain relationships or failure criteria can be obtained from simulative analysis based on a model such as Kawai's Model.

3. Existence of so-called Large Scale Yielding is questionable

As the plastic deformation increases, slips inevitably appear discretely, and the rigid body movement along the slip lines becomes distinguished while the strain itself does not change substantially.

H. OKAMURA

Leere Seite
Blank page
Page vide